UNIVERSITY OF NAVARRA

TECHNOLOGICAL CAMPUS, TECNUN

SAN SEBASTIÁN

tecnun
Universidad
de Navarra

AUTOTHERMAL THERMOPHILIC AEROBIC DIGESTION: DESIGN OF CONTROLLERS AND BENCHMARKING VALIDATION

THESIS SUBMITTED
to obtain the Degree of Doctor in Industrial Engineering
presented by

JESÚS ALBERTO ZAMBRANO BALLESTERO

Supervised by:

Ion Irizar Picón, PhD.

San Sebastián, November 2011

Thesis committee members:

Dr. Eduardo Ayesa Iturrate (chairman)	University of Navarra, Spain
Dr. Jaime Luis García de las Heras	University of Navarra, Spain
Dr. Jairo Gomez	NILSA, Spain
Dr. Montserrat Gil-Martinez	University of La Rioja, Spain
Dr. Jean-Philippe Steyer	INRA, France
Dr. Enrique Aymerich	University of Navarra, Spain
Dr. Joaquín Suescun	Veolia Water Systems Ibérica

This dissertation was approved by:

Dr. Ion Irizar Picón (promotor)	University of Navarra, Spain

Part of this work is the continuation of previous studies developed by Dr. J. Gomez at CEIT in collaboration with NILSA-Navarra de Infraestructuras Locales, Pamplona, Spain.

This work was part of the Gaitek project "Design and development of advanced automatic control strategies for Autothermal Thermophilic Aerobic Digestion processes (ATAD technology)" in collaboration with the Spanish companies MSI Soc. Coop and ATM S.A. This project was financially supported by the Basque Government.

This study was also part of the research project "Design of automatic control strategies in treatment plants of solids residues from a methodology based on the mathematical model and systems simulation", in collaboration with Public University of Navarra. This project was financially supported by the Spanish Ministry of Science and Innovation (DPI2006-15522-C01-C02).

The research described in this thesis was carried out at the Environmental Engineering Area, CEIT-Centro de Estudios e Investigaciones Técnicas de Gipuzkoa (Center of Studies and Technical Investigations of Gipuzkoa), Paseo de Manuel Lardizabal 15, 20018 San Sebastian, Spain.

J.A. Zambrano
Autothermal Thermophilic Aerobic Digestion: Design of controllers and benchmarking validation.
Ph.D. Thesis, University of Navarra, San Sebastian, Spain.

Author's email: jazambranob@gmail.com

Dedicated to the memory of my mother

Aurora Zambrano

(1949-2009)

CONTENTS

INDEX OF FIGURES

INDEX OF TABLES

ABSTRACT

This thesis presents the design and validation by simulation of new automatic control strategies applied to the **A**utothermal **T**hermophilic **A**erobic **D**igester, (ATAD) technology, for sludge treatment.

Every proposed control solution was oriented toward covering different requirements in the treated sludge: reducing aeration costs or increasing sludge stabilization. But in all applied strategies, digester stability was considered in the control performance.

In addition to the ATAD reactor, for direct industrial application of these control strategies, the control scenario selected included a pre-holding tank, a typical scenario for this kind of process in Spain.

The different tasks assessed in this thesis are based on simulation studies, showing the possibilities of the employed mathematical model as a tool in the design, validation and evaluation of the proposed control strategies.

Considering previous work on different simulation benchmarks for activated sludge processes, a specific protocol for sludge digestion employing the ATAD technology was developed, in order to have a platform to design and validate control strategies for this process. Therefore, a detailed definition of the scenario is described here, including the definition of the influent sludge to be treated, the layout configuration, and the available online instrumentation.

Regarding the control problem, the control strategies proposed were designed based on the behavior of some relevant signal profiles during the digestion phase. In this case, like in many biological processes, the depletion of specific signals gives information about the status of a certain part of the process. In the ATAD process, this depletion in the temperature profile is linked to the lack of

biodegradable organic matter, and therefore, a bending-point detection algorithm is implemented as a tool for control strategy approaches.

The implemented simulation protocol was used to validate two different controls strategies for aeration (ST1 and ST2). In terms of the designed benchmark, the validation of the control solutions showed an improvement in overall plant operation. Indeed, in comparison to a conventional open-loop operation, simulation results showed that the ST1 strategy was able to save aeration costs of around 2-4%.

Unlike the ST1 strategy and conventional operation, the ST2 strategy achieved a maximum sludge stabilization reduction by around -18%, but at the expense of higher aeration costs of around 3%. These results are reference values, since they are associated to the plant-layout characteristics, the raw sludge to be treated and the maximum air flow-rate applied.

The uncertainty analysis applied to these strategies shows that while ST2 is more sensitive to variability in the space of the parameters considered, the average response obtained concerning the quality and thermal energy in the effluent reflects a better performance when this strategy is compared to ST1 and OL operation.

As a result, when there is a requirement to save on aeration costs or on sludge stabilization, control strategies ST1 and ST2 can overcome these restrictions: ST1 provides a thermal energy saving, and ST2 brings an improvement in effluent quality.

Keywords: autothermal thermophilic aerobic digester; modeling; robust tuning; bending-points; uncertainty.

1

Introduction

Chapter 1 Introduction

This thesis deals with the control applied to an Autothermal Thermophilic Aerobic Digester (known as ATAD technology). The main focus of the thesis was to try to improve ATAD operation, which was motivated by the fact that the digested sludge is very important for reutilization, and the amount of air used in this kind of process can be reduced. Therefore, the final goal was to improve sludge digestion, save energy costs and obtain better effluent quality.

The outline of this chapter is as follows: In **Section 1.1**, a description of different characteristics for the aerobic treatment of sludge is given. In **Section 1.2**, an introduction to ATAD technology is presented, where the most important process characteristics are shown. **Section 1.3** briefly describes the available instrumentation for the ATAD process. Quality assurance and the relevant norms are explained in **Section 1.4**. The state-of-the-art in mathematical models and control approaches are depicted in **Section 1.5** and **1.6**, respectively.

1.1. Sludge treatment

Sludge that is produced as a by-product of wastewater treatment usually needs additional treatment prior to its further use or disposal. The main goal of plant operators and design engineers is to reduce the quantity of biosolids while simultaneously improving their quality for possible further utilization. The processes employed have the aim of reducing the volume, organic biodegradable content and/or pathogen content of sludge. Sludge treatment techniques can be classified as biological, chemical and thermal. The most

suitable techniques are those that allow the re-use of sludge in agriculture as a valuable commodity that is rich in nutrients (Cheremisinoff, 2002).

Biological sludge treatment can be divided into categories according to the temperature employed as well as according to whether it is carried out in an oxygen-free environment (anaerobic) or in the presence of oxygen (aerobic). In this introduction, only the different process temperature and the aerobic technologies are detailed.

1.1.1. The process temperature

The temperature of the process determines the kind of microorganism population carrying out the digestion. Every living organism can only live between certain temperature ranges. The growth and metabolism of microorganisms are constrained to certain temperature intervals within which an optimum temperature is found. As a general rule, within this range the chemical and biochemical reaction rates double every 10 ºC. The optimum temperature for metabolism is close to the maximum temperature. A brief overview of the types of microorganisms relevant to sludge treatment are described below (Prescott et al., 2002):

- *Phychrophiles*: they grow well at 0 ºC and have an optimum growth temperature of 15 ºC or lower, with the maximum being around 20 ºC. They are readily isolated from Arctic and Antarctic habitats. Because 90% of the ocean is 5 ºC or colder, it constitutes an enormous habitat for psychrophiles.
- *Mesophiles*: their optimal growth is at around 20 to 45 ºC; they often have a minimum temperature of 15 to 20. Their maximum is 45 ºC. Most microorganism fall within this category. Almost all human pathogens are mesophiles, as their environment is a fairly constant 37 ºC.
- *Thermophiles*: they can grow at temperatures of 55 ºC or higher; their minimum growth is at around 45 ºC and their optimum temperature is between 55 and 65 ºC. These organisms flow in many habitats, including

composts, hot water lines, and hot springs. Thermophiles differ from mesophiles in that they have much more heat-stable enzymes and a protein synthesis system that is able to work at high temperatures. The active thermophilic microflora in aerobic thermophilic sludge is very homogeneous and is almost entirely made up of neutrophilic Bacilli (Ponti et al., 1995). The microbes living at thermophilic temperatures are not only capable of stabilizing sludge, but also of treating wastewater. Its full potential can be employed in the case of warm wastewater. Bruce and Newman (1992) found that higher temperature rates allow higher rates of microbial metabolic activity, leading to a shorter retention time in order to reach a given level of solid destruction and a good degree of pathogenic organism inactivation.

1.1.2. Aerobic processes

Regarding the aerobic processes, several variations can be found. These include high-purity oxygen digestion, low-temperature aerobic digestion, dual digestion and mesophilic digestion. Each of these is explained in further detail below.

- **High-Purity Oxygen Digestion**

Here oxygen is used instead of air injection. The process is typically carried out in a closed tank similar to the activated sludge process for wastewater using oxygen. The high-purity oxygen atmosphere is maintained in the space above the liquid surface, and oxygen is transferred into the sludge via mechanical aerators. The process can also be performed in open tanks, in which case oxygen is introduced into the sludge in minute bubbles with special diffusers. The bubbles dissolve before they reach the liquid surface. It is expensive to generate pure-oxygen; therefore, it is cost-effective only when used in conjunction with a pure-oxygen-activated sludge system. The principal advantage of such a system is that it enables high temperatures to be reached

with very low energy requirements, in addition to enabling faster digestion and higher pathogen kill.

- **Low-Temperature Aerobic Digestion**

Aerobic digesters in small package-type wastewater treatment plants have been studied in order to provide better operational control at temperatures lower than 20 ºC. Investigations at treatment plants in British Columbia, Canada have indicated that the sludge retention time (SRT) must be increased as operating temperatures decrease in order to ensure acceptable volatile solids reduction (Koers and Mavinic, 1977; Mavinic and Koers, 1979). At temperatures between 5 and 20 ºC, the system should operate at 250 to 300 degree-days (the product of SRT in terms of days and operation temperature in ºC) in order to maintain an acceptable level of volatile solid reduction. Heated air can be used to keep the digesters from freezing.

- **Dual Digestion**

Dual digestion, a system used extensively in Europe, has two stages: first there is a process of aerobic thermophilic digestion, followed by a second stage of mesophilic anaerobic digestion (see **Figure 1.1**). Residence time in the aerobic digester is typically 18 to 24 hours at 55-65 ºC, and residence time in the anaerobic digestion is about 10 days. Hydrolysis in the aerobic digester results in increased degradation of the sludge during subsequent anaerobic digestion and gas production. Advantages of dual digestion are: (1) increased levels of pathogen reduction, (2) improved volatile solids reduction, (3) increased methane gas production in the anaerobic reactor, (4) fewer odors from the stabilized sludge, and (5) one-third less capacity required than for a single-stage anaerobic digester.

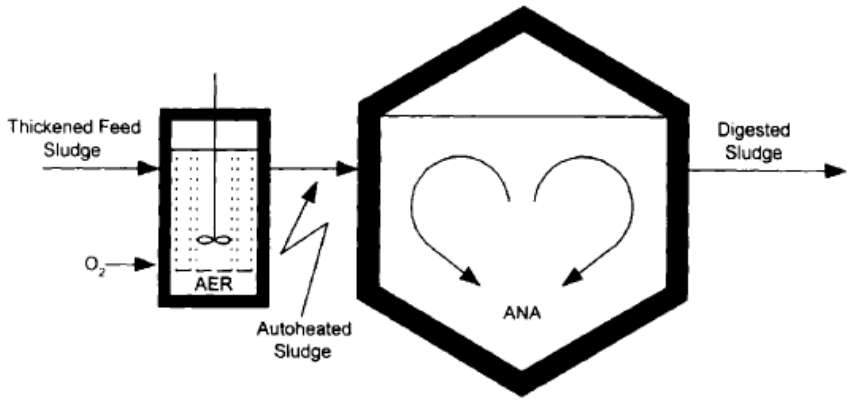

Figure 1.1 Layout of a dual digestion process

- **Mesophilic Aerobic Digestion**

Mesophilic aerobic digestion is a process that includes sludge thickening followed by two or three stages of treatment in aerobic reactors.

In order to achieve the heat balance required for the process, the sludge has to be pre-thickened to 4-5% solids. In the first stage of digestion, the SRT is from 8 to 16 days, the dissolved oxygen is kept between 0.2 to 1 mg/L, and the temperature reaches 20 to 35 ºC. In this stage, ammonium bicarbonate alkalinity keeps the pH between 6.8 and 9. In the second stage, the SRT is from 10 to 17 days, the dissolved oxygen is kept between 0.2 and 1 mg/L, the temperature is kept between 15 and 30 ºC, and the pH is 6.5 to 7.5. A third stage may also be added with a SRT of 10 to 17 days.

The SRT in all stages can be reduced by maintaining temperatures in the range of 30 to 35 ºC in the first stage. The mesophilic aerobic digestion process meets the requirements for significantly reducing pathogens; however, compared to conventional aerobic digestion, use of this process is limited, due to high capital and operating costs.

- **The Autothermal Thermophilic Aerobic Digestion (ATAD)**

A relatively new technology for raw sludge treatment is the **A**utothermal **T**hermophilic **A**erobic **D**igestion, (ATAD) technology. As the aerobic process is exothermic, thermophilic digestion, without much external heat input, can occur by using the heat released during the microbial oxidation of organic matter to heat the sludge.

With properly designed thermophilic aerobic digesters (including the ATAD), the following advantages result (Gurjar, 2001):

- Production of class A biosolids.
- Cost-effective compact facilities.
- Significant volume reduction.
- Better biosolids dewaterability.
- Temperatures above 55 ºC can be reached even during the winter months, provided the digester is well insulated.
- Flexibility of operation; it can be operated batch-wise or semi-continuously, depending on the sludge load.

However, ATAD, as with any sludge treatment, has three main operational difficulties:

- It is usual for sludge not to be well mixed in the raw sludge storage tank. Sludge settles out into bands of thick sludge and water. If care is not taken during digester feeding and this sludge is fed to the digester, the temperature rise is not as high or as rapid as usual, because the amount of the biodegradable material available is limited.
- If there is no grit removal, the sludge entering the digester has high grit content, which causes problems in excessive wear on the pump impeller and excessive grit deposition in the base of the digester. However, since uprated pump impellers and wear plates are used, wear is minimized.

Future digesters are expected to incorporate features designed to facilitate grit removal.

- Rag causes the pump to block and the foam cutter to fail. Raw sludge screening and/or maceration are, therefore, required prior to digestion.

ATAD is a very efficient stabilization process because its facilities are more compact (when compared to conventional aerobic digestion). This compactness:

- Reduces capital costs and annual energy, operation, and maintenance costs
- Enables capture of gas for better odor control
- Can provide those owners with existing available tanks significant tank capital cost savings

From this point forward, the rest of the chapter will focus on the principal characteristics involved in the ATAD technology, starting with an explanation of the biological process, then moving to a discussion of the operational conditions, and ending by talking about the mathematical modeling and control approaches.

1.2. The ATAD technology (process characteristics)

The ATAD technology is an aerobic and exothermic process where sludge is typically subjected to temperatures greater than 55 ºC without supplemental heat. The process is described as autothermal because, after initial start-up, it requires no other heat source (other than mixing energy). The primary aim of the process is to reduce the volume of waste sludge for final disposal.

The ATAD technology is capable of achieving a high degree of stabilization due to the high degree of degradation of volatile solids. Since the microbial metabolism occurs at elevated temperatures, it reaches a high degree of pathogen reduction as well, resulting in biologically stable and pathogen-free biosolids as an end-product (Scisson, 2003). **Figure 1.2** depicts the layout of an ATAD.

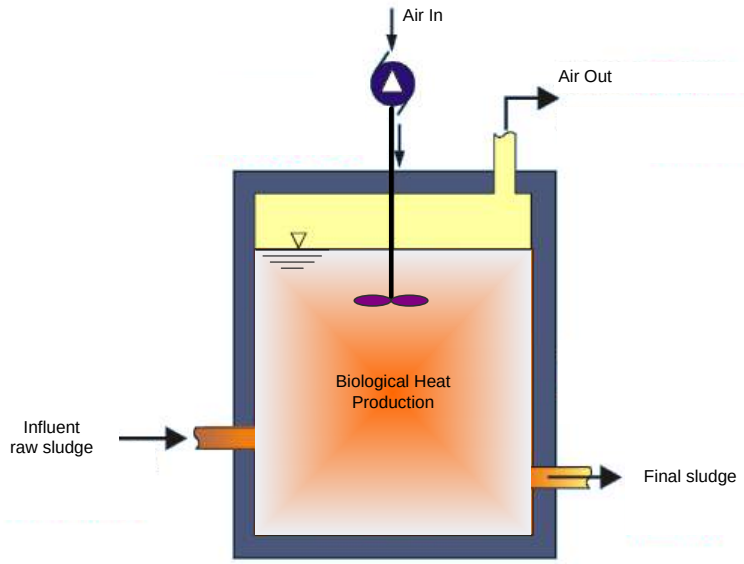

Figure taken from Kelly (2006)

Figure 1.2 Layout of an ATAD

This technology does not only reduce the level of pathogens, parasites and viruses and vector attraction in the biosolids. Because of the high biological reaction rates, it is also able to achieve these reductions within a relatively short SRT of 6-12 days, as compared to the 20-30 days of anaerobic digestion. Furthermore, the higher reaction rates and short sludge digestion time means that less space is required as compared to other conventional processes such as anaerobic digestion. As the biosolids produced by the ATAD reactor have less

organic material and produce few odors, they can be reused by being applied them on lands without any restrictions (provided that the ATAD technology has been operated in compliance with local and national legislation).

The most disadvantageous feature of the process is the high amount of energy needed to operate the aeration and mixing devices both from a capital and an operational point of view. The report EPA/625/10-90/007 of the US Environmental Protection Agency (USEPA, 1990) estimated a value of 1.42 kgO_2 per kg VSSd (VSSd refers to volatile suspended solids destroyed), from full-scale results at the plant in Gemmingen (Germany) direct estimation of field oxygen transfer rates were made in ATAD systems equipped with Fuchs aerators, values ranged from 1.5 to 3.7 kgO_2 per kWh were considered, giving a range of 9-22 kW per kg of organic matter destroyed. There are conflicting reports relating to the costs and energy efficiency of the ATAD process. The operational costs are associated with running the aeration devices and treatment of side streams (i.e., odor control, dewatering). Kelly (1999) compared three thermal sludge treatment processes (indirect drying, thermal chemical treatment and ATAD) and concluded that ATAD was the most cost effective operation. Other researchers also conclude that ATAD is competitive on an economic basis when compared with a single or multi-stage treatment process and a traditional anaerobic process (Deeny et al., 1991; Riley and Forster, 2002). On the contrary, Le (2006) suggests that ATAD is costly and energy inefficient.

1.2.1. First experiences with ATAD

ATAD was developed in the late 1960s for the stabilization of waste biological sludge. For the most part, development has come from the United States and from Germany, though Great Britain, Canada and other countries have also contributed to knowledge about and improvement of this technology.

United States

Interest in the auto-heating of sludge in the USA began with the paper by Kambhu and Andrews (1969). In 1971, sludge auto-heating was demonstrated at the Hamilton Ohio plant. A sludge digester, treating 4% combined primary and secondary municipal sludge, was converted from anaerobic to aerobic operation with diffused aeration, unexpectedly reaching operating temperatures of 38 ºC. However, tests were discontinued due to excessive odors from the uncovered tanks at the higher temperatures (Smith et al., 1975).

In 1972, Union Carbide started pilot plant work using pure oxygen for aeration at the Tonawanda research facility in New York. Researchers felt that pure oxygen was necessary because of the low aeration efficiency of the aerators they were familiar with. The experiments were done in a 200L covered insulated reactor (Matsch and Drnevich, 1977). Other studies were done with pure oxygen in open tanks: Cohen and Puntenney (1973) did batch tests in Denver, Colorado in 1973 with 6.4 m^3 open tanks reaching operating temperatures of 44.5 ºC (Smith et al., 1975).

ATAD using air aeration began in the USA in 1977, the same year that the Vilsbiburg plant opened in Germany. Jewell and Kabrick (1980) were working in Binghamtom, NY, with Delaval self-aspirating aerators, whose design was based on works by Deeny et al. (1985). A 5% thickened primary and secondary sludge was treated in a 33.4 m^3 reactor.

Germany

In 1968, Hurbert K. E. Fuchs observed the autothermal conditions during the aeration of agricultural manure (Breitenbucher, 1984). Much of the development work was done in Germany by Popel (ASCE & WEF, 1998). Kambhu and Andrews (1969) performed the first detailed analysis on thermophilic aerobic sludge digestion, demonstrating through computer simulation that autothermal operation was possible with a high efficiency aeration system and an influent of 4-6% solids content.

A recirculation type aerator using air that Fuchs has developed was used to digest animal manure in tanks of 20-45 m^3 capacity (Deeny et al., 1985). In the early 1970's the tests were expanded to include wastewater Pöpel and Ohnmacht (1972). This work led to the commissioning of a full-scale Fuchs aeration ATAD plant in Vilsbiburg in 1977. The next municipal sludge plant was built at Gemmingen in 1980 as a federal research project. Autothermal operation was empirically demonstrated by Matsch and Drnevich (1977) using high-purity oxygen aeration and by Jewell and Kabrick (1980) via self-aspirating aeration units using air.

Basic research was continued there for the next two years (Breitenbucher, 1984). By 1982, there were 10 ATAD plants operating in West Germany (Wolf, 1982). Further experiments in Germany were focused on treating thin sludge (Vismara, 1985); Salmonella kill using Thieme's proprietary aeration system (Deeny et al., 1985); dual digestion (Loll, 1984); and the effect of heavy metals on the thermophilic process (Loll et al., 1986). Tsang and Smith (2005) concluded that the development of the aspirating aeration was a key factor to the process's success.

Great Britain

The interest in ATAD in Great Britain started in the early 1970's. By 1975, a 9 m^3 pilot plant at the Ponthir sewage works in Wales was successfully operating using pure oxygen. The plant was subsequently converted to a new type of venture compressed air system. In 1979, the air-operated pilot plant reached 61 ^oC (Morgan and Gunson, 1987). In 1981, the entire Ponthir plant was converted to autothermal thermophilic sludge digestion with continuous sludge feed. Operating temperatures were dependent on the ambient temperatures, since the tanks used were the old open digestion tanks, which were not well insulated (Morgan et al., 1983).

Experiments at the Palmersford plant in Wessex in 1980 began using pure oxygen in an above ground insulated 60 m^3 digester (Booth and Tramontini, 1983). Subsequent tests with air aeration attained operating temperatures of up

to 67 ºC (Morgan et al., 1986). Because of excessive foaming, the operating volume was reduced to 24-30 m^3 (Wolinski, 1985).

Rest of the world

In the early 1980's interests in ATAD began to spread to the rest of the world. In Switzerland, interest was mainly in dual digestion systems. Sonnleitner (1983) and Sonnleitner and Fiechter (1983a; 1983b) studied the microbiology of the thermophilic organisms developed in the aerobic pre-stage pilot plant at Altenheim. Mason et al. (1987) studied how thermophilic microorganisms digested mesophilic organisms, in this case yeast cells.

In Norway from 1983-84, Langeland and Paulsrud (1984) studied the fate of salmonella in a three-stage, full-scale pure-oxygen pilot plant. Similar studies took place in South Africa, where Trim (1984) operated an 8 m^3 pure oxygen plant for 3 years.

In Canada, ATAD systems were designed in 1987. Full-scale Fuchs units were installed at Ladysmith, British Columbia (B.C.), and Banff, Alberta. Venturi-style aeration plants were built at Gibsons and at Whistler, both in B.C., and an existing system in Salmon Arm, B.C., was upgraded to ATAD, using a locally designed and built aspirating aeration system commercially marketed as Turborator Technology.

1.2.2. How ATAD works

The aerobic digestion process, which requires the presence of a sufficient level of oxygen, consists of two principal steps:

- Direct oxidation of biodegradable matter
- Oxidation of microbial cellular matter (endogenous respiration)

Heat production from biological activity is the by-product of these two separate processes that take place simultaneously in the bioreactor (Shammas and Wang, 2007). During the synthesis of biomass, heat is released as a result of the free energy change due to growth while biodegradable organic matter degrades. A simplified process can be represented as:

$$\text{Organic matter} + O_2 \xrightarrow{bacteria} \text{Cellular material} + CO_2 + H_2O + \text{Heat}$$

In the endogenous respiration heat is produced as a result of the oxidation of cellular material. A simplified process can be represented as:

$$\text{Cellular material} + O_2 \xrightarrow{bacteria} \text{Digested sludge} + CO_2 + H_2O + \text{Heat}$$

The above is the predominant reaction in aerobic digestion systems. Throughout the biodegradation of the organic matter, heat energy is also being released.

The microbial diversity of ATAD reactors are not fully investigated, though what is known is that nitrifying bacteria, floc-forming organisms and protozoa are not present. The species or organisms that can proliferate in the reactors include Bacillus, which tends to be the dominant species, i.e., thermus and actinomycetes.

Kelly and Warren (1995) state that secondary waste activated sludge is a more suitable substrate than primary sludge for the thermophilic bacteria, as the former substrate is in a more readily available form. The main substrate for the thermophilic microorganism is the biodegradable organic part of the secondary waste activated sludge, which mostly consists of the cell tissue of the mesophilic biomass. When sludge is introduced to the reactor the mesophilic organisms present are subjected to a thermal shock, which deactivates them. The exoenzymes (proteases) of the thermophilic seed sludge cause lysis of the

cell structure, thus releasing the readily biodegradable content of the cell (Haner et al., 1994).

During the lysis stage, the nutrients remaining in the dead cells diffuse out to furnish the remaining cells with substrate, known as cryptic growth. When the available substrate from this carbon source is in short supply, in a process that is similar to the activated sludge process, the microorganisms begin to consume their own protoplasm to obtain energy for cell-maintenance reactions. When this occurs, the microorganism are said to be in the endogenous phase. Both lysis products and extracellular metabolic products supplement the pool of suitable nutrients available to the process culture (Lapara and Alleman, 1999). As a result, the mesophilic biomass is aerobically oxidized to carbon dioxide, water and nitrogen by-products in the ATAD reactor, which, leads to a reduction in the sludge's volatile solids (VS) content. Indeed, between 15 to 80% of the cells' tissue can be oxidized, and the remainder consists of inert components and organic compounds that are not biodegradable.

1.2.3. Fundamentals of process operation

Part of the conservation energy of the organic matter is dissipated into the environment as heat when the organics are converted. Consequently, aerobic thermophilic digestion processes are exothermic, i.e., they generate heat. Since the primary objective of this process is to operate under thermophilic conditions (45-65 ºC) without supplemental heat beyond what is supplied by mixing energy and during digestion itself, heat conservation is crucial. In order to meet the objective of achieving autothermal conditions, controlling the heat generated and the heat lost from the system is very important. The general requirements for maintaining appropriate thermophilic temperatures without external heating and minimizing excessive heat loss are as follows (Stover and Joshua Samuel, 1998; Stentiford, 2001):

- The heat energy produced by the biodegradation of VS is the main contributor to the rise in temperature in ATAD reactor vessels. Therefore, a sufficient level of biodegradable organics must be supplied to the process to provide heat from oxidation. 3% (or lower) of total solids (TS) of thickened sludge might not be able to provide enough energy for thermophilic temperature operations. Studies from Kelly and Warren (1997) suggested that a COD concentration of 40 to 60 $g \cdot l^{-1}$ or as a substitute measurement VS between 3 and 4% are typical requirements (4-6% TS). On the other hand, the TS concentration cannot be over a certain limit since a high concentration would not allow for sufficient mixing. Typically, TS of thickened sludge should not be greater than 6% (maximum 7%). Usually a pre-thickener is used to reach the abovementioned targets. Temperature increment limitations occur at the organic loading rates at which the biological system capacity cannot compensate for heat losses in the effluent with sufficient matter conservation (Jewell and Kabrick, 1980).
- Insulated reactors and low net heat loss system must be designed in order to reduce heat loss to the surroundings.
- Effective aeration system and adequate oxygen transfer efficiency. It is critical for the ATAD system operation to supply sufficient amount of oxygen for the microorganisms. If insufficient oxygen is provided, anaerobic conditions are promoted, resulting in the accumulation of volatile fatty acids and odors (USEPA, 1990). Oversized aeration not only increases the heat loss through the exhaust air, but also increases the operating costs of the aeration device. The over-aeration also has a knock on effect on the exhaust air treatment. To keep aerobic conditions in the reactor is mainly up to the application of the right aeration system.
- Adequate mixing in order to keep the whole vessel aerated.
- Adequate Hydraulic Retention Time (HRT) must be selected.

1.2.4. Operating conditions

Temperature

The operating temperature during the aerobic process influences the microbial population present in the reactors, which affects the microbial organic material degradation kinetics and the degree of stabilization. As in most biological systems, the reaction rates increase with the temperature, such as in the degradation of biodegradable organic matter. In engineering terms, this reduces the size of the reactor required for treating a particular influent. This is one of the advantages of ATAD, and operating in the thermophilic temperature range is thus considered more favorable than in the mesophilic range. However, this is valid up to a certain point; if the sludge temperature exceeds a certain point then it inhibits biological activity.

In the literature there is no precise temperature at which this decline begins, but previous work has shown that above 65 ºC the rate rapidly drops to zero (Stentiford, 2001) and that further cell lysis occurs at extreme temperature above 65 ºC (USEPA, 1990). It has been reported that the reaction rate reaches its maximum at 55 ºC and decreases to zero at a temperature of 75 ºC.

Temperature also affects the inactivation of pathogenic microorganisms as function of incubation time. The higher the temperature, the lower the concentration of surviving microorganisms, and this includes pathogens. Thus, from the point of view of pathogen reduction, it is desirable to attain the highest possible temperature at which it is warm enough to keep the bacteria in good conditions, but it is not so elevated that digestion is shut down.

Feed Cycle

Influent sludge can be introduced into the reactor in three ways: continuously, intermittently, or in batches.

In continuous operation (where tank contents are continuously displaced by an inflow of feed) and in semi-continuous operation (where tanks are partially displaced or drained and filled intermittently, usually in intervals of hours,

throughout the day) some pathogens could short-circuit the reactor through the potential cross-contamination between the incoming and outgoing sludge streams. This undermines the disinfection level, and thus, makes guaranteed sanitization difficult. The main disadvantage with continuous operation is that it is unable to meet pathogen reduction regulations.

Operation in batch mode is when the tank is completely filled, it operates in isolation over the period of hydraulic retention time (HRT) and the tank is fully drained at the end. In semi-batch, on a daily basis the tank is partially drained and filled with a volume equal to the reactor volume divided by the HRT. The ATAD process usually operates in semi-batch mode due to the fact that the full batch mode requires 6 to 10 days of storage upstream of a single reactor facility. For this reason, in this thesis the semi-batch mode is considered.

Mixing Energy Levels

High mixing energy levels are required in an ATAD to keep the digestion solids in suspension, and to ensure good oxygen and substrate transfer to the microorganism. USEPA (1990) recommends 85-105 $W \cdot m^{-3}$. Kelly (1990) recommends 250 $W \cdot m^{-3}$, based upon the minimum mixing energy requirements cited in ASCE and AWWA Water Treatment manuals.

Some of the temperature rise observed in an ATAD is due to the kinetic energy transmitted by mixing. A measure of this energy is the mixing system power draw. Not all of this energy is transmitted to the liquid since motors are not 100% efficient. Usually about 85% is transmitted (Reid Crowther and Partners Ltd., 1987).

The HRT

Typical system design residence times are 6 to 10 days. Residence time over 12 days can decrease process efficiency as temperatures drop due to the lack of volatile solids to fuel the aerobic reactions which generate heat (Burnett, 1994).

The Volatile Solids Destruction

Diverse ranges of VS reduction have been reported for full-scale ATAD installations. Jakob et al. (1989) stated that with a minimum HRT of 6 days, an organic reduction between 25 and 35% can be achieved. Jewell and Kabrick (1980) showed that in both batch tests and full-scale continuous feed operation, a VS reduction of about 33% could be achieved using a 6-day SRT. Their experiments also showed that as the VS loading rate decreased, the rate of VS removal decreased. VS reduction has also been reported to vary with the level of oxygen supply. Wolinski (1985) found that the VS reduction increased with the kgO_2 supplied per kg of TS fed.

Aeration and mixing equipments

One of the main factors in ATAD performance is aeration and mixing efficiency. The system must transfer enough oxygen to the bulk liquid to satisfy the metabolic requirements of the thermophilic bacteria without removing too much heat from the system in the form of water-saturated gas.

Regarding aeration, several types of aeration devices have been used successfully to meet the oxygenation and mixing requirements. These include diffused air, mechanical surface aeration, mechanical submerged turbines, draft-tube aeration, jet aeration, and combined systems. For instance, Booth and Tramontini (1983) reported efficiencies as high as 87% with a venture aeration system. Wolinski (1985) measured transfer efficiencies as high as 100%, but his system was insulated by a deep biological foam layer, which also exhibited an oxygen uptake. Trim (1984) reported on the implementation of the patented Vitox oxygen injection (BOC Gases, 1998) system in an autothermal aerobic digester. The Vitox works by injecting oxygen gas into the throat of a venture injector in a pressurised sidestream of the liquor (see **Figure 1.3**).

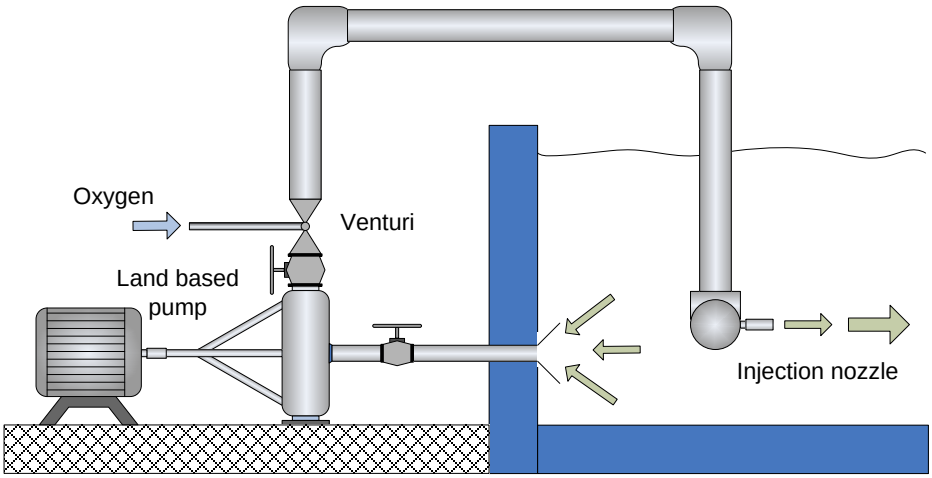

Figure taken from BOC Gases (1998)

Figure 1.3 The Vitox system

Oxygen Transfer Efficiency (OTE) is a good indicator of aeration efficiency, but due to the difficulty in measuring it, design is usually based upon empirical values such as air flows with a given type of aeration system. The EPA manual cites the air flows required for the sufficient aeration of an ATAD system of 4 (m^3 air)/(h·m^3 of active reactor volume), assuming a feed VSS of 2.5 to 5% and a Fuchs aspirating aerator. Kelly (1990) suggests that air flow requirements for ATAD aerators are in the 0.5 to 2.5 air flow-rate/volume of sludge [$m^3 \cdot m^{-3} \cdot h^{-1}$] range, and quotes Wolinski as using 0.25 to 0.5 $m^3 \cdot m^{-3} \cdot h^{-1}$.

Regarding mixing, some energy input is required to mix the biomass and substrate, and to ensure good mass transfer conditions for substrates and gases. Taking advantage of the mixing/aeration effect obtained from the performance of certain devices, modern ATADs another kind of mechanical mixing/aeration systems called recirculation aerators (see **Figure 1.4**). Wolinski (1985), using a venture aeration system with compressed air, found that 17.6% of input heat came from the influent sludge flow, 55.1% came from biological heat production, and 27.3% came from mechanical heat input. Booth and Tramontini

(1983), using a similar system but supplying pure oxygen rather than air, found that 24% of input heat came from the pump, and the rest from reaction heat.

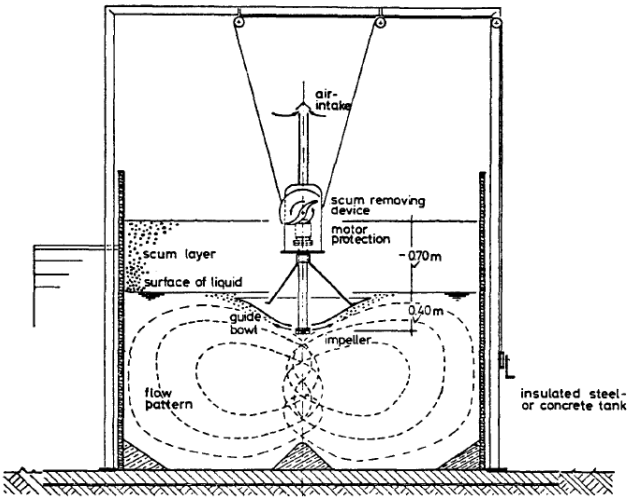

Figure taken from Pöpel and Ohnmacht (1972)

Figure 1.4 Recirculation aerator.

Heat Gain

When bacteria degrade organic molecules into their simpler constituents of carbon dioxide and water, energy which was stored in the bonds between the atoms is released. Some of this energy is used to fuel the inner working of the bacteria and some is used to create more bacteria, but most of the energy is released as heat.

Pöpel and Ohnmacht (1972) found that the total energy produced per gram of organic matter oxidized varied with both sludge type and the type of organism involved. Primary sludge contained 3.033–3.411 $kcal \cdot g^{-1}$ organic solids. Activated sludge ranged between 3.136 $kcal \cdot g^{-1}$ organic solids for high rate sludge, to 3.765 for extended aeration sludge.

Jewell and Kabrick (1980) stated that the oxidization of most organic matter will release 3.5 kcal·(g COD)$^{-1}$ in the substrate. Since 1 kcal of heat will raise the temperature of 1 liter of water by 1 ºC, the resulting approximate temperature change in sludge resulting from COD oxidation would be:

$$\Delta^{o} C = 3.5 \cdot (\Delta\ g\ COD) \qquad (1.1)$$

Loll (1984) later corrected this expression to 3.5–4.0, including heat from mechanical aeration. Therefore, if the COD concentration in waste is high enough and if heat is not lost to the surrounding environment, the temperature of the waste will rise as it is degraded by bacteria. One example of this phenomenon is found in solid waste composting facilities, where temperature in compost piles has been recorded above 70 ºC (Haug, 1993).

Heat Loss

Keohan et al. (1981) reported that there are three sources of heat loss: loss to surroundings by convective radiation, loss through the release of moisture-laden exhaust gas (both through evaporation and loss of sensible heat[1]), and loss through the emptying of digested sludge from the system, of those three, the most important losses are via effluent sludge and off-gas. Wolinski (1985) showed that with his system, 56.9% of the heat loss was from emptying of digested sludge, 41.8% was from convection, and 1.3% was lost through effluent gas. Booth and Tramontini (1983) found that 60.6% was lost in effluent sludge, and 38.3% from convection, with negligible loss from the pure oxygen gas flow. Jewell and Kabrick (1980) using aspirating gas aerators estimated that 60% of the heat lost was due to the emptying of the digested sludge and 40% was lost thorough convection and gas discharge.

[1] "Sensible heat" is defined as the heat that causes a change in temperature in an object. It is different from "Latent heat", defined as the heat that causes a change in the state with no change in temperature.

pH

pH generally does not need special attention, as the thermophilic temperature achieved during digestion suppresses nitrification of the reactor and as a result the pH depression commonly experienced in nitrifying environments does not occur. Typically the pH is above 8.0 when a feed of pH 6.5 is supplied (USEPA, 1990). In this thesis the pH profile is not included for studies.

Foam

A substantial amount of foam is generated in ATAD reactors because cellular proteins, lipids, oil and grease materials break down and are released into the solution. Control of the foam layer is important; however, the exact role of the foam layer has not been completely explained. The foam layer seems to improve oxygen utilization, provides insulation, and enhances biological activity. However, excessive foam inhibits air from entering the digesting sludge mass.

Scisson (2003) claims that ATAD systems inevitably produce foam as a consequence of protein degradation but in order to have an effective system the growth of this foam layer has to be controlled rather than eliminated. Uncontrolled excessive foam can lead to the loss of solids from the reactor. A controlled foam layer is beneficial because it helps to insulate the tanks. Schwinning (1996) suggests that foam contributes to autothermal conditions and also to the overall heat transfer coefficient. Stentiford (2001) reports that most manufacturers use a mechanical foam cutter, which cuts or beats the foam layer and thus limits its growth to typically less than 300-500 mm.

The design and operation of foam cutters are empirical and must consider the surface area of the reactors, the solids concentration of sludge in the reactors, and the type and intensity of aeration.

Odors

Because there is not nitrification and because of the high temperature in the ATAD system, a relatively high concentration of ammonia is released, meaning that the gases emitted by the ATAD can be extremely odorous. Schwinning et al. (1997) state that excessive high operating temperatures, feed management and ineffective odor control contribute to odor problems with ATADs.

Odors can be controlled if proper operating temperatures are achieved and the reactors are adequately mixed and aerated. It is also possible to find odor controlling arrangements that use either gas scrubbers or the combination of scrubbers with compost/soil filters. Odors can also come from the storage of sludge after ATAD treatment, caused mainly by ammonia and hydrogen sulphide.

Oxidation Reduction Potential (ORP)

The ORP is a measurement of the activity of oxidation-reduction reactions in an aqueous environment. ORP in a sewage sludge solution is affected by many parameters, including pH, DO concentration, NOx, and PO4 concentration (Peddie et al., 1988). ORP can also indicate the aerobic state of a solution. Koch et al. (1988) showed that for a Bio-P pilot plant, 50 to 100 mV could be interpreted as aerobic, -75 to -225 mV as anoxic, and -300 to -450 mV as anaerobic. This relationship can be observed in **Figure 1.5**.

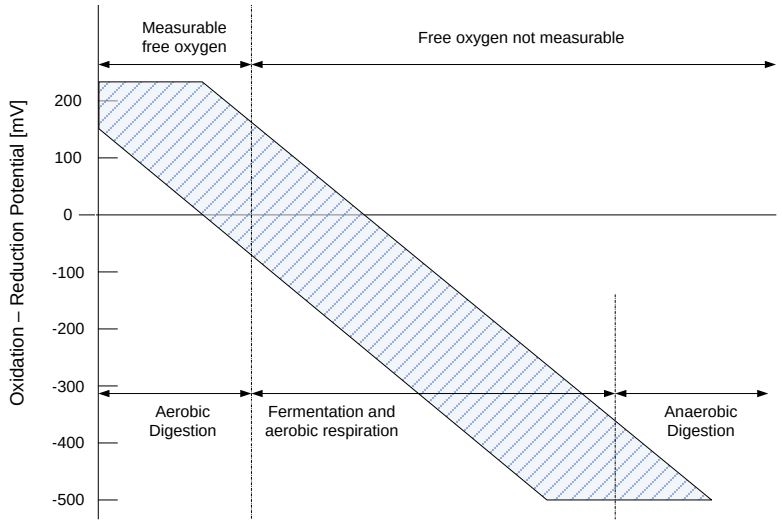

Figure taken from Kelly (1990)

Figure 1.5 Relationship of ORP to Aeration State.

1.2.5. Generations of ATAD

First Generation ATAD

In the 1970's, the first generation of ATAD technology was investigated and high temperatures were produced when pig and volatile wastes were aerated. The initial ATADs developed in this generation were characterized by the following design and operating features (Scisson, 2003):

- Short solid retention time (SRT), generally less than 10 days for the whole series of reactors.
- Aspirating air systems: hollow tube aerators, aspirated pumps or aspirated jet systems.
- Two or three serially operated reactors.
- Mechanical foam cutters protruding through the tank ceiling.
- An invariable air supply and no aeration control.

Over 50 “first generation” ATAD systems have been installed in Europe, and there are over such 20 facilities in the USA. Several of these American facilities have been shut down because of excessive odor generation and other issues.

Due to the serial configuration, the temperature is typically maintained at approximately 45 ºC in the first “preheat” reactor and at approximately 60 ºC in the second and third reactors. A fourth reactor is typically required for cooling and storage to enhance thickening and dewatering performance and supernatant/filtrate quality. Heat is typically extracted from the ATAD biosolids through heat exchangers to heat the incoming “cold” feed solids. Most of the “first generation” ATAD systems are operated in batch, semi-continuous, or continuous mode.

With regard to the foam level, ineffective process control in the “first generation” ATAD systems often let to excessive foam generation and numerous maintenance problems. Mechanical foam cutters are often used to control foam generation.

The biggest issue with these early ATADs was the generation of excessive odors. An ATAD with improper mixing and process control typically produces an odorous off-gas that includes a high concentration of ammonia, amines, and reduced sulphur compounds. Successful odor treatment systems for “first generation” ATAD systems incorporate multiple serial odor treatment technologies, including wet scrubbers, ozone, and three-stage scrubbers.

Second Generation ATAD

In the 1980’s, the second generation of ATADs appeared after a two-year study showed high oxygen transfer efficiencies promoted and maintained thermophilic conditions by aerating sludge with ambient air (Jewell & Kabrick 1980; Deeny et al. 1985; Strauch 1987). The principal advantages of the “second generation” ATADs are as follows (Scisson, 2003):

- Longer SRT (12 to 14 days) compared to the “first generation” ATAD process of 5 to 8 days. This allows for better stability and reduction of volatile solids.
- Jet aeration thoroughly mixes the ATAD process tanks “from the bottom up” and maintains aerobic conditions. The mixing system also uses conventional out-of-basin pumps and compressors with variable-speed drives that are already familiar and accessible to operating and maintenance staff.
- Use of a single reactor with oxidation-reduction potential (ORP) control that matches oxygen supply to variable process demands and provides a more stable and complete digestion process with minimal odor generation.
- A unique and patented foam Splashcone system that recirculates and controls foam with hydraulic energy and has no internal moving parts to maintain.

Several of the ATAD that have been retrofitted with the “second generation” process have reported more than a 60% reduction in biosolids product from the wastewater treatment plant (WWTP) site due to both greater mass destruction and drier cake solids concentration (less water) as compared to conventional aerobic and anaerobic digestion processes.

The ATAD designs mostly differ in the aeration device; the most common types according to Kelly and Warren (1997) are aspirator-mixer aerators, combination recirculation pump/venture arrangements, and turbine and diffused air.

1.3. The Instrumentation issue

The lack of robust and reliable online sensors is still a limitation that has hindered the deployment of monitoring and control tools for these systems. For

example, industrial sensors for dissolved oxygen or suspended solids are manufactured for use in the secondary treatment, where temperatures and solids concentration are not excessive. However, they are not appropriate for withstanding aggressive operational environments such as those in ATADs.

Regarding dissolved oxygen (DO) concentration, Loll (1984) reported that the oxygen meters he used did not have adequate temperature compensation and the electrodes quickly wore out. Booth and Tramontini (1983) reported that a modified “phOx” (tradename) probe correctly recorded DO concentration in a water bath, but readings oscillated when the probe was installed in the ATAD sludge piping.

A few researchers have reported success with Orbisphere probes developed in Switzerland. Jewell and Kabrick (1980) stated that the meter was only used for spot checks, and it was specially developed for high temperatures and high organic content applications. Morgan et al. (1983) also used the meter only for spot checks.

Nowadays, just the ORP and temperature signal sensors fulfill the technical features required for operation. Therefore, any control strategy applied to ATAD technology only has to take these sensors into account.

1.4. Quality assurance and norms

Sludge is rich in nutrients such as nitrogen and phosphorus, and it contains valuable organic matter that is useful when soils are depleted or subjected to erosion. These two elements – nutrients and organic matter – make waste sewage sludge a source of plant nutrients. Accordingly, the use of sewage sludge in agriculture is encouraged. However, the spread of this kind of waste on land as a fertilizer or an organic soil can only be beneficial provided that it is safety recycled. Safe recycling takes into account these two of sludge and tries

to minimize their possible adverse impacts on the environment, making it possible to obtain an agricultural benefit from sludge land application.

Pasteurization

One important factor to be addressed when sludge is used on land is pathogen concentration, due to the effect on human health. The type and number of pathogens that sewage, and therefore sludge, contains can vary not only geographically but also over time at the same site.

There is a lack of consensus on the definition of the pasteurization criteria. The EU recommendation applicable to batch digesters recommends thermophilic aerobic digestion at a temperature of 55 ºC for 20 hours in batch-mode, without admixture or withdrawal during treatment. Fuchs and Fuchs (1991) established the same criteria, but they also reported pasteurization effects when sludge is treated at more than 55 ºC for at least 10 hours. Furthermore, at a temperature between 50 ºC and 70 ºC and an appropriate SRT, disinfection is safely assured. At 50 ºC, one day between two feeding cycles will be enough. With temperatures in excess of 65 ºC, even a time of three hours between two feeding cycles will be sufficient to obtain a complete disinfection.

To meet USEPA guidelines for Class A biosolids for thermophilic sludge of less than 7% total solids, the time required at a given temperature varies according to the equation depicted in **Figure 1.6** (USEPA, 1990; Eyma et al., 1999).

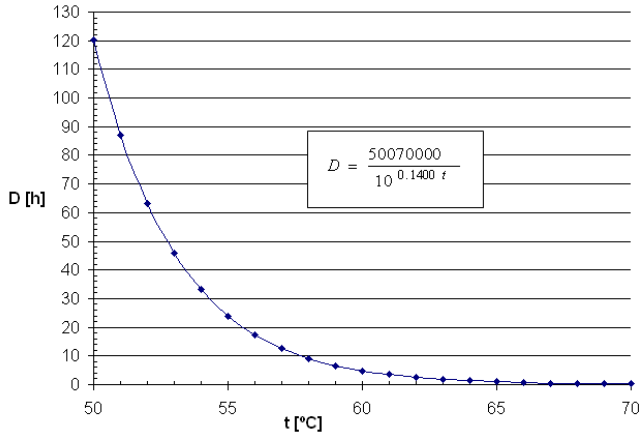

Figure 1.6 Time-temperature requirement to achieve Class A biosolids

D is the time required (in hours) and *t* is the temperature (in ºC). This gives the following time-temperature relationship: 5 days at 50 ºC, 23 hours at 55 ºC or 5 hours at 60 ºC.

Stabilization

Another negative characteristic of raw sludge is that it is malodorous and contains a large amount of organic matter that attracts pest such as flies, mosquitoes and rodents. If the sludge is to be applied to land as a soil additive or fertilizer, this vector attraction characteristic must be minimized.

The definition of sludge stabilization is probably one of the most difficult notions involved in sludge treatment systems (Tsang and Smith, 2005). Vesilind (2001) refers to it as one of the most difficult concepts to define, and sometimes this difficulty has led to inappropriate standards for sludge disposal. Sludge cannot be deposited on land without some pre-treatment because of two constraints: (i) it contains chemicals and microbes that can be a health hazard to people; and (ii) it often smells bad.

These two constraints are imperceptible because there is not a single measure of sludge stability. What is needed are specific criteria and standards for the end use of sludge (taking into account whether the sludge will be used as fertilizer, whether the farm is close to the people who would be offended by odors, whether the plants grown on the farm are for human consumption, etc.).

A review of existing policies and guidelines for sludge management in different countries shows the diversity of criteria used to specify requirements for sludge stabilization. Indeed, such requirements are strongly conditioned by the type of treatment used for digestion. For instance, as far as aerobic digestion is concerned, the American Regulation 40 CFR Part 503 (USEPA, 1993) established three options for complying with the vector attraction reduction requirements (i.e., sludge stabilization):

- Option 1: A reduction of at least 38% in volatile solids during sewage.
- Option 2: A reduction of less than 15% of additional volatile solids during bench-scale aerobic batch digestion for 30 additional days at 20 ºC.
- Option 3: A Specific Oxygen Uptake Rate (SOUR) of less than 1.5 mg O_2/h/(g total sewage sludge solids) at 20 ºC.

Option 3 is only applicable to mesophilic aerobic digesters; Option 2 is only valid for aerobically digested sewage sludge with 2% or less solids. Unlike Options 2 and 3, Option 1 is not restricted to any specific treatment technology; however, this option has certain limitations since it is not completely appropriate for treatments where the incoming sludge has been partially pre-stabilized (for example, sewage sludge from secondary treatments operated at medium/large SRT). In these situations, Option 2 should be used instead.

Therefore, a common consensus for evaluating requirements for pasteurization and stabilization in the ATAD technology is necessary; as it will allows the process's performance to be improved and the sludge reuse to be available.

1.5. State-of-the-art in mathematical models of ATADs

The ATAD is part of a type of thermal process where the temperature profile gives important information about the process behavior. Thus, one of the most important aspects of ATAD modeling relies on good thermodynamic modeling. Additionally, the most important parameters to consider in the modeling are: (i) the concentration of sludge supplied, and (ii) the system aeration applied.

Using a mathematical model, Kambhu and Andrews (1969) demonstrated that bio-heating (or auto-heating) of organic waste was theoretically possible. The model showed that by supplying sufficient substrate to a microbial population and minimizing heat loss to the surrounding environment, thermophilic temperatures could be reached. In the project summary of Keohan et al. (1981) a description of the components involved in heat entering and leaving an aerobic digester is given (see **Figure 1.7**).

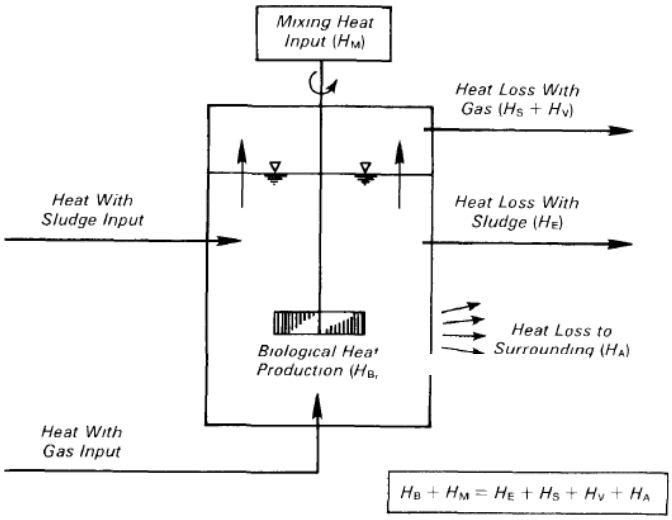

Figure taken from Keohan et al. (1981)

Figure 1.7 Heat Balance in the ATAD.

The following factors must be considered in the heat inputs:

- Biological heat generation by aerobic organisms.
- Energy required to mix the sludge.
- Influent sludge mass.

As explained previously, the biological heat generated depends of the type of solids being oxidized, the type of organisms present, and the concentration of biomass available for oxidation. Temperature affects the rate at which the reactions progress, and therefore the rate at which more heat is generated. The SRT determines how much of the organic solids are oxidized, as well as the rate of oxidation as the availability of the food for the microorganisms decreases with time.

Previous works on the dynamic prediction of temperatures in biological tanks have been assessed. In Vismara (1985) and Messenger et al. (1990), the basis of the heat balance model were beginning to be established. The modeling of dynamic temperature changes in tanks have been also successfully modeled by Sedory and Stenstrom (1995) and Scherfig et al. (1996). These models incorporate the different gains/losses over the basins. They require, however, a large amount of input data (i.e., operational and meteorological conditions), which are not always easy to collect, especially at the design stage of the plant.

In recent years, there have been significant advances in the dynamic modeling of ATAD systems. Kovacs et al. (2007) propose several adaptations of the standard Activated Sludge Model Nº 1 (ASM1), which is aimed at incorporating thermophilic bacteria and their respective biochemical transformations. The ASM1 model allows the system to consider the utilization of biomass as a substrate, which is especially suitable for describing the thermophilic aerobic digestion system. For other models, such as ASM3, however, the death-regeneration concept is not considered. Also, ASM1 is one of the simplest models that allows modifications.

Gomez et al. (2007a) and Gomez (2007b) bring together existing formulations on biochemical reactions, physico-chemical transformations and thermal energy balances, in order to develop a comprehensive model for the ATAD that includes dynamic prediction of liquid and gas compounds as well as temperature.

A further step in any mathematical model of processes is the use of models for control studies. Therefore, it is necessary to adapt the model in order to respond to manipulated variable actions.

In the ATAD as a case study, it is necessary to adapt ATAD mathematical models in order to have dependence with respect to the variables manipulated such as the amount of influent and/or effluent sludge and the air flow-rate injected. Regarding the air flow-rate, its variation during the process has a significant effect in terms of biological heat generation, gas convection and evaporation. Therefore, for control objectives, an adaptation of the thermo-dynamical terms of this model is required.

1.6. Control approaches in ATAD

Automatic control in ATAD technologies is limited to the use of very simple strategies for aeration. Breider and Drnevich (1981) probably hold the first patent based on a real-time air control of ATAD by means of the sludge temperature observation, seeking to keep the sludge temperature in a certain range. Trim (1984) reported an oxygen input control in an autothermal aerobic digester, via the dissolved oxygen measurement.

Aeration in all aerobic biological systems is one of the most important considerations, since it affects both the quality of the effluent and the total operational costs. The ATAD system is not an exception; here the influence of aeration is even more marked. Over-aeration increases costs without leading to a significantly better quality of treated sludge. Moreover, in the case of air-

based aerating systems, over-aeration involves a cooling effect on the slurry with the subsequent risk of not reaching pasteurization temperatures (Cheng and Zhu, 2008). On the other hand, under-aeration limits efficiency for stabilization and heat generation. Also, under-aeration promotes anaerobic conditions, which can increase the potential for undesired odors in the outlet off-gas (Staton et al., 2001).

The first-generation ATADs didn't consider any air regulation; it was only in the second-generation ATADs that automatically manipulated air was considered (Scisson, 2003), where the ORP signal is used to control the oxygen supply to match the demand during digestion time. This is reported to ensure aerobic conditions in the reactor, limiting odors and improving the destruction of volatile solids.

After an extensive evaluation of ATAD performance in Ireland and other ATAD facilities in Europe and North America, Layden (2007) reported that optimizing the aeration rate, with better control of spiral aerators, would enhance process control, but further research is needed to improve the current understanding of airflow, oxygen transfer efficiency, and oxygen utilization in the ATAD process.

Results from Wareham et al. (1994) show a sludge digestion control using the ORP signal. The research was carried out in two lab-scale digesters working in an aerobic-anoxic fashion. The approach is based on controlling the total length of the cycle upon the distinctive "nitrate breakpoint" occurring in the ORP-time profile. Studies from Staton et al. (2001) showed that with appropriate ORP signal processing the depletion of biodegradable organic substrate can be detected, and from this behavior it would be possible to apply control strategies for external aeration.

Recently, Kim and Oh (2009) proposed an aeration control for Thermophilic Aerobic Digesters (TAD) using fluorescence monitoring of biological compounds as an indicator of the physiological activity of the living thermophilic microorganisms obtaining good results in terms of stability, maintenance and response time. Giffin (2009) reported a control for a

continuous ATAD process in full-scale, where the temperature was controlled by keeping the solid content of the feed as high as possible, generally between 4-6% solids, and supplying sufficient oxygen. Due to undersized aerators being installed, aeration was supplemented with pure oxygen. This was supplied in liquid form and stored on site in a cryogenic pressure vessel.

Nevertheless, the lack of appropriate, robust and reliable sensors for aggressive environments (those with high temperatures and solid concentration) like in ATAD is still a limitation. Today, industrial sensors for dissolved oxygen or suspended solids are manufactured for use in secondary treatment where temperature and solids concentrations are not excessive. Nowadays, just ORP and sludge temperature sensors can satisfy the technical requirements for ATAD conditions.

Sludge temperature can give important information about the digestion status of the ATAD. The applicability of industrial sensors and recent approaches in ATAD modeling makes it possible to study and verify new control strategies for this process.

2

Objectives

Chapter 2 Objectives

2.1. Research questions

The general objective of this thesis is to design and validate new control strategies in an Autothermal Thermophilic Aerobic Digester (ATAD). The control strategies seek to improve the pasteurization and stabilization effects in the final product. Therefore, the strategies proposed will try to keep the process stability, and be robust against disturbances.

Considering previous methodology used for the design and validation of control strategies in activated sludge processes, the general objective of this thesis includes the achieving of these partial objectives:

- To demonstrate the possibility of adapting existing mathematical model for ATAD in order to carry out control studies in this process.
- To propose new control strategies applied to the ATAD technology that can be implemented in industrial scenarios.
- To establish a benchmark or simulation protocol in order to validate any control strategy applied to the ATAD technology.
- To be able of quantifying the performance of the control strategies proposed.
- To propose a methodology for tuning control strategy algorithms based on trend analysis.

2.2. Research planning

Every chapter of this study will try to give solutions to the research questions. A brief summary of the Chapters is described below:

In **Chapter 1** the principal characteristics of the ATAD technology have been introduced, describing the process fundamental, the operational conditions, the benefits and the necessity to improve the process operation by means of control strategies. As part of the state-of-the-art, a scope concerning the instrumentation, the mathematical modeling and the control approaches was introduced.

This chapter describes the objectives considered in the thesis, and the research planning taken for the problems.

In **Chapter 3** the mathematical model used in this thesis is described. A brief scope of the biological phenomena is shown, describing the variables, the biochemical and physico-chemical transformations.

The **Chapter 4** describes the different control strategies proposed. Starting from the control problem definition and the specifications and requirements to accomplish, some control strategies (alone or combined) will cover partially or totally the involved specifications.

In **Chapter 5**, a benchmarking for the validation of control strategies is described. The benchmark definition includes the sludge influent characteristics, the plan-layout configuration, the mathematical model, the performance indices, and the simulation protocol.

In **Chapter 6**, in agreement with some control strategies proposed in **Chapter 4**, a methodology for tuning bending-point based detection algorithms for biological processes is proposed. The ATAD technology is selected as a case study.

Chapter 7 shows the results obtained when the different control strategies are applied following the benchmark protocol proposed in **Chapter 5**. Moreover, in

this chapter, in order to complete the simulation study, an uncertainty consideration in the mathematical model is considered; with the purpose of evaluate the controller's sensitivity as well as the performance for different operational conditions. Furthermore, preliminary experimental results are also presented.

Chapter 8 gives some general conclusions about the results. Directions for future research and perspectives are also briefly discussed.

3

The mathematical model

Chapter 3 The mathematical model

In this chapter, the mathematical model implemented to describe the adopted plant configuration is presented. The plant configuration is formed by a pre-holding tank (HT) followed by an autothermal thermophilic aerobic digester (ATAD).

In order to be able of predicting the temporal evolution of the mass and temperature components in the system, the mathematical model includes biochemical and physico-chemical transformations, the mass/energy transport model is associated to the influent/effluent mass flows, and the heat fluxes.

The chapter is organized as follows: previous considerations and the notation employed are presented in **Section 3.1**. A description of the global model, considering mass and energy balances in the HT and ATAD are given in **Section 3.2**. The description of the transport phenomena is given in **Section 3.3**. At last, the model of biochemical and physico-chemical transformations is provided in **Section 3.4**.

3.1. Introduction

The mathematical model employed for every unit process (pre-holding tank and ATAD) follows a state variables structure. Considering mass and energy balances in every tank, a set of ordinary differential equations is obtained, and the temporal evolution of the states (masses and enthalpies) in the liquid and gaseous phase is obtained.

The energy balance applied in every unit process allows describing the temporal evolution of the temperature, considering the following effects: (i) temperature related to the influent and effluent mass flows; (ii) gaining heat from the mixing equipments and, (iii) heat fluxes due to the superficial convection and to the conduction/convection effect trough the walls.

3.1.1. Previous considerations

The mass flows (Q) and heat fluxes (HF) are depicted in **Figure 3.1(a)** and **3.1(b)** respectively.

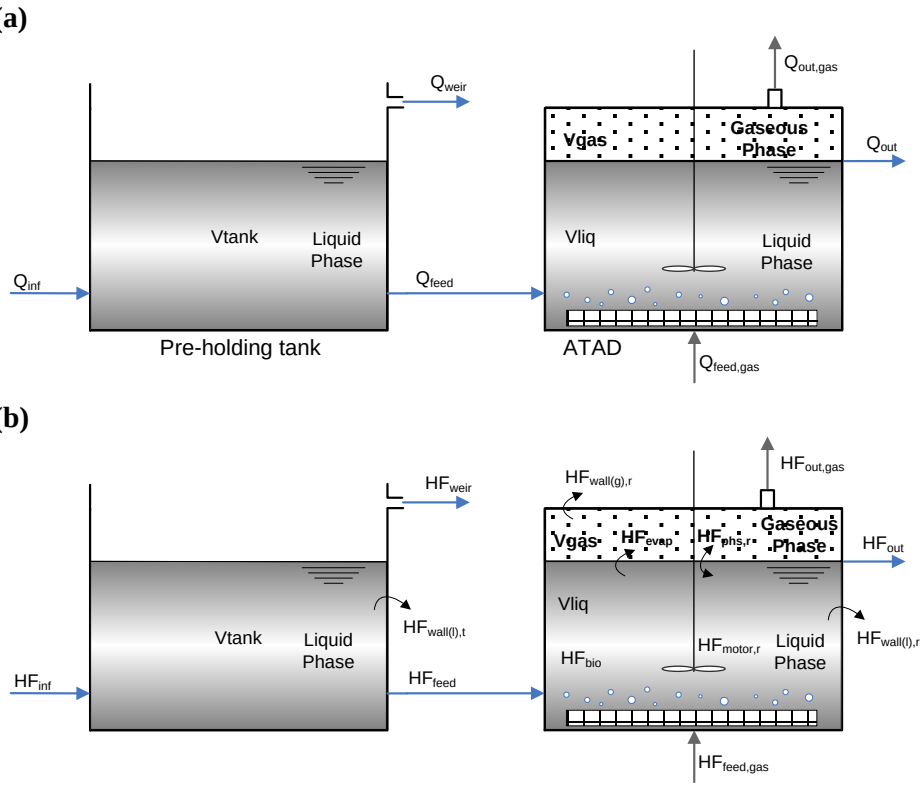

Figure 3.1 Plant representation. **(a)** Mass flows. **(b)** Heat fluxes

Regarding the HT, the following assumptions were adopted:

- The HT is modeled as a variable volume (V_{tank}) and completely stirred tank, biological and physico-chemical reactions were no considered.
- An open tank and a uniform section.
- There are two types of outlets in the tank: pump-type (Q_{in}) for normal operation, and weir-type (Q_{weir}) for abnormal situations.

Concerning the ATAD, this reactor was modeled under the following hypothesis:

- Two variables and perfect mixed volumes or phases were considered: sludge or liquid phase (V_{liq}) and gaseous volume (V_{gas}).
- A uniform section is assumed. Despite V_{liq} and V_{gas} are variable volumes, the total digester volume (V_{ATAD}) is constant, therefore:

$$V_{liq}+V_{gas} = V_{ATAD} \tag{3.1}$$

- The ATAD has two outlets: one for the treated sludge (Q_{out}) and one for the off-gas ($Q_{gas,out}$).
- The influent and effluent of the liquid phase are controlled by two independent pumps: Q_{feed} and Q_{out}.

The notation employed in the plant representation is listed in **Table 3.1**. This notation is used throughout this chapter.

Table 3.1 Notation employed in the plant representation

Type	Symbol	Description	Unit
Volume	V_{HT}	Volume of water in the HT	m^3
	V_{liq}	Liquid phase volume in ATAD	
	V_{gas}	Gaseous phase volume in ATAD	
Flow rate	Q_{inf}	Sludge influent to the HT	$m^3 \cdot d^{-1}$
	Q_{weir}	Sludge effluent from the HT due to overflow	
	Q_{feed}	Sludge influent to the ATAD	
	Q_{out}	Sludge effluent from the ATAD	
	$Q_{feed,gas}$	Influent gas to the ATAD	
	$Q_{out,gas}$	Off-gas from the ATAD	
Heat flux	HF_{inf}	Heat input due to influent sludge to the HT	$kJ \cdot d^{-1}$
	HF_{feed}	Heat loss with sludge from the HT due to pumping	
	HF_{weir}	Heat loss with sludge from the HT due to overflowing	
	HF_{out}	Heat loss with effluent sludge from the ATAD	
	$HF_{feed,gas}$	Heat input due to gas injected to the ATAD	
	$HF_{out,gas}$	Heat loss by the off-gas from the ATAD	
	$HF_{walls,t}$	Heat loss by conduct./convect. through walls in liq. phase in HT	
	$HF_{walls(l),r}$	Heat loss by conduct./convect. through walls in liq. phase in ATAD	
	$HF_{walls(g),r}$	Heat loss by conduct./convect. through walls in gas. phase in ATAD	
	$HF_{motor,r}$	Heat input due to mixing equipments in ATAD	
	$HF_{phs,r}$	Heat exchange between liquid and gaseous phases in ATAD	
	HF_{bio}	Heat gain by biological activity	
	HF_{evap}	Heat loss by water evaporation	

3.1.2. State variables of the model

The state variables model definition is determined by the set of transformation equations employed to describe the aerobic digestion. The mass components

considered in the model are described below; the transformations will be described in the next section.

A list of generic mass components involved in the liquid and gaseous phase is shown in **Table 3.2**. The liquid phase includes soluble and particulate states. The gaseous phase includes all the gaseous forms of those dissolved states that suffer a phase transformation from liquid to gas.

Table 3.2 Components of the model

Component	Symbol	Description
Liquid phase	Sh2o	Water
	Ss	Readily biodegradable substrate
	Si	Soluble inert organic matter
	So2	Dissolved oxygen
	Shco3	Bicarbonate
	Sco2	Carbon dioxide
	Sn2	Nitrogen
	Snh4	Ammonium
	Snh3	Ammonia
	Sh	Ion of hydrogen
	Soh	Ion of hydroxyl
	Sh2po4	De-hydrogen phosphate
	Shpo4	Hydrogen phosphate
	Xs	Slowly biodegradable substrate
	Xr	Readily solubilizable substrate
	Xbh	Active heterotrophic biomass
	Xi	Particulate inert organic matter
	Xinor	Inorganic matter
Gaseous phase	Gh2o	Vapor of water
	Gco2	Carbon dioxide gas
	Go2	Oxygen gas
	Gn2	Nitrogen gas

From the model components, the states vector can be obtained. This vector also includes the enthalpy components, and is depicted in **Table 3.3**.

Table 3.3 State vector

State	Phase	Description	Pos. (i)	Symbol	Unit
Mass $\overline{M}$	Liquid $\overline{ML}$	Water	1	MS_{H2O}	kg H_2O
		Soluble organic	2	MSs	kg COD
			3	MSi	kg COD
		Soluble Inorganic	4	MSo2	kg O_2
			5	MShco3	kg C
			6	MSco2	kg C
			7	MSn2	kg N
			8	MSnh4	kg N
			9	MSnh3	kg N
			10	MSh	kg H
			11	MSoh	kg H
			12	MSh2po4	kg P
			13	MShpo4	kg P
		Particulate organic	14	MXr	kg COD
			15	MXs	kg COD
			16	MXbh	kg COD
			17	MXi	kg COD
		Particulate inorganic	18	MXinor	kg
	Gaseous $\overline{MG}$		19	MGh2o	kg H_2O
			20	MGco2	kg C
			21	MGo2	kg O
			22	MGn2	kg N
Enthalpy $\overline{H}$	Liquid		23	H_{liq}	kJ
	Gaseous		24	H_{gas}	kJ

The state vector consists in a total of 24 states, this vector contains a sub-vector $\overline{M}$ of 22 mass states [1 to 22] and a sub-vector $\overline{H}$ of 2 enthalpies [23 and 24]. Regarding the sub-vector $\overline{M}$, 18 states correspond to the liquid phase $\overline{ML}$ [1 to 18] and 4 correspond to the gaseous phase $\overline{MG}$ [19 to 22].

Some lumped variables can be defined from the state variables of the model; this allows linking the model components with analytical measurements. These variables are defined as follows:

bCOD: biodegradable Chemical Oxygen Demand [kg COD·m^{-3}]

VS: Volatile Solids [kg·m^{-3}]

TSS: Total Suspended Solids [kg·m^{-3}]

According to the components model described in **Table 3.2**, the above variables can be expressed as follows:

$$bCOD = Ss + Xs + Xr + Xbh \tag{3.2}$$

$$VS = \begin{pmatrix} Ss\cdot\gamma_{TOD,Ss}^{-1} + Si\cdot\gamma_{TOD,Si}^{-1} + Xs\cdot\gamma_{TOD,Xs}^{-1} + \\ Xr\cdot\gamma_{TOD,Xr}^{-1} + Xbh\cdot\gamma_{TOD,Xbh}^{-1} + Xi\cdot\gamma_{TOD,Xi}^{-1} \end{pmatrix} \tag{3.3}$$

$$TSS = Xs\cdot\gamma_{TOD,Xs}^{-1} + Xr\cdot\gamma_{TOD,Xr}^{-1} + Xbh\cdot\gamma_{TOD,Xbh}^{-1} + Xi\cdot\gamma_{TOD,Xi}^{-1} + X_{inor} \tag{3.4}$$

Where $\gamma_{TOD,i}$ is defined as the amount of required oxygen to oxidize the elements that conform an organic or inorganic compound into its reference compounds (Gujer et al., 1999). These lumped variables will be considered in

Chapter 5, as part of the evaluation criteria defined for the ATAD process benchmarking.

3.2. Global model

3.2.1. Mass and energy balance in the pre-holding tank

The temporal evolution of the mass states in the pre-holding tank is a consequence of hydraulic effects. It can be expressed as follows:

$$\left(\frac{d\overline{M}_{HT}}{dt}\right)_{global} = \left(\frac{d\overline{M}_{HT}}{dt}\right)_{transport} \tag{3.5}$$

As depicted in **Figure 3.1**, the temporal evolution of the enthalpy in the pre-holding tank is obtained considering thermal effects associated to the liquid and gaseous mass transport, to the convection trough the free surface (transference between phases) and to the walls conduction, expressed as follows:

$$\left(\frac{d\overline{H}_{HT}}{dt}\right)_{global} = \left(\frac{d\overline{H}_{HT}}{dt}\right)_{transport} - HF_{phs,HT} - HF_{walls,HT} \tag{3.6}$$

3.2.2. Mass and energy balance in the ATAD

Concerning the ATAD reactor, the temporal evolution of mass states is expressed as the sum of the mass transport terms and of bio-chemical and physico-chemical transformations, expressed as follows:

$$\left(\frac{d\overline{M}_{ATAD}}{dt}\right)_{global} = \left(\frac{d\overline{M}_{ATAD}}{dt}\right)_{transport} + \left(\frac{d\overline{M}_{ATAD}}{dt}\right)_{transf} \tag{3.7}$$

The temporal evolution of the enthalpy in the ATAD is obtained considering thermal effects associated to the mass transport, to the enthalpy variation given by the bio-chemical and physico-chemical transformations, and to a set of thermal gain and losses terms. Hence, for the liquid phase this set of terms includes the mixing equipment, the conduction-convection effect trough walls and the transference between phases. For the gaseous phase, this set of terms includes the conduction-convection effect trough walls and the transference between phases. It can be expressed as follows:

$$\left(\frac{dH_{ATAD}}{dt}\right)_{global} = \left(\frac{dH_{ATAD}}{dt}\right)_{transport} + \left(\frac{dH_{ATAD}}{dt}\right)_{transf} + \begin{Bmatrix} HF_{motor,ATAD} - HF_{walls(l),ATAD} \\ - HF_{phs,ATAD} - HF_{walls(g),ATAD} \\ + HF_{phs,ATAD} \end{Bmatrix} \tag{3.8}$$

The next section shows an overview of the transport and transformation equations for every tank in the plant. For more details, see **Annex A**.

3.3. Model equations of transport phenomena

In this section the mass and energy balance applied to the pre-holding tank and ATAD is presented, in order to describe the temporal variation in the mass and the enthalpy due exclusively to hydraulic effects.

Some auxiliary variables are introduced in this section to facilitate the model description:

- The liquid phase volume is calculated considering just the mass of water and its density:

$$V_{liq} = \frac{MS_{H2O}}{\delta_{H2O}} \tag{3.9}$$

- The concentration of components in every phase is calculated as the ratio between the mass and the volume in the phase where the component is defined:

$$L_i = \frac{ML_i}{V_{liq}} \quad i \in [1,18] \quad ; \qquad G_i = \frac{MG_i}{V_{gas}} \quad i \in [19,22] \tag{3.10}$$

Where L_i [kg·m^{-3}] and G_i [kg·m^{-3}] are the concentrations in the liquid and gaseous phase respectively.

- The thermal fluxes associated to the mass transport are directly linked with the in/out mass flux temperature. Regarding the liquid flows, a generic heat flux (*HF*) is obtained considering the calorific capacity of the water, as follows:

$$HF = Q \cdot \delta_{H_2O} \cdot c_{p,H_2O} \cdot T \tag{3.11}$$

Where T [ºC] represents the flow mass temperature, Q [m^3·d^{-1}] is the flow-rate and $c_{p,H2O}$ [kJ·kg^{-1}·ºC^{-1}] is the calorific capacity of the water. This expression is applied to the influent and effluent heat fluxes (HF_{inf}, HF_{feed}, HF_{weir}, HF_{out}) depicted in **Figure 3.1**.

Regarding the gaseous heat flows in the ATAD, these values are obtained considering the calorific capacity $c_{p,i}$ [kJ·kg^{-1}·ºC^{-1}] of every compound in the influent and effluent gas, as follows:

$$HF_{feed,gas} = Q_{feed,gas} \cdot T_{feed,gas} \cdot \sum_{i=19}^{22} G_{i(\,feed\,),ATAD} \cdot c_{p,i} \tag{3.12}$$

$$HF_{out,gas} = Q_{out,gas} \cdot T_{gas,ATAD} \cdot \sum_{i=19}^{22} G_{i,ATAD} \cdot c_{p,i} \tag{3.13}$$

- The enthalpy in the liquid and gaseous phase is directly related to the enthalpy of the volume associated. Therefore, regarding the liquid phase, the liquid temperature can be obtained as follows:

$$T_{liq} = \frac{H_{liq}}{M_{H_2O} \cdot c_{p,H_2O}} \tag{3.14}$$

Concerning the gaseous phase, the gaseous temperature can be obtained considering the gaseous enthalpy and the calorific capacity of every compound in the total gas:

$$T_{gas} = \frac{H_{gas}}{V_{gas} \cdot \sum_{i=19}^{22} G_{i,ATAD} \cdot c_{p,i}} \tag{3.15}$$

3.3.1. Transport sub-model in the pre-holding tank

The mass flows and heat fluxes in the HT are depicted in **Figure 3.2**.

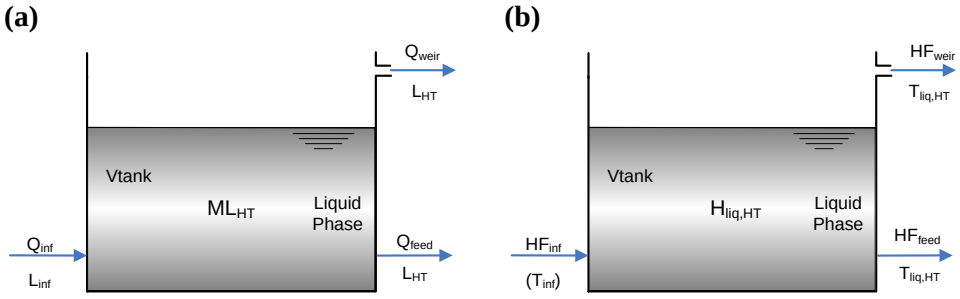

Figure 3.2 Flows representation in the HT. **(a)** Mass flows; **(b)** Heat fluxes.

From theses figures, the temporal evolution of the mass and enthalpy components by hydraulic effects can be obtained after applying the following balance equations:

$$\left(\frac{dM_{h2o,HT}}{dt}\right) = \delta_{H2O} \cdot \left(Q_{\inf} - Q_{feed} - Q_{weir}\right) \tag{3.16}$$

$$\left(\frac{d\overline{ML}_{HT}}{dt}\right) = \overline{L}_{\inf,HT} \cdot Q_{\inf} - \overline{L}_{HT} \cdot \left(Q_{feed} + Q_{weir}\right) \tag{3.17}$$

$$\left(\frac{dH_{liq,HT}}{dt}\right) = HF_{\inf} - HF_{feed} - HF_{weir} \tag{3.18}$$

The equation (3.16) describes the temporal evolution of the mass of water, the equation (3.17) describes the temporal evolution of the components in liquid

phase, and the equation (3.18) describes the enthalpy variation in the liquid phase considering the heat fluxes associated to the influent and effluent mass flows.

3.3.2. Transport sub-model in the ATAD

The mass and calorific flows in the ATAD are depicted in **Figure 3.3**.

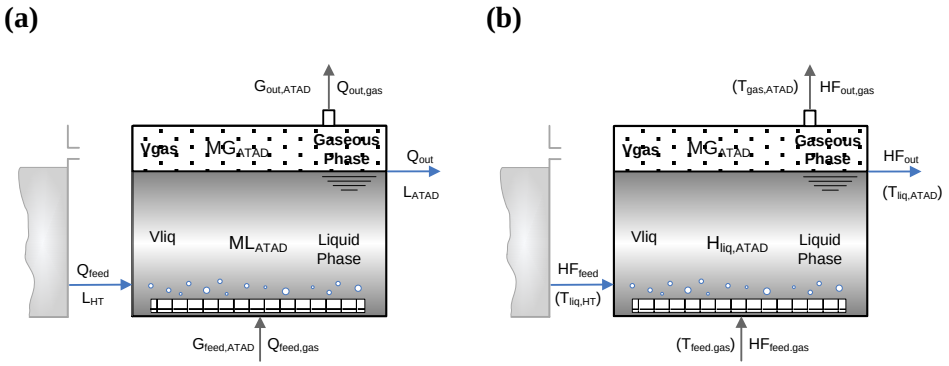

Figure 3.3 Flows representation in the ATAD. **(a)** Mass flows; **(b)** Heat fluxes.

As it was detailed in the HT, for the ATAD reactor the temporal evolution of the mass and enthalpy components in the liquid phase by hydraulic effects can be also obtained after applying the following balance equations:

$$\left(\frac{dM_{h2o,ATAD}}{dt}\right)_{transport} = \delta_{H2O}\cdot\left(Q_{feed} - Q_{out}\right) \tag{3.19}$$

$$\left(\frac{d\overline{ML}_{ATAD}}{dt}\right)_{transport} = \overline{L}_{HT}\cdot Q_{feed} - \overline{L}_{ATAD}\cdot Q_{out} \tag{3.20}$$

$$\left(\frac{dH_{liq,ATAD}}{dt}\right)_{transport} = HF_{feed} - HF_{out} \tag{3.21}$$

The equation (3.19) describes the temporal evolution of the mass of water, the equation (3.20) describes the temporal evolution of the mass states, and the equation (3.21) describes the enthalpy variation in the liquid phase considering the heat fluxes associated to the influent and effluent mass flows.

In the same way, the temporal evolution of the mass and enthalpy components in the gaseous phase can be obtained after applying the following balance equations:

$$\left(\frac{d\overline{MG}_{ATAD}}{dt}\right)_{transport} = \overline{G}_{feed,ATAD} \cdot Q_{feed,gas} - \overline{G}_{ATAD} \cdot Q_{out,gas} \tag{3.22}$$

$$\left(\frac{dH_{gas,ATAD}}{dt}\right)_{transport} = HF_{feed,gas} - HF_{out,gas} \tag{3.23}$$

The equation (3.22) describes the temporal evolution of the gaseous components, and the equation (3.23) describes the enthalpy variation in the gaseous phase considering the heat fluxes associated to the influent and effluent mass flows.

3.4. Model of biochemical and physico-chemical transformations

In this section, the model used to describe the temporal evolution of the states in the unitary processes due to biochemical and physico-chemical transformations is presented. Since there are not biochemical reactions in the pre-holding tank, this model is only applied to the ATAD reactor.

The model stoichiometry is presented in the matrix format suggested by (Petersen, 1965). The matrix representation allows rapid and easy recognition of the fate of each component. In the matrix, the rows are associated to bio-chemical and physico-chemical transformations; the columns are associated to a model component.

The kinetic expressions for every individual transformation j is denoted as ρ_j [kg·m^{-3}·d^{-1}], therefore the vector $\overline{\rho} = \{\rho_1, \rho_2, ..., \rho_m\}^T$ represents the set of all the kinetic equations of the model. The elements of the stoichiometric matrix are called stoichiometric coefficients (v_{ij}) and represent the mass relationship between the different components within every individual reaction. Therefore, a variation in the mass of component i due to the transformation j is obtained by multiplying its stoichiometric coefficient (v_{ij}) by the correspondent kinetic equation ρ_j.

In this way, by moving down a column for a specific component, the full differential equation with all the biological process may immediately be formulated, giving the temporal evolution of this component.

The stoichiometric matrix of the mathematical model includes the mass relationships between components and transformations either in liquid or gaseous phase.

3.4.1. Description of transformations

In this mathematical modeling only those reactions that can describe the aerobic digestion, the chemical equilibriums and the mass transformation between phases are considered.

In the next section, the set of transformations considered in the liquid and gaseous phase will be presented. Details of the equations and the stoichiometry, kinetics and physico-chemical parameters are included in **Annex A**.

3.4.1.1. Liquid phase transformations

The transformations presented in the liquid phase are presented below.

3.4.1.1.1. Biochemical transformations

The biochemical transformations of the implemented model are summarized in **Table 3.4** and represented in **Figure 3.4**, involving from the substrate solubilization until the lysis step.

Table 3.4 Biochemical transformations

Transformation	Description
Thermal solubilization	Solubilization of Xr
Hydrolysis	Hydrolysis of Xs
Aerobic degradation	Degradation of Ss
Lysis	Lysis of Xbh

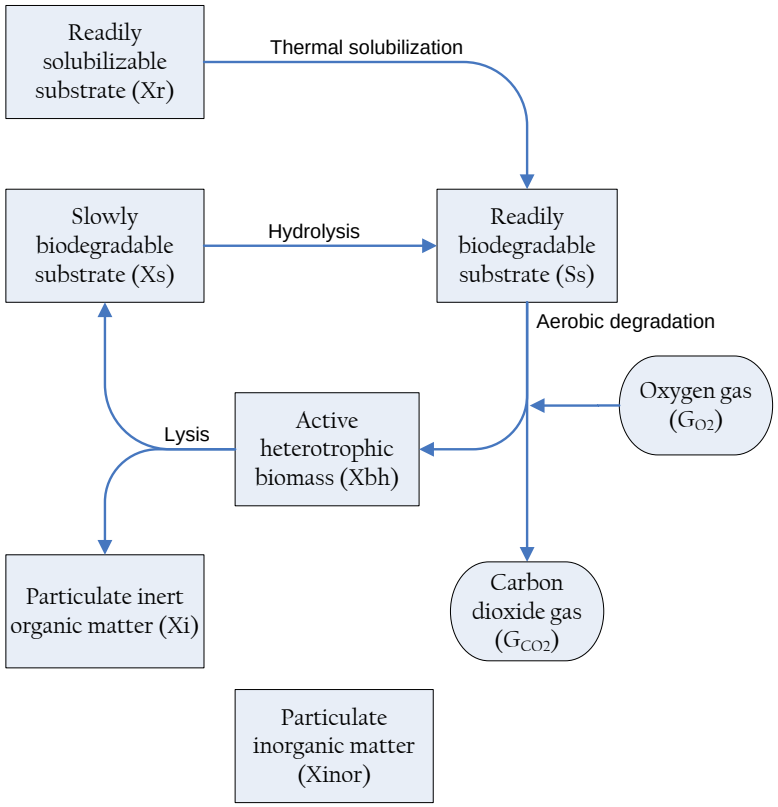

Figure 3.4 Biochemical transformation of the aerobic digestion model

Thermal solubilization

This extracellular reaction represents the fast solubilization of one portion (Xr) of the raw sludge due to the thermal shock effect when it is introduced in the digester. The product obtained is a readily biodegradable substrate (Ss).

Hydrolysis

This extracellular reaction represents the slowly solubilization of the other part (Xs) of the raw sludge. This disintegration also contributes to produce readily biodegradable substrate (Ss).

Aerobic degradation

In this reaction the degradation of the readily biodegradable substrate (Ss), due to the thermal solubilization and the hydrolysis, is produced by the heterotrophic bacteria (Xbh). As an aerobic reaction, it requires the presence of the dissolved oxygen to facilitate the transformation.

Lysis

This reaction represents the bacteria decay by effects of endogenous respiration and cellular death. It is considered that part of the lysis of Xbh produces particulate inert organic matter (Xi) and part produces slowly biodegradable substrate (Xs).

3.4.1.1.2. Chemical equilibriums

These transformations correspond to the chemical equilibrium between different components of the model; this includes equilibrium between inorganic compounds and the equilibrium of water. The chemical equilibriums are depicted in **Table 3.5**.

Table 3.5 Chemical equilibrium

Transformation	Description
Inorganic compounds	Equilibrium of carbon
	Equilibrium of nitrogen
	Equilibrium of phosphorus
Water	Equilibrium of water

3.4.1.2. Transformations involving liquid and gaseous phase

These transformations correspond to physico-chemical reactions that involve the interaction between the liquid and gaseous phases. This includes gas dissolution to the liquid phase of all gaseous compounds considered in the model (CO_2, O_2 and N_2) in the gaseous phase; the water evaporation-condensation is also included in this group of transformations. Theses transformations are listed in **Table 3.6**.

Table 3.6 Physico-chemical transformations

Transformation	Description
Dissolution	CO_2 dissolution
	O_2 dissolution
	N_2 dissolution
Evaporation-condensation	H_2O evaporation

3.4.2. Kinetics vector

The previous transformations are included in a kinetics vector $\overline{\rho}$, this vector contains a total of 12 individual processes where different components of the model are involved. The kinetics vector of the model is detailed in **Table 3.7**.

Table 3.7 Kinetics vector of the model

Type	Transformation	Description	Pos. (j)
Biochemical	Thermal solubilization	Solubilization of Xr	1
	Hydrolysis	Hydrolysis of Xs	2
	Aerobic degradation	Degradation of Ss	3
	Lysis	Lysis of Xbh	4
Chemical	Inorganic compounds	Equilibrium of carbon	5
		Equilibrium of nitrogen	6
		Equilibrium of phosphorus	7
	Water	Equilibrium of water	8
Physico-chemical	Dissolution	CO_2 dissolution	9
		O_2 dissolution	10
		N_2 dissolution	11
	Evaporation-condensation	H_2O evaporation	12

3.4.3. Sub-model of bio-chemical and physico-chemical transformations

In this section the mathematical expressions to describe the temporal variation of the model states due to the transformations kinetics vector $\overline{\rho}$ are presented. Since the set of transformations are not considered in the pre-holding tank, the differential equations are zero. For further details about the mathematical expressions see **Annex A**.

Using the previous notation, a set of differential equations that involve the biological transformations in the ATAD is obtained considering every individual transformation; this can be written as follows:

$$\left(\frac{d\overline{M}_{ATAD}}{dt}\right)_{transf} = \sum_{i=1}^{22}\sum_{j=1}^{12} \nu_{(i,j)} \cdot \rho_j \cdot V_{phs} \qquad (3.24)$$

Where $V_{phs} = V_{liq}$ for $j \in [1,11]$ (for the biochemical, chemical, and dissolution transformations), and $V_{phs} = V_{gas}$ for $j = 12$ (for the evaporation-condensation transformation).

As it was referred before, the terms v_{ij} refer to the stoichiometric coefficients of the stoichiometry matrix, and describe the mass relationship between the 22 mass states for the 12 transformations considered in this model. Concerning the enthalpy variation due to the model transformations, only two transformations are considered in the liquid phase: the heat produced by the aerobic degradation and the water evaporation effect. The heat produced or consumed by the rest of transformations is neglected.

For the enthalpy variation due to the aerobic degradation, it is obtained considering the enthalpy variation associated to heterotrophic biomass growth, i.e. the enthalpy per unit of biomass generated [kJ·(kg COD)$^{-1}$], it can be expressed as:

$$HF_{bio} = \Delta H_{bio} \cdot \rho_3 \cdot V_{liq} \qquad (3.25)$$

For the enthalpy variation due to the water evaporation effect, it is obtained considering the evaporated mass flow of water multiplied by the latent heat (ΔH_{evap} [kJ·kg^{-1}]) at the liquid phase temperature, it can be expressed as:

$$HF_{evap} = \Delta H_{evap(Tliq,ATAD)} \cdot \rho_{evap} \cdot V_{gas} \qquad (3.26)$$

The enthalpy due to aerobic degradation is considered as a thermal gain, whereas the enthalpy due to water evaporation is considered as a thermal loss. Consequently, the enthalpy variation in the liquid phase due to the transformation can be expressed as:

$$\left(\frac{dH_{liq,ATAD}}{dt}\right)_{transf} = HF_{bio} - HF_{evap} \tag{3.27}$$

The water evaporation effect could has been included in the enthalpy variation of the pre-holding tank, but it was not considered in this model since this tank is at low temperature, thus the heat produced or consumed by these transformations is neglected.

Changes in the ATAD modeling

The air flow-rate injection to the ATAD is one of the few possible control handles for this reactor, hence, when the mathematical model presented in this chapter is used for control proposes, some thermal equations have to be adapted in order to have an air flow-rate dependence. Regarding this consideration, two principal thermal effects taken from the mathematical model proposed by Gomez et al. (2007a) and Gomez (2007b) were adapted: (i) the thermal exchange between the liquid and gaseous phase, and (ii) the condensation/evaporation effect. These thermal effects will be explained as follows:

(i) In that study, the thermal exchange between the liquid and gaseous phase was proposed as follows:

$$HF_{phs,ATAD} = k_{qa} \cdot \left(T_{liq,ATAD} - T_{gas,ATAD}\right) \cdot A_{phs,ATAD} \cdot \left(1 + \lambda\right) \tag{3.28}$$

Where k_{qa} denotes the heat conduction kinetic coefficient, $A_{phs,ATAD}$ is the area between phases and λ refers to an increasing contact area coefficient that depends on the mixing and aeration systems.

This coefficient varies with the amount of air flow-rate injected, thus the previous equation can be rewritten as follows:

$$HF_{phs,ATAD} = k_{qa(Q_{air})} \cdot \left(T_{liq,ATAD} - T_{gas,ATAD}\right) A_{phs,ATAD} \tag{3.29}$$

Where $k_{qa(Qair)}$ summarizes the total contact surface between liquid and gas when there is a variation in the air flow-rate injected. The variation of this coefficient was modeled as follows:

$$k_{qa(Q_{air})}\left[kJ \cdot d^{-1} \cdot {}^{o}C^{-1} \cdot m^{-2}\right] = k_{qa}^{(o)} + \lambda_{qa} \cdot Q_{air} \tag{3.30}$$

(ii) The heat loss by the water evaporation-condensation effect is modeled following this equation:

$$\rho_{evap} = k_{ma} \cdot \left(G_{h2o}^{sat} - G_{h2o}\right) \tag{3.31}$$

It the current study, it was assumed that the higher the air flow-rate injected is, the more the evaporation effect is produced. Therefore, the water evaporation rate coefficient (k_{ma}) was modeled following a variation with respect to the air flow-rate injected:

$$k_{ma(Q_{air})}\left[d^{-1}\right] = k_{ma}^{(o)} + \lambda_{ma} \cdot Q_{air} \tag{3.32}$$

Values for λ_{qa} and λ_{ma} were adopted from the values considered by the model approach presented by Gomez et al. (2007a) and Gomez (2007b) for k_{qa} and k_{ma} respectively. Details of these new parameters are detailed in **Annex A**.

4

Controlling the ATAD

Chapter 4 Controlling the ATAD

In this chapter, new control strategies for the ATAD technology working as a single treatment in batch-fashion are proposed. Regarding the overview presented in **Chapter 1** concerning to several control approaches for this process and the different limitations in the instrumentation, the aim is to design new control strategies considering all the possible information about the process behavior during the digestion phase.

The chapter is organized as follows: The control objectives for the ATAD process are detailed in **Section 4.1**. A preliminary simulation study is addressed in **Section 4.2**. In **Section 4.3** some control strategies are explained, where biological fundamentals are included to a better understating of the control background. Finally, some considerations related to the control solutions proposed are given in **Section 4.4**.

4.1. Control objectives

This section explains all the goals involved in the design of control strategies applied to the ATAD process, taking into account the most important limitations and restrictions. These restrictions affect the specifications and features of the control strategies proposed.

One important advantage in the ATAD process is its better stability[2] compared to conventional anaerobic processes (Gurjar, 2001). This leads to focus this kind of process into provide a final sludge fulfilling the pasteurization and stabilization criteria.

Typically, there are three possible control handles in the ATAD process: air flow-rate injection, influent and effluent flow-rate. The correct manipulation of one (or more) of these handles leads to obtain specific control objectives. According to typical ATAD operation, this study will focus on the variation of the air flow-rate injection of an ATAD operated in batch-type, in order to achieve the following objectives: (1) considering air-injection cost saving as priority; (2) considering the maximum sludge stabilization as priority.

For that reason, the design of any control strategy has to consider the following restrictions and limitations that this process has:

- The total volume of sludge to be treated is restricted by the total raw sludge in the influent; therefore the flow-rate manipulation to the ATAD is limited.
- Depending on the ATAD sizing and the total amount of sludge to be treated per cycle, a maximum air flow-rate injection has to be previously defined.
- The pre-holding tank dimensions give a limitation in its proper damping capacity; hence the control strategy has to overcome possible variations in the biodegradable substrate to be digested.
- Due to the batch-type process, the controller has to be implemented considering a limited period of time (the reaction phase).
- Due to the practical application of the control strategies proposed, the monitored variables are subjected to typical instrumentation found in industrial applications.

This set of characteristics reveals that is not possible to apply conventional concepts and techniques of classical control, but it is necessary to apply new

[2] The term “stability” is referred to process control. Do not confuse “stability” with the term “stabilization”, which is referred to reduction of organic substances contained in the sewage sludge.

and different techniques that, knowing the limitations detailed previously, allow achieving the objectives.

In the next sections, a preliminary simulation study will be assessed in order to understand the behavior of the ATAD process in typical conditions of operation. This study will allow presenting two control scenarios (ST1 and ST2). ST1 will focus on the air injection saving; ST2 will focus on to obtain the maximum sludge stabilization.

4.2. Preliminary simulation study

Prior to define the control strategies ST1 and ST2 for the ATAD, a preliminary study of the process was assessed. This study is developed by simulations using the mathematical model explained in **Chapter 3**, where the goal is to identify the diverse biological behaviors involved in the process in order to find out control solutions adapted to the system.

In denitrification and nitrification processes, the “nitrate knee” (in anoxic phase) and “ammonia break-point” (in aerobic phase) are linked respectively to the ORP and DO signals, giving information about the reactions vanish. Regarding the ATAD process, the proposed control strategies rely in this basic idea: to automatically detect the depletion of the biodegradable organic substrate fed into the digester, therefore, it is desirable to have a signal from the process that could bring information about the digestion status and also to be simulated using a mathematical model.

As it was described in **Chapter 1**, the available instrumentation of the process is the ORP and sludge temperature signal. The ORP signal gives an idea of the biodegradable status of the sludge during the digestion, but it can not be modeled.

A set of simulations were assessed in order to study the behavior of the following main variables during the digestion phase: the biodegradable substrate, the dissolved oxygen and the sludge temperature.

Considering a constant air flow-rate applied to the process, the batches can be classified in two groups: (i) when the biodegradable substrate is not completely digested (also known as oxygen limited), and (ii) when the biodegradable substrate is completely digested (also known as substrate limited). These two groups are depicted in **Figure 4.1(a)** and **4.1(b)** respectively

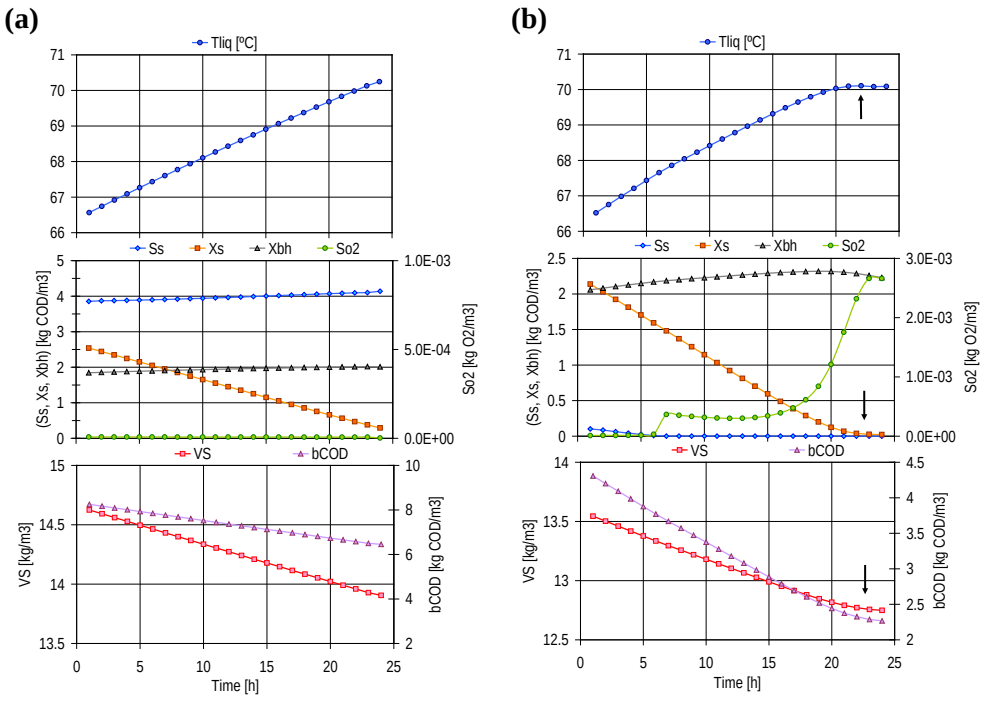

Figure 4.1 Possible batch situations: **(a)** Substrate not completely digested, **(b)** Substrate completely digested (zone indicated with black arrows).

Figure 4.1(a) shows the situation when the ATAD is under aerated, in this condition the digestion of the slowly (Xs) and readily (Ss) biodegradable

substrate is not completed, therefore the dissolved oxygen (So2) in the sludge is at minimum values, the kinetic of the heterotrophic biomass (Xbh) changes according to So2, and the sludge temperature (T_{liq}) ascent rate is directly controlled by the oxygen supplied. The volatile solids (VS) and biodegradable COD (bCOD) follow a linear trend during all the digestion phase.

On the other hand, **Figure 4.1(b)** shows the situation when the ATAD is over aerated, in this condition both the readily (Ss) and slowly (Xs) biodegradable substrate are digested. Indeed, when the reactor runs out Ss the dissolved oxygen increases due to the oxygen consumption rate drop. When there is a lack of Xs there is not more biodegradable substrate to be digested, the lysis of biomass is observed by the decreasing of Xbh, dissolved oxygen (So2) starts to increase again. Here, after 20 hours, the sludge temperature suffers a bending-point, and the linear trend of the volatile solids (VS) and biodegradable COD (bCOD) start to bend (named as “bCOD knee”). The beginning of this situation is indicated with black arrows in **Figure 4.1(b)**.

Therefore, **Figure 4.1(a)** shows that an excess of organic matter at the beginning of reaction can not be digested by the reactor, and **Figure 4.1(b)** shows that for a lack of organic matter at the beginning of reaction the VS and bCOD reach minimum values. In this way, the lack of substrate to be oxidized makes external aeration unnecessary; therefore, this flow-rate can be stopped until the next cycle in order to save energy costs.

If it would be possible to have a measurement of the slowly biodegradable substrate (Xs), a kind of control solution can be implemented to the process, but neither a sensor of Xs, VS or bCOD can be applicable.

Nevertheless, it can be observed that the behavior of the sludge temperature trajectory would give information about the digestion status of the process. In this way, the bending-point occurrence in the sludge temperature during the digestion phase reflects the lack of VS and bCOD.

In conclusion, the sludge temperature has an important behavior during the sludge digestion. It was detailed in **Chapter 3** that the mathematical model of the ATAD includes the modeling of the sludge temperature, therefore a data

processing of this signal can be implemented in order to design new control solutions for the ATAD.

In the next section, some control strategies approaches based on the sludge temperature signal processing will be explained.

4.3. Control strategies based on the sludge temperature

It was observed that when the ATAD is operated in under and over aeration, the typical sludge temperature trajectories are as depicted in **Figure 4.2(a)** and **4.2(b)** respectively.

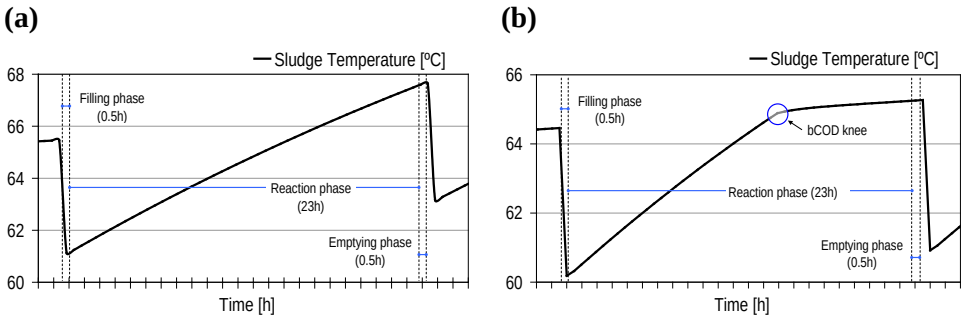

Figure 4.2 Temperature profile: **(a)** Under-aerated batch. **(b)** Over-aerated batch.

The control strategies ST1 and ST2, based on the sludge temperature signal, will have a common factor: the detection of bending-point in the sludge temperature profile. These control solutions will be evaluated following a specific protocol or benchmark, which will be detailed in **Chapter 5**. Some aspects of these control solutions were presented in Zambrano et al. (2009a) and will be explained bellow.

4.3.1. Strategy 1 (ST1): automatic switching-off of external aeration

This strategy uses the bending-point detection algorithm; therefore the followed actions have to be performed:

- At the beginning of every reaction phase, the external aeration is switched on and fixed to a constant air flow-rate (enough air in order to ensure the raw sludge stabilization in the worse conditions).
- During the reaction phase, a real-time signal processing algorithm collects the temperature trajectory with the objective of detecting the occurrence of the bending-point.
- If the bending-point happens, the air supply is automatically switched- off until the beginning of the next cycle.

$$Q_{air}^{(i)}(t) = k_a^{(i)}(t) \cdot Q_{air}^{(o)} \tag{4.1}$$

where

$$k_a^{(i)}(t) = \begin{cases} 1 & \text{if "bending-point" is not detected} \\ 0 & \text{otherwise} \end{cases}$$

The superscript *(i)* denotes the i-th batch cycle, $k_a^{(i)}$ denotes a parameter that changes during the batch time according to the bending-point detection, hence it takes the value “1” at the beginning of every new digestion phase, and will change to “0” if a bending-point occurs during the batch; therefore the air flow-rate is turned-off.

The air flow-rate action can be observed in **Figure 4.3**, where the aeration is constant during the digestion phase, and it is stopped when the bending-point is detected.

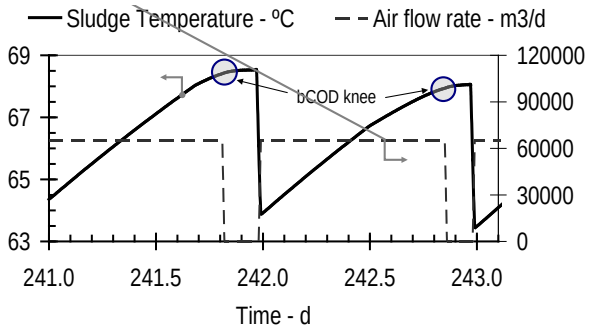

Figure 4.3. ST1 performance: switching-off of aeration when a bending-point is detected.

As it is observed in **Figure 4.3** that, departing from a given air flow-rate used in a conventional open-loop operation, this strategy aims to saving air consumption in those cycles where there is not necessary to apply more aeration to improve the sludge digestion.

Considering 1 year of ATAD operation and a digestion phase of 23 hours for every batch cycle, a roughly comparison between the activate or not of ST1 operation gives about 4% and 8% of air cost saving if the detections occur 1 or 2 hours before the batch ending respectively, these calculations are done considering that there is always a bending-point detection in every batch cycle.

4.3.2. Strategy 2 (ST2): ST1 combined with air flow-rate regulation from cycle to cycle

The ST1 strategy is effective at managing those cycles in which the air flow-rate is greater than that needed to oxidize the sludge fed into the reactor. Nevertheless, it has no provision for any corrective action on the aeration in situation where bending-points repeatedly remain undetected.

ST2 takes into account the above limitation considering an adapting control for the air flow-rate injected. Here the air flow-rate set-point from batch to batch is adapted depending on whether the bending-point is detected or not.

As in ST1, the air flow-rate set-point is constant throughout the reaction phase and is stopped when the knee is detected, but now this air flow-rate increases or decreases from batch to batch. It was assumed that the air flow-rate is working between minimum and maximum values. The ST2 strategy is described by the following equation:

$$Q_{air}^{(i)} = k_a^{(i)}(t)\cdot\left[Q_{air}^{(i-1)} + k_b^{(i-1)}\cdot\Delta Q\right] \tag{4.2}$$

where

$$k_a^{(i)}(t) = \begin{cases} 1 & \text{if "bending - point" is not detected in the i}^{\text{th}}\text{ cycle} \\ 0 & \text{otherwise} \end{cases}$$

$$k_b^{(i-1)} = \begin{cases} 1 & \text{if "bending - point" is not detected in the } (\text{i - 1})^{\text{th}}\text{ cycle} \\ -1 & \text{otherwise} \end{cases}$$

$$\Delta Q = \begin{cases} \Delta Q_{up} & \text{if } k_b^{(i-1)} = 1 \\ \Delta Q_{down} & \text{if } k_b^{(i-1)} = -1 \end{cases}$$

The parameter $k_a^{(i)}(t)$ is as referred in the ST1 operation, $k_b^{(i-1)}$ denotes a variable that allows the increasing or decreasing air flow-rate with respect to the previous batch, ΔQ refers to the air increment (ΔQ_{up}) and decrement (ΔQ_{down}) applied to the next batch, that depends on the value of $k_b^{(i-1)}$. It can be observed that ST1 is a particular case of ST2.

According to the criteria for the air flow-rate variation, an example of the ST2 performance can be depicted in **Figure 4.4**.

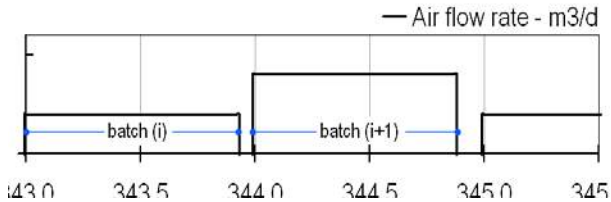

Figure 4.4 ST2 performance: air flow-rate action when a bCOD knee is detected during the batch.

Because these two control strategies consider bending-point detections in the sludge temperature, it is necessary to implement an adequate algorithm in order to detect these bending-points during the digestion phase. This issue will be discussed immediately.

4.3.3. The bending-point detection

In ATAD processes, a data processing can be applied to the sludge temperature profile in order to detect bending-points during the reaction phase. An algorithm based on linear regression applied to a moving-window data processing was considered in this study for two reasons: (i) data from the beginning of the reaction phase is not useful for detections, and (ii) querying the entire history may be impractical.

Estimating the derivative of the temperature profile

There are many mathematical ways to detect changes in a signal trajectory (linear regressions, derivates, curvatures, etc.). In this research, the bending-point detection via linear regression algorithm is adopted. This method is described as follows:

(i) Consider a set of data registered in a window of size N (even number) in a certain time. Internally, this window is divided into two registers of size N/2: one register stores the newest N/2 data (W_{new}) and the other stores the oldest N/2 data (W_{old}). This array is shown in **Figure 4.5**.

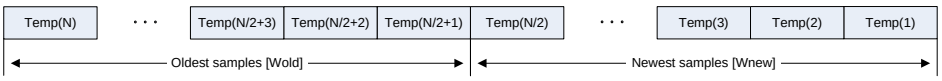

Figure 4.5 Data window divided into two registers

(ii) The changes in the sludge temperature are analyzed by doing a linear regression of the registers W_{new} and W_{old}. Therefore, in a general way, when a new data is received in the window, the time and the signal value are recorded, and the following calculations are done:

$$m[W_{new}] = \frac{\sum_{i=1}^{N/2}\left(t(i)-\overline{t(i)}\right)\left(T_{liq}(i)-\overline{T_{liq}(i)}\right)}{\sum_{i=1}^{N/2}\left(t(i)-\overline{t(i)}\right)^2} \tag{4.3}$$

$$m[W_{old}] = \frac{\sum_{i=\frac{N}{2}+1}^{N}\left(t(i)-\overline{t(i)}\right)\left(T_{liq}(i)-\overline{T_{liq}(i)}\right)}{\sum_{i=\frac{N}{2}+1}^{N}\left(t(i)-\overline{t(i)}\right)^2} \tag{4.4}$$

Where T_{liq} refers to the sludge signal values, t refers to the time value, and N refers to the number of samples in the window.

(iii) For every new data in the window, the change in the signal trend is evaluated by calculating the difference between the slopes of registers W_{old} and W_{new}, as follows:

$$\alpha[^{o}] = \frac{180}{\pi} \cdot \left\{ tg^{-1}\left[m(W_{old})\right] - tg^{-1}\left[m(W_{new})\right] \right\} \qquad (4.5)$$

Where α is the angle between the register W_{old} and W_{new}. A bending-point occurs when α is greater than a certain value. **Figure 4.6(a)** depicts the region where the bending-point occurs; a zoom of that zone is shown in **Figure 4.6(b)**, detailing the angle α used for the bending-point detection algorithm.

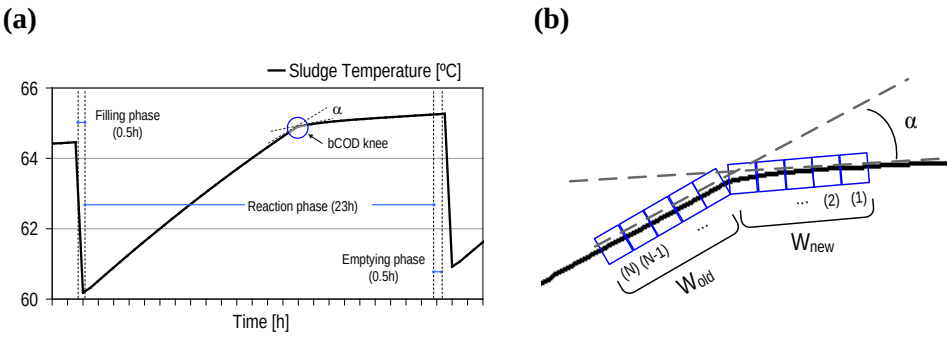

Figure 4.6 Bending-point detection in the temperature signal. **(a)** Batch profile; **(b)** Zoom of the circle in **Figure 4.6(a)** showing the data window used in the algorithm.

Crossing the temperature profile in real time

Because it is required to detect the bending-point during the current digestion phase, the detection algorithm has to be implemented in a moving-window. This moving-window will allow crossing the entire temperature profile. Therefore, in every new sample time the moving-window algorithm executes the following three steps:

- The oldest data is removed from the window.
- All the data set is shifted one-position.
- A new data is stored at the beginning of the window.

To facilitate the illustration, consider a moving-window of length 4. During the sample time (i) the moving-window will store the last 4 data as depicted in **Figure 4.7(a). Figure 4.7(b)** and **(c)** depict the data storing when new data is received, in every sample time the values in the window are shifted to receive new data.

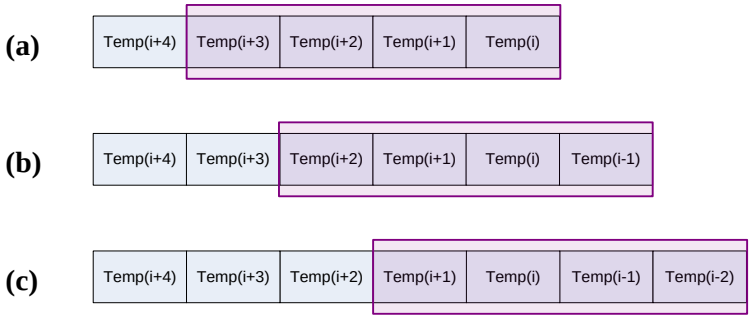

Figure 4.7 The moving-window algorithm. **(a)** Data storing at time (i), **(b)** and **(c)** show the data storing when new data is received.

In order to test the performance of the algorithm for the bending-point detection, ideal and real temperature profiles were considered. **Figure 4.8(a)** and **(b)** depict the α-profile given by the algorithm when ideal and real temperature profiles are evaluated.

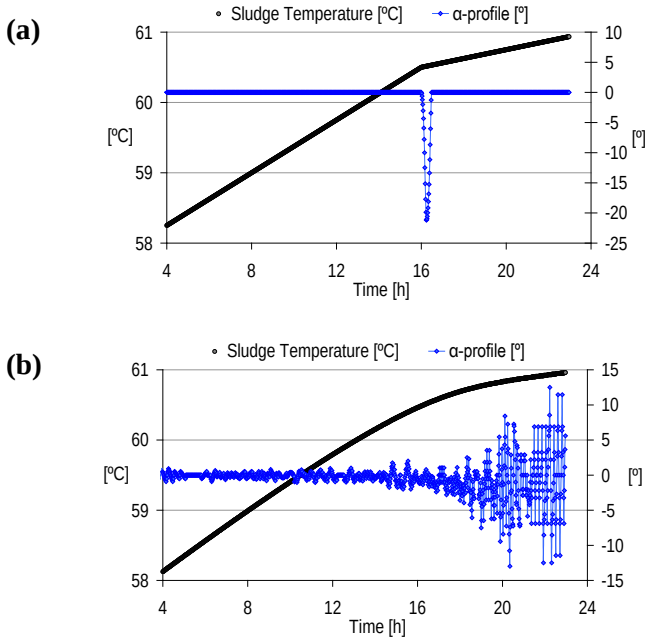

Figure 4.8 Response of α for a temperature profile. **(a)** Considering an ideal temperature profile. **(b)** Considering a real temperature profile.

It can be detailed in **Figure 4.8(a)** that, considering an ideal temperature profile, the change in the α-profile is notorious. But, as shown in **Figure 4.8(b)**, for a real temperature profile the α-profile has a different behavior. Here, the slope of the temperature profile changes smoothly, and any pair of values for the window-size (N) and the angle of detection (α) may give a good (or bad) bending-point detection.

Thus, in order to detect bending-points in this kind of temperature profiles, a selection of proper values for (N) and (α) is required. For this reason, a tuning procedure to obtain appropriate values for these parameters has to be developed. This subject will be undertaken in **Chapter 6.**

4.4. Control considerations

Based on the control structure previously proposed, some considerations must be taken into account for the proper application of control solutions that use algorithms based on bending-point detections, for example:

- **The air flow-rate**

  Because the kinetics of the heterotrophic biomass growth is modulated by the dissolved oxygen concentration, and the temperature ascent rate is directly controlled by the oxygen supplied, the best condition for bending-point detection in the sludge temperature profile is when a constant air flow-rate is applied from the beginning of the batch cycle.

  As a first approach in this study, a constant air flow-rate injection at the beginning of every batch cycle is assumed.

- **When to apply the controller?**

  It was observed that there is a change in the sludge temperature slope at the beginning of the batch cycle, due to the readily biodegradable substrate (Ss) consumption. Then, there is a second change in the sludge temperature slope, due to the lack of slowly biodegradable substrate (Xs). Therefore, the bending-point detection algorithm has to guarantee the detection of the second bending-point to ensure that all the biodegradable substrate was consumed.

- **True and false detections**

  In situations when the biodegradable substrate is consumed, it is necessary to obtain accurate bending-point detections. An early or later detection

could give consequences in the effluent quality and also in the plant operational costs.

Regarding the ST1 controller, if the bending-point is detected before (or if there is a false detection) the correct moment, there will be biodegradable substrate needed to be oxidized, giving higher COD values in the effluent sludge. On the other side, if the bending-point is detected after the correct moment, there will be a certain amount of air injected that was not necessary to apply, giving an increasing in the air consumption.

Concerning the ST2 controller, consecutive earlier or false bending-point detections can be dramatic for the process performance. For instance, several false detections will reduce the air supply in every new cycle batch, giving a worse effluent quality and producing odor problems by promoting oxygen limited conditions. This effect was referred in pilot studies by Schwinning et al. (1997).

- **The best parameters setting**

  Adequate bending-point detection has to consider proper values for the parameters algorithm: the window-size (N) and the angle of detection (α).

  Concerning the window-size (N), a low value will give fast detections but also could give false detections. In the same way, a large value for (N) would overcome the false detection problem but will give a high delay in the detection time.

  Regarding the angle of detection (α), a low value will give false detections for any little change in the temperature trajectory. On the other hand, a large value would overcome false detections but will avoid detecting any bending-point, because the expected angle of detection is higher than the angle obtained.

  Therefore, there will be a pair of (N) and (α) values that gives a good performance in terms of detections and speed of detection for control strategies based on bending-point detection algorithm.

- **The noise effect**

  For a signal with high curvature[3], the noise effect is not significant for bending-point detections. A typical sludge temperature profile in the ATAD process has a low curvature; causing that the bending-point detection may not be precise. However, in industrial application, the noise effect is always presented in sensor and can not be neglected.

  In this way, the set of parameters that give good bending-point detection under ideal conditions (no noise), may give bad results when the noise effect is included in the temperature signal profile.

  Hence, for a practical implementation of bending-point detection algorithm, the noise effect in the sludge temperature signal must be considered.

- **The ORP as a complementary signal**

  It was discussed previously that the ORP signal gives information about the biodegradable status of the sludge during the digestion phase. Although it is not possible to model it, the ORP can be used as a complementary signal to make the bending-point detection algorithm more robust against false detections.

[3] Curvature can be defined as a measure of how sensitive the tangent line is to moving the point to other nearby points.

5

Benchmarking the ATAD

Chapter 5 Benchmarking the ATAD

In this chapter, a new benchmark protocol for the ATAD process is developed based on previous benchmark studies. The aim of this protocol is to establish a simulation platform in order to design control strategies for the ATAD technology, and also, to be a common reference for the validation and evaluation of the proposed strategies.

The development of this benchmark requires a detailed definition of different aspects such as the specifications of a representative scenario of operation, or to introduce a set of indices that allow an objective evaluation of controller performance, both in quantitative and qualitative terms.

The chapter is organized as follows: a general review of the principal works on benchmark protocols is detailed in **Section 5.1**; then a general description of the benchmark specific for the ATAD process is presented in **Section 5.2**; the influent definition is presented in **Section 5.3**; the plant-layout is detailed in **Section 5.4**; the evaluation criteria and simulation procedure are given in **Section 5.5** and **Section 5.6**; the open-loop strategy is described in **Section 5.7**; and some conclusions are given in **Section 5.8**.

5.1. Benchmarks – A review

In the environmental engineering, simulation benchmarks have been employed in the evaluation and quantitative comparison of activated wastewater treatment control technologies. Following this idea, it is established that a simulation benchmark must be independent of any commercial simulation software

employed for it (GPS-X, WEST, Matlab/Simulink, BioWin). Moreover, it is not just a model for simulations, but a complete protocol that includes all the steps for controller's evaluation.

The Benchmark Simulation Model Nº 1 (BSM1) was the first benchmark applied to Waste Water Treatment Plants (Copp, 2002). The BSM1 was designed to evaluate control strategies for wastewater treatment with nitrogen removal. The benchmark plant is composed of a five-compartment activated sludge reactor consisting of two anoxic tanks followed by three aerobic tanks. The activated sludge is followed reactor is followed by a secondary settler. The evaluation protocol consists of a prior controller initialization followed by an evaluation period of 7 days. In this respect, an important point for controller's evaluation, besides quantifying control responses (errors, deviations, etc.), is the index process definition, from which it is possible to measure: (i) effluent quality, and (ii) the cost factors for operation. They are detailed as follows:

(i) The effluent quality (EQ) (kg pollution unit·d^{-1}): is referred as the quantification of the effluent pollution load. The EQ is average over a period of 7 days based on a weighting of the effluent loads of compounds (i.e., readily biodegradable substrate, COD, Kjeldahl nitrogen, nitrates and DBO5) that have a major influence on the quality of the receiving water and that are usually included in the regional legislation. Details of this work can be found in Vanrolleghem et al. (1996).

(ii) The cost factors for operation: takes into account the following terms:

- The sludge production to be disposed (SP) (kg·d^{-1}): is calculated from the total solids flow from wastage and the solids accumulated in the system over an evaluation period of 7 days. Details of the BSM1 equations can be found in Copp (2002).

- The aeration energy (AE) [kWh·d^{-1}]: the aeration energy takes into account the plant peculiarities (type of diffusers, bubble size, depth of submersion, etc.) and is calculated as a function of the k_La.
- The pumping energy (PE) [kWh·d^{-1}]: the pumping energy estimates the pumps energy consumption for influent and effluent flow-rates.
- The consumption of external carbon source (EC) [kg COD·d^{-1}]: calculates the external carbon that could be added to improve denitrification.
- The mixing energy (ME) [kWh·d^{-1}]: it is calculated considering the mixing in the anoxic compartment.

Finally, an Overall Cost Index (OCI) is calculated considering a weighting of the cost factor for operation previously explained.

Later on, some authors have suggest some modifications to the BSM1, such as the work presented by Vanrolleghem and Gillot (2002) who proposed to group the BSM1 indices in two general indices: (1) TCI (Total Cost Index), it summarizes the effluent quality costs and the energy costs; and (2) RI (Robustness Index), it evaluates the sensitivity of TCI between a range of variation for some selected process parameters (influent flow-rate, COD and N load, temperature, etc.). Samuelsson et al. (2007) and Stare et al. (2007) demonstrated how depending on the defined function costs related to the addition of external carbon and the effluent nitrate requirements, the optimal operation criteria for internal recirculation and for addition of methanol can fluctuate significantly.

Although the BSM1 is an important and widely used tool at the beginning, it evidences some limitations, for instance, it is not possible to evaluate control strategies for a longer time scale and on a plant-wide basis. Therefore, some adaptations have been introduced. An extension of the benchmark system for a long-term control and monitoring system performance evaluation (Rosen et al., 2004) was proposed recently in what is known as BSM1-LT. Here the required evaluation period is one year, and for this reason factors as temperature trajectory, temperature dependency and influent file design (considering rain and storm events) were important factors that have been considered.

Subsequently, a new important benchmark protocol was presented by Jeppsson et al. (2006; 2007) and evaluated by Vrecko et al. (2006), where both the water and the sludge line processes were integrated in a same plant-wide layout. In this protocol, known as BSM2, the sludge obtained from the primary and secondary settlers is then treated with a thickener, a conventional anaerobic digester and a dewatering. The BSM2 layout is depicted in **Figure 5.1**.

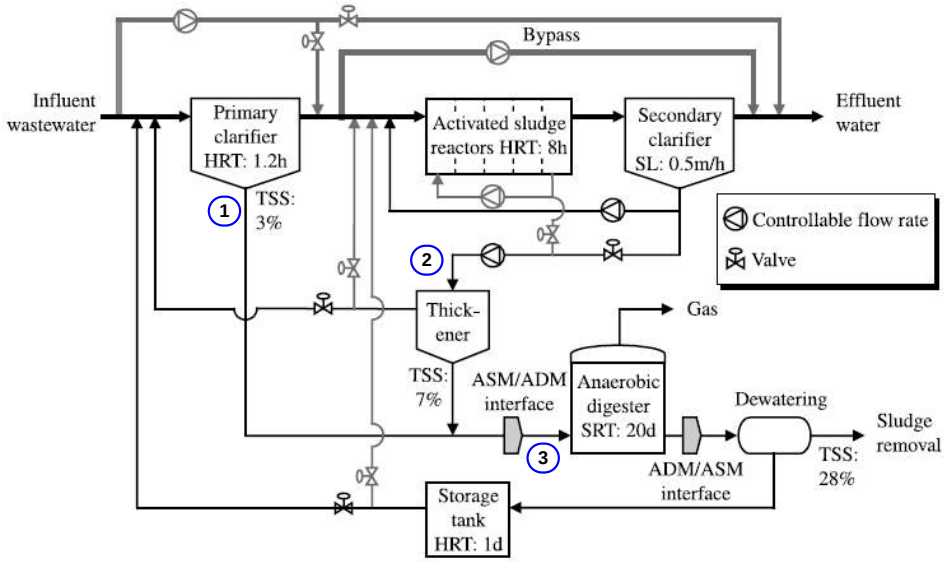

Figure taken from Jeppsson et al. (2007).

Figure 5.1 Layout of the BSM2. Points (1), (2) and (3) refer to primary, secondary and mixed sludge respectively.

The BSM2 gives particular emphasis on the ADM1 description of the digester, the interfaces between activated sludge and digester models, and the reject water storage. Since the anaerobic digester is part of the sludge treatment, the methane production obtained from the anaerobic digester was included in the OCI calculation.

The aeration energy is calculated in a similar way as in the BSM1. For the pumping energy calculation also the primary clarifier underflow, thickener underflow and dewatering overflow are included. Sludge production for disposal is calculated based on the amount of solids that are accumulated in the plant and from the solids that are removed from the plant as dewatered sludge. Mixing energy combines energy used for mixing the AS anoxic tanks and energy used for mixing the AD. Methane production represents an economic benefit, and can be included in the cost index as a negative cost. Net heating energy represents energy that is needed for heating the sludge of the AD in case the assumed heat exchange system together with the heat provided by the gas motor is not sufficient.

Moreover, taking the BSM2 layout, a plant-wide evaluation that includes a SHARON-Anammox process after the sludge treatment system described in the BSM2 was presented (Volcke et al., 2006). Here the impact of reject water streams on the performance of a WWTP is assessed in a simulation study, indicating that significant improvements of the effluent quality of the main wastewater treatment plant can be realized. The Overall Cost Index was used to evaluate the economical aspects of this approach.

On the basis of the standard BSM protocols, an ad-hoc benchmark for the anaerobic process considering a pre-holding tank was specially defined (Alferes and Irizar, 2010). This benchmark (named as AD_BSM) allows the design and validation of control strategy aimed at maximizing methane production and to guaranty appropriate water levels in the pre-holding tank.

Nevertheless, ATAD technology is not supported by any of the existing BSMs and, therefore, studies on ATAD control cannot be carried out with any of the simulations protocols. Seeing the ATAD model approaches in the last few years, the integration of ATAD into current BSM benchmarks or even the definition of a new benchmark protocol especially for ATADs, such as presented in this thesis, becomes feasible.

5.2. The ATAD benchmark definition (AT_BSM)

On the basis of the standard BSM protocols, an ad-hoc benchmark for the ATAD process was specifically designed (henceforth referred to as "AT_BSM"). The implementation of the AT_BSM protocol has involved the following four principal elements (see **Figure 5.2**): (1) Influent definition; (2) Plant-layout and plant-model; (3) Evaluation criteria; and (4) Simulation procedure. The level of definition reached in these components will determine how useful can be the AT_BSM to evaluate control solutions in a scenario close to the reality.

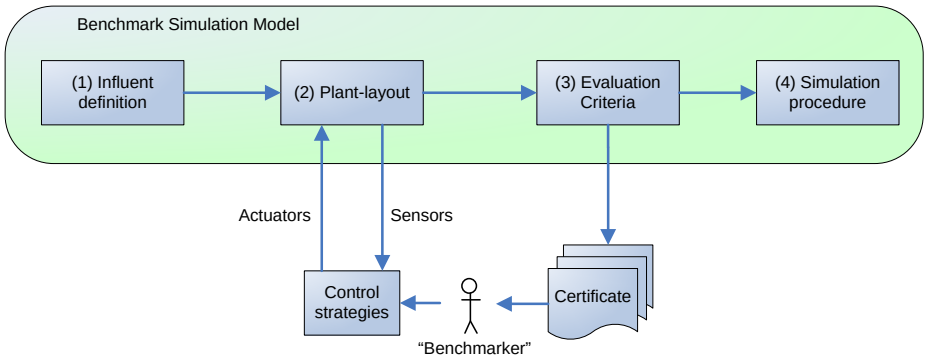

Figure adapted from Jeppsson and Pons (2004).

Figure 5.2 AT_BSM principal elements

The AT_BSM components were defined according to the influent sludge characteristics and the layout selected. Moreover, the definition of evaluation indices will establish a set of criteria to quantify the effects of applying different control strategies in the benchmark, under a systematic validation protocol.

A "certificate" is also indicated in the figure, which describes that the proposed control strategy and its performance evaluation would finally be issued to the user. This certificate serves as "quality insurance" that the proposed strategy

was properly validated and fulfils the AT_BSM criteria. Depending on the final results, the benchmarker can adopt either to improve the control strategy or to develop a new controller.

For a direct industrial application, the evaluation indices developed in this Chapter take into account common used process variables and energetic units observed in a plant operation and supervision.

5.3. Influent definition

From the control point of view, the raw sludge constitutes the principal perturbation to the digester. Therefore, the influent definition has to follow a defined procedure, since the control solutions and the validations assessed by the benchmark will depend on it.

It is always difficult to collect historical data with valuable information about the short and long term characteristics of a typical sludge in a full-scale plant. For that reason, it was decided to automatically generate the data by selecting a representative virtual plant. In this respect, for the sake of simplicity, the virtual plant of the BSM2 was chosen and simulated following the BSM2 simulation procedure (Vrecko et al., 2006).

Therefore, the influent data for the AT_BSM come from the sludge obtained after the thickener (see point (3) in **Figure 5.1**) in the BSM2 layout, referred as mixed sludge. The data obtained were saved at regular intervals of 15 minutes so as to create an influent file that includes all the sludge characteristics (flow-rate, concentrations and temperature). It was adopted a total simulation time of 728 days for the BSM2 in order to obtain the influent data of this study.

Concerning the temperature, since the BSM2 evaluation contains data variation during 728 days, the sludge temperature was an important value to consider. Hence, the temperature was included as part of the sludge characteristics.

5.3.1. Flow-rate, COD and temperature profile

The mixed sludge obtained after the BSM2 simulation contains variations in terms of flow-rate, concentrations and temperature. **Figure 5.3** depicts yearly and weekly trend of these data.

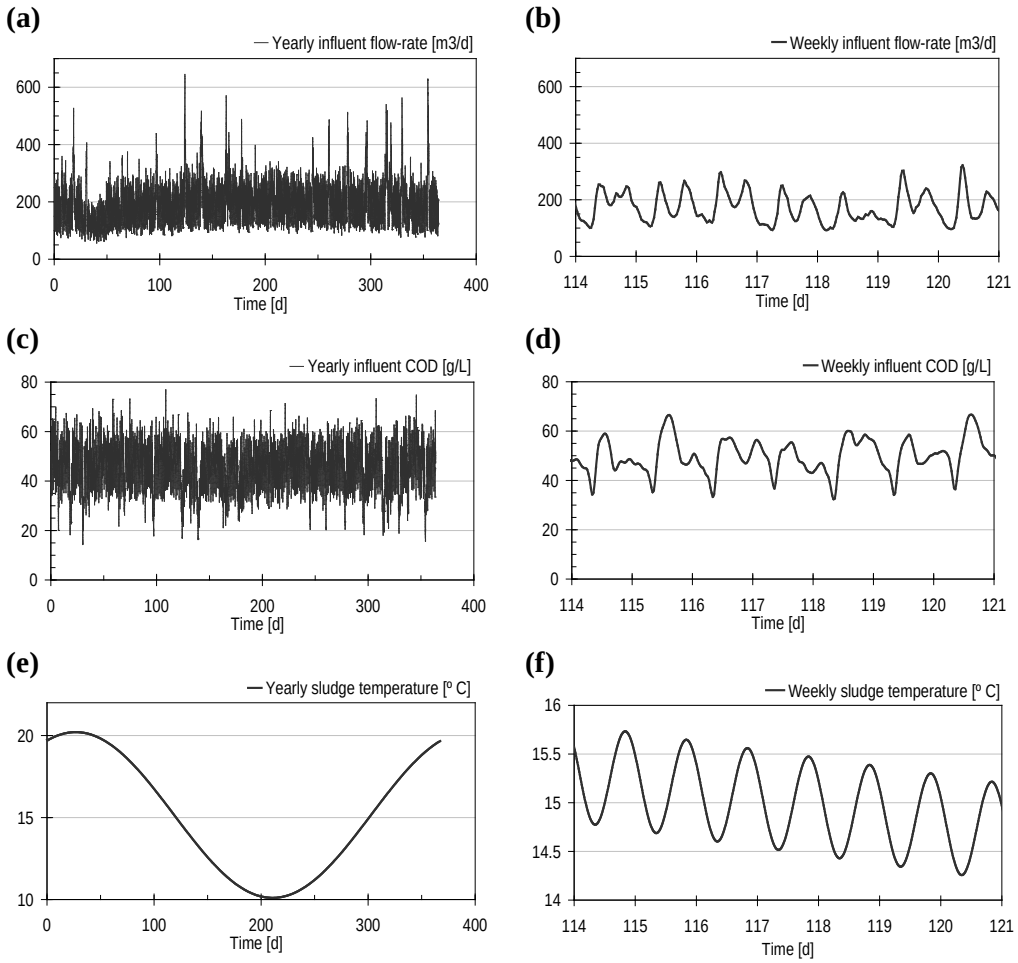

Figure 5.3. Profile variation of the mixed raw sludge. **(a)** yearly influent flow-rate, **(b)** weekly influent flow-rate, **(c)** yearly influent COD, **(d)** weekly influent COD, **(e)** yearly sludge temperature, **(f)** weekly sludge temperature.

Besides the mixed sludge, it was also possible to store data related to the primary and secondary sludge (see points (1) and (2) in **Figure 5.1**). Considering the total variation of the raw sludge, **Table 5.1** summarizes some major features of the obtained data.

Table 5.1. Influent file in the AT_BSM

Sludge features	Min	Max	Average
Flow-rate [$m^3 \cdot d^{-1}$]	39/17/56	544/102/646	148/40/188
COD [$g \cdot L^{-1}$]	2.2/85/14	74/95/77	35/86/47
TSS [$g \cdot L^{-1}$]	1.5/60/10.3	49/67/52	24/61/32
Temperature [ºC]	9.5	20.5	15

Primary/Secondary/Mixed

Compared to average values, it is shown a maximum in the mixed flow-rate of 646 $m^3 \cdot d^{-1}$, and maximum values of COD and TSS of 77 and 52 $g \cdot L^{-1}$ respectively.

5.3.2. Interfacing the raw sludge

Regarding the raw sludge obtained from the BSM2 simulation, an interface was developed in order to adapt the state variables used in the BSM2 to those used in the AT_BSM. This interface allows rewriting the raw sludge composition in terms of the mathematical model adopted in this study (see **Chapter 3**), thus the influent data can be used in this study.

Accordingly, in terms of the state variables used in the AT_BSM, the COD fractionation of the primary, secondary and mixed sludge can be expressed as shown in **Table 5.2**.

Table 5.2 COD fractionation in the AT_BSM influent raw sludge

	Model component	Fractionation (*) [%]	Mean value (*) [kg·m^{-3}]
Soluble COD (100%)	Ss	67/3.5/61.6	0.057/0.001/0.045
	Si	33/96.5/38.4	0.028/0.028/0.028
Particulate COD (100%)	Xs	80.2/55.65/70.25	28.356/47.946/32.721
	Xr	1.1/6.6/3.35	0.387/5.690/1.564
	Xi	18.7/37.75/26.4	6.611/32.531/12.291

(*) Primary/Secondary/Mixed

Table 5.2 reflects that the soluble COD component in the raw sludge is negligible. Regarding the particulate COD, more than 2/3 parts of the mixed raw sludge is due to slowly biodegradable substrate (Xs); the rest is roughly due to inert organic matter (Xi).

5.4. Plant-layout and plant-model

The definition of the plant-layout requires a complete specification of the physical configuration of the plant and the mathematical models employed to describe the process behavior.

Therefore, the plant-layout in the AT_BSM was made up of a pre-holding tank (HT) and a single-stage ATAD reactor (see **Figure 5.4**). Although the ATAD technology supports other design configurations than the single-stage, this one was preferred for two reasons: (i) the tendency in the second-generation ATAD is to provide less complex reaction schemes (Staton et al., 2001); and (ii) in Spain, most of the full-scale ATADs currently in operation have been built according to this layout (García et al., 2007). Additionally, instead of several trends of ATADs working in parallel such as is usual in full-scale facilities; a single-tank approach was adopted for the sake of simplicity.

The ATAD as a single treatment is generally operated in batch-mode (feeding–digestion–emptying), mainly in scenarios where sludge pasteurization is mandatory and where, therefore, it is important to avoid hydraulic short circuits during the digestion phase. Within this benchmark, a batch-mode operation was imposed for the ATAD. This sequencing operation can be achieved by controlling the feeding and emptying steps by pumps. Consequently, in this process there are three possible control handles: the feeding and emptying pumps, and the aeration pump.

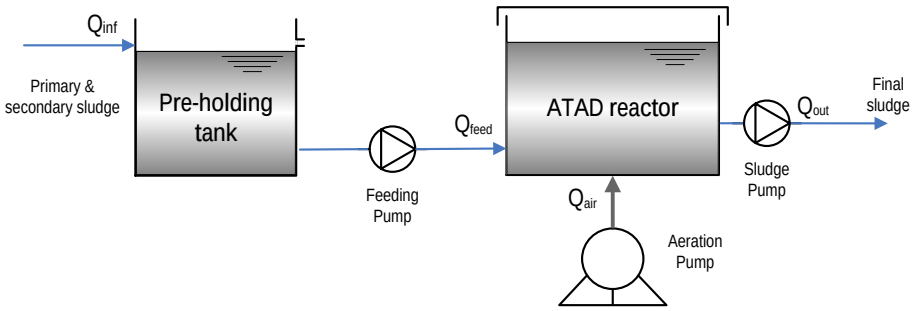

Figure 5.4 Plant-layout of the AT_BSM

Concerning the mathematical model used in the AT_BSM, the equations were described in **Chapter 3**, the details of the model can be found in **Annex A**. The effective volume of HT and ATAD are described below.

Moreover, although it was assumed ideal (no noise and delays) sensors and actuators in the present implementation of the AT_BSM, models of typical sensors were included adopting the study presented by Rieger et al. (2003).

The pre-holding tank (HT) sizing

It was previously discussed that the non-continuous feeding in the ATAD (for pasteurization requirements) makes the utilization of HTs necessary. Therefore,

the role of the HT is to be an available control handle rather than a part of the biological process.

The dimension of this tank has an influence in the posterior ATAD performance. A low tank capacity can produce the following effects: (i) perturbations to the ATAD influent sludge; and (ii) overloading and emptying effects.

On the other hand, big HT causes the following effects: (i) it requires space and increases the construction costs; (ii) may produce a pre-digestion step (acting as an anaerobic digestion); (iii) may give an over lamination of the raw sludge.

It is understandable that the size of HT depends on the raw sludge influent profile, and on the amount of sludge to treat daily. The overloading and emptying effect have to be avoided.

The HT sizing has taken into account the entire raw sludge profile described in **Section 5.3**, especially when the sludge reaches critical values (minimum and maximum flow-rates).

An analysis of the influent data file was performed to obtain appropriate values for the effective volume of both the HT and the ATAD. Consequently, two mean influent flow-rates (Q_{feed}) to the ATAD were defined (for summer and winter season). Q_{feed} = 170 $m^3 \cdot cycle^{-1}$ was adopted for summer season, and Q_{feed} = 200 $m^3 \cdot cycle^{-1}$ was adopted for winter season.

Furthermore, two additional parameters were added to avoid hydraulic problems and keep the damping capacity of the tank: the minimum volume (V_{min}) and the re-start volume (V_{rst}), where $V_{min} < V_{rst}$. Consequently, the feeding control to the ATAD depends on two situations:

- If the volume in HT is below V_{min}, the flow-rate to the ATAD is stopped (emptying situation in the HT).
- When the volume in HT is higher than V_{rst}, it leads to reactivate the influent flow-rate to the ATAD.

V_{min} and V_{rst} were set in 150 and 500 m^3 respectively, giving a HT volume of 2000 m^3. Just to remark, the emptying situation in HT is not referred to an empty HT, but a minimum volume reached in it.

The ATAD sizing

Reactor sizing involved the determination of the active volume, selecting dimensions for a circular tank (classical shape), considering a height/diameter (h/d) ratio, and adding additional height for foam management and freeboard.

The minimum active volume was based on the sludge retention time (SRT). For ATAD as a single-treatment, a 10-15 days SRT is commonly established to provide a better operation (Scisson, 2003; Eyma et al., 1999). Based on this range and considering the average influent flow-rate previously defined, the active volume reactor (V_{liq}) size resulted in 2350 m^3. This value is equivalent to a SRT of 12.7 days.

A typical range of 0.5 to 1.0 for h/d was considered during reactor sizing (USEPA, 1990). To accomplish this requirement h/d = 0.75 was adopted for this study. Thus, the dimensions of the active volume of ATAD resulted as follows: d = 15.86 m; h = 11.9 m.

An additional height was required to allow a space for the gaseous phase and, in industrial application, for foam management. It is not possible to model the foam effect but it is necessary to define a gaseous volume for the model adopted, therefore, additional 2 m were considered. The resultant final dimensions of the ATAD are: Diameter = 15.86 m; Total height = 13.9 m.

This resulted in a gaseous volume (V_{gas}) and a total reactor volume (V_{ATAD}) equal to 395.11 m^3 and 2745.11 m^3 respectively.

5.5. Evaluation criteria

Following the criteria form the standard benchmark protocols, three major performance indices were incorporated into the AT_BSM in order to compare control strategies: (1) Overall Cost Index (OCI); (2) the Pasteurization Quality Index (PQI); and (3) the Stabilization Quality Index (StQI). These indices were presented in Zambrano et al. (2009b) and will be detailed below.

Due to the non-continuous operation of the process, the evaluation criteria are based on discrete sums, considering the results obtained after the filling, the digestion and the emptying phases.

- **Overall Cost Index (OCI):**

The OCI takes into account all the energy costs involved in the operation of the ATAD reactor: aeration energy (AE), pumping energy (PE) and mixing energy (ME), using the following expressions:

$$AE[kWh{\cdot}d^{-1}] = \frac{0.04}{N{\cdot}t_{cycle}} \sum_{i=1}^{N} \left(\int_{ti}^{tf} Q_{air}(t)dt \right) \tag{5.1}$$

$$PE[kWh{\cdot}d^{-1}] = \frac{0.04}{N} \left\{ \frac{1}{t_{feed}} \sum_{i=1}^{N} \left[Q_{feed}^{(i)} \right] + \frac{1}{t_{out}} \sum_{i=1}^{N} \left[Q_{out}^{(i)} \right] \right\} \tag{5.2}$$

$$ME[kWh{\cdot}d^{-1}] = P_m{\cdot}t_{cycle} \tag{5.3}$$

Where t_{cycle} [days] is the time required to complete the digestion phase, t_{feed} [days] is the time required for the feeding cycle, t_{out} [days] is the time required

for the emptying cycle, N is the total number of batch cycles, *i* is the *i-th* batch cycle. In PE both the feeding and the withdrawal of the sludge are considered; for ME only the energy required for mixing the ATAD is considered. The costs involved in PE and ME are constant during the evaluation, only the costs involved in AE will change (depending on the strategy selected for the air flow-rate injection). Finally, the OCI was calculated in a similar way to that undertaken in BSM2 but using a non-weighted sum:

$$OCI[kWh \cdot d^{-1}] = AE + PE + ME \tag{5.4}$$

- **The Pasteurization Quality Index (PQI):**

PQI was included into the benchmark to represent the percentage of ATAD cycles in which the sludge leaving the treatment can accomplish the norms. In this case, according to the EU recommendation, and since in the more general case the decant volume per cycle (V_{out}) might change from cycle to cycle, the index PQI was formulated in terms of mass fluxes per cycle, as follows:

$$PQI[\%] = \frac{\sum_{i=1}^{N}\left[k_{paste}^{(i)} \cdot V_{out}^{(i)} \cdot TSS_{out}^{(i)}\right]}{\sum_{i=1}^{N}\left[V_{out}^{(i)} \cdot TSS_{out}^{(i)}\right]} \cdot 100 \tag{5.5}$$

where

$$k_{paste}^{(i)} = \begin{cases} 0 & if \quad PTime^{(i)} < 20h \\ 1 & if \quad PTime^{(i)} > 20h \end{cases}$$

TSS_{out} [$kg \cdot m^{-3}$] is the total suspended solids concentration in the treated sludge. $PTime^{(i)}$ [hours] represents the total time in which the sludge has been at a

temperature greater than 55 ºC during the aerated reaction phase of the *i-th* batch.

- **The Stabilization Quality Index (StQI):**

Recalling the option for compliance with vector attraction reduction requirements (sludge stabilization) discussed in **Section 1.4**, Option 1 (38% reduction in volatile solids during sewage) and Option 2 (less than 15% additional volatile solids reduction during bench-scale aerobic batch digestion for 30 additional days at 20 ºC) are valid for aerobic thermophilic digestion. Therefore, the following expression was decided for StQI:

$$StQI[\%] = \frac{\sum_{i=1}^{N}\left[k_{st}^{(i)} \cdot V_{out}^{(i)} \cdot VS_{out}^{(i)}\right]}{\sum_{i=1}^{N}\left[V_{out}^{(i)} \cdot VS_{out}^{(i)}\right]} \cdot 100 \qquad (5.6)$$

where

$$k_{st}^{(i)} = \begin{cases} 1 & \begin{cases} if \;\; Option\ 1^{(i)}\ is\ met \\ else \\ if \;\; Option\ 2^{(i)}\ is\ met \end{cases} \\ 0 & Otherwise \end{cases}$$

VS_{out} [kg COD·m^{-3}] refers to the volatile solids concentration in the effluent sludge. Option 1$^{(i)}$ and Option 2$^{(i)}$ are Boolean variables whose values result from the evaluation at the end of the *i-th* batch cycle of the respective Option 1 and 2 previously defined.

Finally, complementary to PQI and StQI, three additional indicators were included in the evaluation criteria: (1) the withdrawal volume (WV_{out}); (2) the thermal energy in the treated sludge (ThE_{out}); and (3) the biodegradability of the treated sludge ($bCOD_{out}$). These additional criteria are detailed bellow.

- **The withdrawal (WV_{out}):**

This indicator represents the mean volume taken out from the plant.

$$WV_{out}\left[m^3 \cdot d^{-1}\right] = \frac{\sum_{i=1}^{N} V_{out}^{(i)}}{N \cdot t_{cycle}} \tag{5.7}$$

With the WV_{out} index, a qualitative indicator to compare the requirements for sludge dewatering is provided. Differences obtained in the WV_{out} value are directly related to a higher or lower evaporation effect in the ATAD sludge.

- **The Thermal Energy in the treated sludge (ThE_{out}):**

This indicator is included in the indices in order to know the thermal energy obtained in the sludge at the end of every batch cycle, providing an indicator of the heating potential of the treated sludge.

$$ThE_{out}\left[Mcal \cdot d^{-1}\right] = 2.39 \cdot 10^{-4} \cdot \frac{\sum_{i=1}^{N}\left[c_{p,H_2O} \cdot \delta_{H_2O} \cdot V_{out}^{(i)} \cdot T_{out}^{(i)}\right]}{N \cdot t_{cycle}} \tag{5.8}$$

Where T_{out} [ºC] refers to the sludge temperature before the emptying period. It was assumed that the sludge temperature value is approximately equal to the liquid temperature.

- **The biodegradability of the treated sludge ($bCOD_{out}$):**

This indicator represents the percentage of biodegradable COD reduction in terms of the final effluent organic flow-rate.

$$bCOD_{out}\left[kg\,O_2 \cdot d^{-1}\right] = \frac{\sum_{i=1}^{N}\left[V_{out}^{(i)} \cdot bCOD_{out}^{(i)}\right]}{N \cdot t_{cycle}} \tag{5.9}$$

Where $bCOD_{out}$ [kg COD·m^{-3}] refers to the biodegradable COD concentration in the total effluent sludge.

From the definition of the evaluation criteria, it can be observed that higher values in ThE_{out} mean higher temperatures in the treated sludge; therefore, for a given value of PQI, the higher the value of ThE_{out} is, the higher is the degree of pasteurization obtained. Analogously, for a given value of StQI, the lower the value of $bCOD_{out}$ is, the higher is the degree of stabilization.

5.6. Simulation procedure

A proper evaluation and comparison between control strategies studied in the AT_BSM, based on the evaluation criteria defined previously, require that every control strategy must be validated under the same simulation procedure. In this way, it is guaranteed that the evaluation indices are calculated under the same operational conditions.

According to the BSM protocols, a simulation procedure based on 4 events was defined, with a total simulation time of t_{sim} = 728 days, considering stationary and dynamic simulations. This procedure is depicted in **Figure 5.5** and will be explained bellow. For software implementation, the time (t) used in the mathematical model was named as t_{sim}.

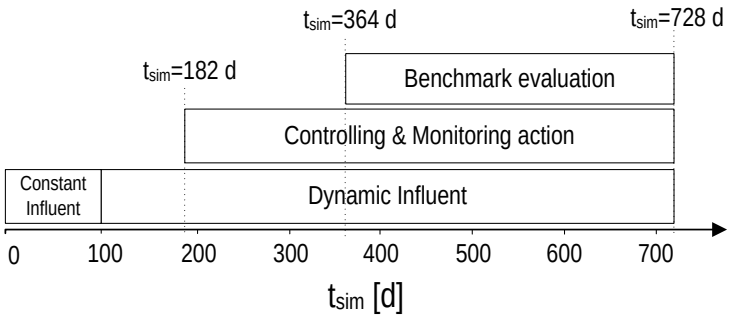

Figure 5.5 Protocol of simulations to validate the control strategies.

At t_{sim} = 0 d, the plant was simulated during 100 days under fixed operational conditions in order to reach the steady state. In this case, the influent file corresponds to a constant influent built from the medium values of flow-rate and concentrations of the raw sludge (see **Table 5.1**). The final mass states reached in the holding-tank and ATAD were used as initial values for the dynamic simulations. At t_{sim} = 100 d, the dynamic influent was applied to the plant. This influent includes daily fluctuations in flow-rate and sludge composition. At t_{sim} = 182 d, the control strategy to be evaluated was activated under the dynamic conditions started at t_{sim} = 100 d. At t_{sim} = 364 d, the calculation of the different evaluation indices was activated. Average values were totalized at the end of the simulation time.

5.7. Reference strategy: open-loop operation

In order to have a reference basis to compare and validate the different control strategies proposed in the AT_BSM, the proposed benchmark included one strategy in open-loop. This strategy, henceforth referred to as OL, referred to a typical operation where constant air flow-rate is injected high enough in order to guaranty an acceptable operation of the overall process.

OL strategy in the AT_BSM was defined considering the following aspects: (i) it has to be guaranteed a feeding event to the ATAD during all the simulation time (i.e., avoiding emptying events in the HT); (ii) appropriate SRT and air flow-rate settings were required to accomplish pasteurization and stabilization criteria.

Consequently, the operational parameters for the OL strategy (Q_{feed}, cycle time, Q_{air}) were obtained according to the HT and ATAD sizing (for more details see **Section 5.4**). The air flow-rate was obtained according to the biological characteristics of the influent sludge. The OL strategy was defined as follows:

- For summer time (T_{amb} >= 15 ºC), feeding volume of Q_{feed} = 170 $m^3 \cdot cycle^{-1}$. For winter time (T_{amb} < 15 ºC), feeding volume of Q_{feed} = 200 $m^3 \cdot cycle^{-1}$. These flow-rates gave an adequate hydraulic performance in the process.
- A sequencing operation with a cycle time of 24 h distributed as follows: feeding phase of 0.5 h, reaction phase of 23 h and emptying phase of 0.5 h. This was adopted in compliance with EU requirements (European Commission, 2000) for sludge pasteurization in batch systems.
- According to the raw sludge characteristics, it was assumed an aeration flow-rate of Q_{air} = 65000 $m^{3} \cdot d^{-1}$ applied during the reaction phase. The aeration is turned-off during feeding and emptying phases.

The performance indices obtained after running the OL strategy are shown in **Table 5.3**. These results were used as a reference to evaluate the performance obtained when the rest of strategies were simulated with this benchmark.

Table 5.3. Performance results for the OL strategy

Evaluation index	Value	Unit
PQI	100	%
StQI	100	%
WV_{out}	174.94	$m^3 \cdot d^{-1}$
ThE_{out}	12324	$Mcal \cdot d^{-1}$
$bCOD_{out}$	623	$kg\ O_2 \cdot d^{-1}$
OCI	5351	$kWh \cdot d^{-1}$
AE	2457	$kWh \cdot d^{-1}$

5.8. Conclusions

Knowing the important results that the BSM1 protocols has played to obtain automatic control in WWTP layouts, the implementation of similar protocols for the sludge treatment is an opportunity to integrate improved control into sludge treatment technologies.

In this way, the results achieved with the protocols BSM1-LT and BSM2 were the basic idea to design a procedure that takes into account the sludge treatment.

In this new benchmark the aeration cost and the biodegradable COD conformed two of the fundamental indices in control evaluation, and will give relevant information about the control strategies performance.

Concerning the increasing interest in improving the performance of sludge treatments in WWTPs, the proposed AT_BSM protocol try to be useful in testing and analyzing control strategies applied to the ATAD technology as a robust process for sludge reduction.

6

Methodology for robust tuning of bending-point detection algorithm

Chapter 6 Methodology for robust tuning of bending-point detection algorithm

Chapter 4 presented the algorithms corresponding to the control strategies based on the detection of bending-points in the temperature signal. Now, it is time to go with tuning their parameters.

A control strategy based on bending-point detections is not a classical control strategy (like a P, PI, PID, etc) as it is referred in classical control theory. As a first try, initial values for different parameters can be tested, but accurate results can be obtained only when proper methodology to tune the different parameters is established.

Consequently, it is necessary to develop some kind of tuning procedure adapted to this specific problem. This chapter deals with the development of a new methodology for a robust tuning of the parameters when an algorithm based on bending-point detections is implemented. Although the methodology can be applied to any process, it will be particularized to the ATAD.

The robustness aspect in this approach relies on considering all the possible profiles that can occur in real situations. For that, slow and fast dynamic responses of the process were analyzed.

From the total of profiles generated, a resolution of an optimization problem is designed to give proper values for the parameters of the algorithm; the objective in this optimization is to find the best set of parameters to maximize the true detections and to reduce the false detections.

The outline of this chapter is as follows: in **Section 6.1** the occurrence of bending-points in biological systems is discussed. **Section 6.2** gives a short

overview of the PCA method (that will be used in the methodology). In **Section 6.3** the new methodology for tuning bending-point detection algorithms is detailed. In **Section 6.4** the ATAD technology is used as case study to implement the methodology. The effect of noise in the sensor signal is evaluated in **Section 6.5**. Finally, some conclusions are presented in **Section 6.6**.

6.1. The bending-points in WWTP

In some non-continuous biological processes, which are common solutions when dealing with biological technologies treating wastes (either liquids or solids), the bending-point occurrence gives important information about the status of specific reactions. Just to mention a few of them, Sequencing Batch Reactors (SBR), Biodenitro/Biodenipho, and ATAD are three examples of technologies where operation relies on the application of a cyclic sequence to both the hydraulic pattern and the external aeration.

Conditioned by the fact that it is in the scenario of small systems that batch-oriented biological processes acquire most relevance, studies on phase-length control were undertaken under the assumption that only low-cost instrumentation is available for use, namely online signals for dissolved oxygen (DO), ORP and pH. Fortunately, an analysis of the trajectories that these signals follow during the cycle reveals the occurrence of bending-points totally connected with depletion in either denitrification or nitrification. Thus, what it is referred to as phase-length control is nothing else than real-time algorithms aimed at detecting automatically the occurrence of such bending-points.

Depending on whether these bending-points are detected or not, the algorithms determine whether the ongoing phase of the cycle is forced to end or not. Indeed, control strategies based on bending-point analysis can be found in Sequencing Batch Reactors (SBR) and in intermittently aerated continuous

systems, using ORP and/or pH as the measured signals. Bending points on the ORP give information about the “ammonia break point” and “nitrate knee”, on the pH refer to the “ammonia valley” and ”nitrate apex”. Aeration is switched-off when the “ammonia break-point” or the “ammonia valley” is detected, and is switched-on when the “nitrate knee” or “nitrate apex” is detected. In this way, the lengths of the aerobic and anoxic phases are controlled to be just sufficient for complete nitrification and denitrification, respectively. Plisson-Saune et al. (1996) used the two ORP bending points to control a lab-scale plant treating domestic wastewater. Al-Ghusain et al. (1994) and Al-Ghusain and Hao (1995) used the two pH bending points to control a lab-scale sludge digestion process. Nearly complete nitrogen removal was achieved.

The concerns about the reliability of the bending-point detection have initiated the idea of combining ORP and pH for the aeration control. In Yu et al. (1997), the derivatives of ORP and pH with respect to time were calculated simultaneously. The combination of the two derivative signals, together with an artificial neural network predictor, which calculates the time and magnitude of the bending point detection, significantly improved the reliability of the bending point detection and hence the performance of the controller.

Signal treatment has been applied in water treatment plant controllers for bend-point detection, for instance, Ga and Ra (2009) presented a real-time control based on the moving slope changes of pH(mV)-time profile applied to a (SBR for swine wastewater treatment. Won and Ra (2011) evaluated this strategy using the ORP-time profile.

It was found during this thesis that another situation of bending-point occurs at the temperature signal in batch-type ATAD digesters when biodegradable organic matter vanishes, thus causing exothermic aerobic reactions to slow down.

Although specific researches have been reported to detect the occurrence of bending-points, the underlying idea behind all of them is basically to get an estimate of the first derivative on the signal trajectory. With the values of the first derivative, comparisons with pre-set threshold values are performed in

order to detect the occurrence of a bending-point. On the other hand, the main difference between these works relies on two factors: (1) the manner of estimating the first derivative; and (2) the value assigned to the threshold parameter. Some authors propose the combination of moving windows with linear regression methods to estimate derivatives (Chen et al., 2002). Others, instead, opt for filtering the raw signal to then estimate the derivative on the filtered signal as a direct difference between consecutive samplings (Pavselj et al., 2001; Kim et al., 2004; Marsili-Libelli et al., 2008).

Nonetheless, whatever algorithm is implemented, an appropriate tuning of its parameters (sampling time, filter coefficient, threshold values, etc.) is crucial to achieve satisfactory performance. At this point, none of the aforementioned algorithms is accompanied with a rigorous and systematic description of the tuning procedure, the latter being the reason that has motivated to develop a new methodology for tuning bending-point detection algorithms.

6.2. Using PCA - Overview

The continuous increasing in process monitoring capacity leads to use large amount of data. It is important to use efficient techniques to get high quality information from this great volume of data. In engineering applications, it is usual to find cross-correlation between the variables space. In these cases, multivariate analysis has proved to be a powerful statistical technique. Piovoso et al. (1992) present a brief tutorial about applications of multivariate statistics to process analysis, monitoring and control.

Principal Component Analysis (PCA) utilizes directly the information from data, compacted in the form of a covariance matrix, to extract more relevant information and to generate new variables named as principal components. The mathematical details are presented in **Annex C**.

Many times PCA has been applied as a dimension reduction tool prior to other costly computations (Eleyan and Demirel, 2005; Song et al. 2008). The division in scores and residuals performed in PCA is very useful in Multivariate Image Analysis domain (Prats-Montalbán et al., 2011).

The application of fault detection techniques based on PCA as a dimension reduction method was proposed by Yoon and MacGregor (2001 and Tomita et al. (2002). Rosen and Olsson (1998) show disturbance detection in wastewater treatment systems using principal components and partial least-squares (PLS). Raich and Çinar (1995) propose to utilize multivariate statistical techniques (PCA and discriminant analysis) to detect states out of control and to diagnose abnormal operation conditions and disturbance that cause poor process behavior.

In next section, the PCA technique will be employed within the methodology to quantify the correct uncertainty space for all parameters and variables that affect signal trajectories.

6.3. The proposed methodology

State variables in biological processes follow different time-scales. In this way, the effect of some variables can only be evaluated in a long-time scale; on the other hand, there are variables where effects can only be evaluated in a short-time scale.

For instance, compared to the soluble substrate, some of the particulate substrate in a reaction presents a slow response when changes in the influent or effluent flow-rate occur, but other kind of perturbations (for instance, changes in the influent fractionation or in the air injected) can produce a faster response.

Moreover, if the objective is to analyze the profile of a target variable of the process, the behavior of this variable can be influenced by several elements, as follows: inputs, model parameters and changes in state variables.

Considers a biological process represented by f, the state vector by $\bar{x}$, the input variables by $\bar{r}$, the model parameters by $\bar{p}$, the target variable by x_i, and time represented by t. The dynamic of the target variable can be described as follows:

$$\frac{dx_i}{dt} = f(\bar{r}, \bar{p}, \bar{x}, t) \tag{6.1}$$

Where $\bar{r}$ (inputs variables)=[r_1, r_2, …, r_r]; $\bar{p}$ (model parameters)=[p_1, p_2, …, p_p] and $\bar{x}$ (state variables)=[x_1, x_2, …, x_i, …, x_k].

Since the aim is to establish a robust tuning procedure for bending-point detection algorithms in the target variable, it is required to generate all possible profiles which would be analyzed by the algorithm. This requires considering the uncertainty in the inputs and model parameters, and quantifying the uncertainty in the state variables both in short and long time scale. Therefore, in the present methodology, these dynamics are analyzed separately.

Basically, the methodology can be explained in three steps:

(i) Firstly, the effect observed in a long-time scale is analyzed. This is done by considering a low variability of the model inputs ($\bar{r}$) and parameters ($\bar{p}$), and executing steady-state simulations. Named as nominal or mean operating points.

(ii) Later, the effect observed in a short-time scale is analyzed. This is done by considering a high variability of the model inputs ($\bar{r}$) and parameters ($\bar{p}$), and evaluating the response after one cycle. Final states obtained in (i) are used as initial states in this evaluation.

(iii) Finally, after the steady state and one-cycle evaluations, a group of different profiles (with or without bending-points) are obtained. A parameters optimization problem is designed to find proper values for the bending-point point detection algorithm.

A block diagram describing the methodology is depicted in **Figure 6.1**, every part of the diagram and the mathematical notation will be explained in the next sections.

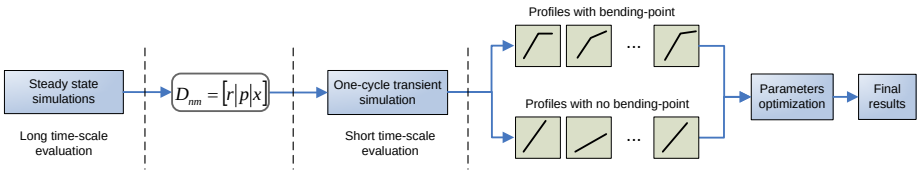

Figure 6.1 Blocks diagram describing the methodology.

6.3.1. Steady state simulation

From the entire variability of the terms involved in the dynamic of a target variable, some of these terms show a slow dynamic effect. This effect can only be analyzed in a long-time evaluation.

Therefore, the response in a steady state simulation is required. This is done by applying a low variability in the mean values of considered input ($\bar{r}$) and parameters ($\bar{p}$), and simulating the process until reaching steady state conditions. This allows quantifying the uncertainty in the state variables ($\bar{x}$).

In this study, because a constant influent is applied and the process is batch-type, the process is considered to reach the steady-state when each of its process states at the end of every batch remains in a certain constant value.

After every simulation, the vectors ($\bar{r}$), ($\bar{p}$) and ($\bar{x}$) can be stored in the rows of a matrix *D*. Therefore, after n-simulations this matrix has the following expression:

$$D_{nm} = \left[\begin{array}{cccc|cccc|cccc} r_{11} & r_{12} & \cdots & r_{1r} & p_{11} & p_{12} & \cdots & p_{1p} & x_{11} & x_{12} & \cdots & x_{1k} \\ r_{21} & r_{22} & \cdots & r_{2r} & p_{21} & p_{22} & \cdots & p_{2p} & x_{21} & x_{22} & \cdots & x_{2k} \\ \vdots & \vdots & \ddots & \vdots & \vdots & \vdots & \ddots & \vdots & \vdots & \vdots & \ddots & \vdots \\ r_{n1} & r_{n2} & \cdots & r_{nr} & p_{n2} & p_{n2} & \cdots & p_{np} & x_{n1} & x_{n2} & \cdots & x_{nk} \end{array}\right] = \left[r_{nr} \middle| p_{np} \middle| x_{nk}\right]$$

For instance, in the study of ammonia valley and nitrate apex in the pH of a SBR process, the input vector ($\overline{r}$) can be made up by the influent fractionation, parameters vector ($\overline{p}$) can consist of parameters of the mathematical model and parameters of operation like air flow-rate and SRT, and the state vector ($\overline{x}$) would include the state variables considered in the mathematical model.

6.3.2. Determining the uncertainty space from steady state simulations (PCA study)

This is a midway step between the steady state and the one-cycle transient simulations. Departing from the data matrix *D*(*n x m*) obtained in the steady-state evaluation, the one-cycle transient simulation requires applying a high variability in the inputs and parameters of every of these n-simulations. Indeed, in order to obtain the different profiles in the one-cycle evaluation, it is necessary to generate multiple profiles for every of the *n* steady-state simulations.

From the structure of matrix *D* it can be observed that, after every run, the final states depend on the inputs and parameters values considered in the simulation, i.e., the data in every row of matrix *D* is correlated.

One way to manage the amount of profiles to generate in the one-cycle evaluation and also to reduce the correlation in matrix *D* is by applying PCA. The PCA transforms a matrix with correlated data in such a way that a maximum of the variance is explained by a new matrix of mutually uncorrelated variables (Jolliffe, 2002). A data processing of matrix *D* by applying Principal Component Analysis (PCA) technique can be useful, because it finds a sub-space in the space of the variables where data mostly vary. The original (*m*)

variables commonly correlated can be linearly transformed into low number of (*l*) uncorrelated variables. As a result, just possible cause/effect scenarios can be obtained.

Let matrix *D* (*n x m*) represented by data (*n* = simulations, *m* = variables), applying PCA it is possible an optimal factorization of *D* into two matrices, *T (n x l)* called the scores matrix, and *L (m x l)* called the loading matrix, plus a matrix of residuals *E (n x m)*. *l* (with $l < m$) is the number of factors considered for the optimal factorization. Therefore, matrix *D* can be expressed as follows:

$$D = TL^T + E \tag{6.2}$$

The condition of the optimality on the factorization is that the Euclidean norm of *E* must be minimized for the given number of factors. It is useful to view PCA as a linear mapping of data from R^m to R^l.

Taking $L^TL=I$ without loss of generality, the mapping has the form $T=DL$. Matrix *T* can be seen as the coordinates of *D* in the new space. The loadings *L* are the coefficients for the linear transformation (also known as eigenvectors). Departing from this mapping, it is possible to reconstruct the measurement vector by reversing the projection back to R^m, that is:

$$\hat{D} = TL^T \tag{6.3}$$

where $\hat{D} = D - E$ is the reconstructed measurement vector. The smaller the dimension of the feature space is, the greater the resulting error.

Figure 6.2 shows the data processing between the steady state simulations and the fast dynamic simulations using the PCA technique.

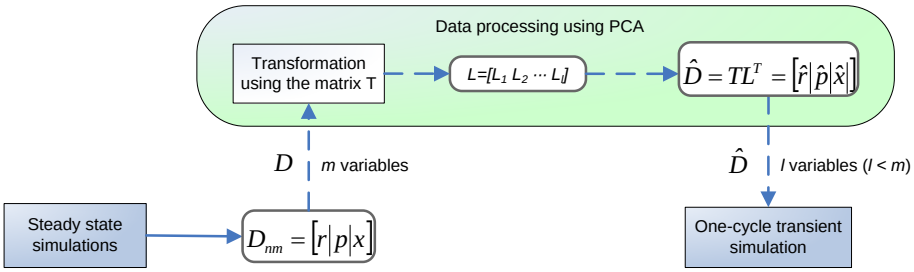

Figure 6.2 Blocks diagram describing the data processing using PCA

Regarding the factors (l), there are many criteria to optimize the amount of factors to take (Jolliffe, 2002; Bouhouche et al., 2007), such as: Cumulative Percent Variance (CPV), Residual Percent Variance (RPV), Size of variance of Principal Components, Minimum Description Length (MDL), Average Eigenvalue (AE), Parallel Analysis (PA), Autocorrelation (AC), scree graph. The CPV, the size of variance of Principal Components and the scree graph are ad-hoc rules which, despite some efforts to put them on a more formal basis, are still intuitive methods. In this case study just CPV and scree graph will be employed. Concerning the CPV rule, to separate the noisy eigenvectors from the smooth ones, the following expression is used:

$$CPV(l) = 100 \cdot \left(\frac{\sum_{j=1}^{l} \lambda_j}{\sum_{j=1}^{m} \lambda_j} \right) \% \qquad (6.4)$$

Where l refers to the index of the principal components, m refers to the number of process variables and λ_j are the eigenvalues. Optimal number of factors (l) is obtained generally when 98% of global change of the considered index (CPV or RPV) is attained.

Regarding the *scree* graph, this is a visual method to determine the number of factors (*l*) to adopt. The scree graph, which was discussed and named by Cattell (1966) but which was already in common use, is even more subjective in its usual form, as it involves looking at a plot of λj against j, and deciding at which value of j the slopes of lines joining the plotted points are "steep" to the left of j, and "non steep" to the right. This value of j, defining an "elbow" in the graph, is then taken to be the number of components *l* to be retained. An alternative to the scree graph, which was developed in atmospheric science, is to plot log(λj) against j; this is known as the log-eigenvalue (or LEV) diagram (Farmer, 1971).

6.3.3. One–cycle transient simulation

Some other terms involved in the dynamic of a target variable show a fast dynamic effect. This effect is notable when a big variation is considered in these terms and a short period of evaluation is assessed. It is assumed one cycle as a short-term evaluation for batch-type processes.

Thus, the aim in this step is to study the fast dynamic response of the target variable considering high variability in some components of vector ($\bar{r}$) and ($\bar{p}$), and obtaining the response after one cycle.

Based on **Equation 6.3**, for any combinations in the loading matrix *L* and by means of the score matrix *T*, it is possible to obtain any point in the m-dimensional space. Indeed, by applying any sample technique (i.e., random, LHS, etc.) in matrix *L*, a matrix $\hat{D}$ (*q x m*) with (*q*) operational points (*q* can be higher or lower than *n*) in R^m can be obtained. Since matrix *D* is composed by vectors ($\bar{r}$), ($\bar{p}$) and ($\bar{x}$), the correspondent ($\hat{r}$), ($\hat{p}$) and ($\hat{x}$) for the *q* new profiles can be generated.

Therefore, the following steps are executed for every of the *q*-simulations:

(i) A sampling (using random, LHS, etc.) is applied to matrix *L* in order to obtain the vectors ($\hat{r}$), ($\hat{p}$) and ($\hat{x}$) according to **Equation 6.3**.

(ii) A high variability is applied to those terms in ($\hat{r}$), ($\hat{p}$) that have a short-term effect in the target variable.

(iii) The final states ($\hat{x}$) are become the initial states for the one-cycle transient evaluation.

(iv) The simulation of one-cycle is assessed.

(v) The profile of the target variable is stored and classified into two groups: U-type profiles (with bending-point) or V-type profiles (with no bending-point).

The total of profiles generated by the one-cycle evaluation will be employed for the tuning algorithm parameters explained in the next section.

6.3.4. Tuning algorithm parameters

This step focuses on to establish a series of requirements in order to obtain proper parameters for the algorithm of bending-point detections.

The profiles obtained from the one-cycle transient evaluation are classified into two groups: profiles with bending-point and profiles with no bending-point. For a robust tuning of the parameters, the following requirements have to be considered: (i) minimization of false detections; and (ii) about true detections: Minimization of the detection time obtained by the algorithm with respect to the detection time expected.

True detection is considered when the algorithm detects a bending-point in a profile in which the organic substrate is digested, and this detection time is equal or higher than the detection time expected.

False detection is considered in three cases: (i) when the algorithm detects a bending-point in a profile where the organic substrate is not completely digested; (ii) when the algorithm does not detect a bending-point in a profile where the organic substrate is already digested; and (iii) when the detection time obtained by the algorithm in a profile with organic substrate digested is lower than the detection time expected.

These requirements can be solved by means of an optimization problem, where the objective is to find proper values for a set of parameters [a_1, a_2,…, a_z] for the algorithm of bending-point detections. The optimization problem can be expressed as follows:

$$\min_{[a_1,a_2,...,a_z]} \left\{ \frac{1}{U}\sum_{u=1}^{U}\left[t_b^{(u)} - t_a^{(u)}\right] + \frac{1}{V}\sum_{v=1}^{V} t_b^{(v)} \right\} \tag{6.5}$$

$$\text{subject to: } \begin{cases} \left[t_b^{(u)} - t_a^{(u)}\right] \geq 0 \quad \text{for every} \quad u \in U \\ a_1 \in \left[\underline{a_1}; \overline{a_1}\right];\ a_2 \in \left[\underline{a_2}; \overline{a_2}\right];\ ...;\ a_z \in \left[\underline{a_z}; \overline{a_z}\right] \end{cases}$$

Where *U* denotes the group of profiles with bending-point, *V* denotes the group of profiles with no bending-point, the terms *u* and *v* denote the *u-th* and *v-th* profile being evaluated from the total of *U* and *V* profiles respectively, t_b denotes the bending-point detection time obtained by the algorithm, and t_a denotes the detection time expected, these detection times are represented in **Figure 6.3**.

Minimum $\left(\underline{a_k}\right)$ and maximum $\left(\overline{a_k}\right)$ values for the set of *a*-parameters $\left[a_1,a_2,...,a_z\right]$ must be known before implementing the parameters optimization problem.

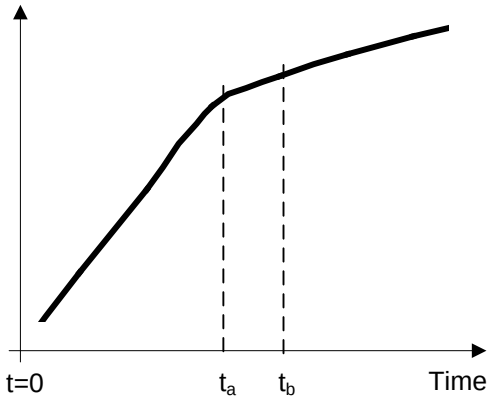

Figure 6.3 Representation of t_a and t_b in a profile with bending-point.

It is expected that the detection time obtained by the algorithm (t_b) is higher or at least equal to the detection time expected (t_a).

Finally, the best set of parameter values are obtained from the optimization problem resolution. The true and false detections obtained as well as the mean detection time of the true detections are stored in matrices; the analysis of these matrices can be assessed via checkerboard plots representation, where the best and worse zones of bending-point detections can be observed.

6.4. ATAD as case study

In **Chapter 1** the ATAD was described as a technology that uses the air as a source of oxygen to aerate the sludge, promoting the substrate digestion. The operation is autothermal, i.e., the heat required for the increase in temperature is supplied completely from the exothermic breakdown of organic and cellular material.

Form the ATAD mathematical model explained in **Chapter 3**, the sludge temperature tendency during the digestion can be expressed mainly by the following expression:

$$\frac{dT_{liq}}{dt} \approx k \cdot \frac{S_s}{K_s + S_s} \cdot \frac{S_{o2}}{K_{oxi} + S_{o2}} \cdot X_{bh} \cdot V_{liq} \quad [^{o}C \cdot day^{-1}] \qquad (6.6)$$

Where k includes the product of some terms (the stoichiometric term related to the yield, the specific biological heat production and the water specific heat), Ss is the readily biodegradable substrate, S_{o2} is the dissolved oxygen which is generated from the air flow-rate (Q_{air}), X_{bh} is the heterotrophic biomass, K_s is the half-saturation coefficient for growth, K_{oxi} is the half-saturation coefficient for oxygen and V_{liq} is the liquid volume in the reactor.

Equation 6.6 reflects that the sludge temperature tendency depends on the dynamic responses of some state variables of the model, and the influence of inputs and model parameters. Changes in the influent/effluent flow-rate, ambient temperature and biomass concentration present a long-term effect in the sludge temperature evolution. On the other hand, the air injection and the influent fractionation (specifically the readily biodegradable substrate) present a short-term effect. In order to find all possible sludge temperature profiles, these short and long term dynamics must be studied separately.

In **Chapter 4** two control strategies were developed for the ATAD, these strategies include an algorithm based on the bending-point detection applied to the sludge temperature tendency. The application of these strategies without any tuning of the algorithm parameters may results in bad results of these control solutions, therefore, it is necessary to find appropriate values for the algorithm parameters, i.e.: the angle of detection (α) and the window-size (N), for a good performance of these strategies.

Thus, the idea is to apply the methodology presented in this Chapter in order to obtain the best pair of parameters for the bending-point algorithm in an ATAD

plant-layout, taking into account all the possible temperature profiles that the influent and the plant can generate.

As it was defined in the methodology, the slow and fast dynamics are studied separately. For this, a plant-layout and input uncertainty variables are established to apply the methodology in this particular case. The results are describes as follows.

6.4.1. The plant model selection

For this case study, the mathematical model of the ATAD is based on the model explained in **Chapter 3**. The features of the ATAD plant-layout (dimensions, sludge influent) were adopted from the AT_BSM protocol discussed in **Chapter 5** (see **Figure 6.4**).

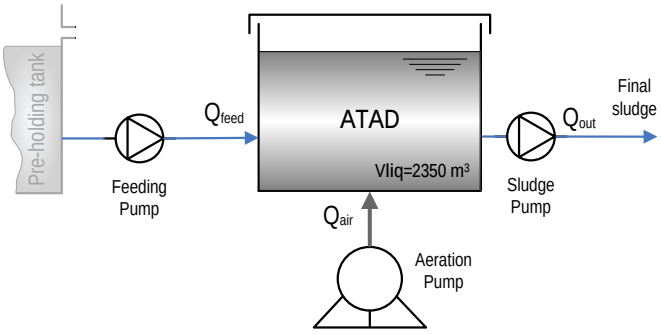

Figure 6.4 Plant-layout of the AT_BSM

6.4.2. Input uncertainty ranges

The following terms were considered for uncertainty: the total influent COD and fractionation parameters for the readily and the slowly biodegradable substrate (f_{Xr} and f_{Xs}), the influent/effluent flow-rate (indirectly referred by the SRT), the air injected (Q_{air}) and the ambient temperature (T_{amb}).

Regarding the influent, the medium input uncertainty values are considered from the raw sludge used in the BSM2 evaluation. All the uncertainty terms are assumed to have uniform probability distribution and a pre-defined variability around the mean value. The uncertainty ranges are summarized in **Table 6.1**.

Table 6.1 Input uncertainty ranges considered

	Steady state evaluation		One-cycle evaluation		
Parameter	Lower bound	Upper bound	Lower bound	Upper bound	Units
COD_{total}	42	48	31	58	g COD·m^{-3}
fXs	69%	71%	65%	75%	g COD·(g COD_{total})$^{-1}$
fXr	2%	4%	1%	5%	g COD·(g COD_{total})$^{-1}$
SRT	11	13	11	13	day
Q_{air}	55000	75000	42000	94000	m^3·day^{-1}
T_{amb}	14	16	10	20	ºC

Sampling technique

Latin Hypercube Sampling (LHS) is adopted to sample the parameters space. This technique has proved to give an effective coverage for the total parameters uncertainty (McKay et al., 1979). In the Matlab/Simulink® platform, the function *lhsdesign* was used for the LHS. For further details about the LHS technique see **Annex B**.

6.4.3. Application of the methodology

Steady state simulations

For this step, a region for steady-state conditions is obtained considering the bounds of uncertainty referred in **Table 6.1**. Employing the notation detailed in **Section 6.3**, the elements considered for this evaluation can be grouped in

vectors ($\bar{r}$) and ($\bar{p}$) as follows: $\bar{r} = [f_{Xr}, f_{Xs}, COD]$ and $\bar{p} = [SRT, Q_{air}, T_{amb}]$.

Therefore, considering the vectors ($\bar{r}$), ($\bar{p}$) and the mass and enthalpy elements of the state variables in the mathematical model (see **Table 3.3** in **Chapter 3**), every row in matrix *D* has the following elements:

$$\left[\bar{r} \;\middle|\; \bar{p} \;\middle|\; \overline{M} \;\; \overline{H}\right] = \left[f_{Xr} \; f_{Xs} \; COD \middle| SRT \; Q_{air} \; T_{amb} \middle| MS_s \; MS_{o2} \; MS_{hco3} \; MS_{co2} \; MS_{n2} \; MS_{nh4} \; MS_{nh3} \; MS_h \; MS_{oh} \; MS_{h2po4} \; MX_s \; MX_{bh} \; MX_i \; MX_{inor} \; MG_{h2o} \; MG_{co2} \; MG_{o2} \; MG_{n2} \; MH_{liq} \; MH_{gas}\right]$$

The element MS_{H2O} was used to calculate the mass elements for the rest of the variable states in liquid phase and was not included in matrix *D*, the elements [MS_i, MS_{hpo4}, M_{Xr}] were neglected since their values were close to 0.

It is assumed that the average operation of the ATAD satisfies the pasteurization and stabilization criteria; therefore, all the profiles obtained in the steady state evaluation have to achieve these requirements. It was decided to obtain a total of 2000 profiles that satisfy these requirements, resulting in a matrix *D* of 2000 x 26 elements (rows corresponds to simulations, columns correspond to data).

Determining the uncertainty space from steady state simulations (PCA study)

In this step, the aim is to explain a maximum of the variance of the correlated data in matrix D (2000 x 26) by a new matrix of uncorrelated variables defined by the number of factors (*l*). Therefore, the application of PCA to the matrix D is assessed. It is crucial to determine (*l*) since a low number of these factors will not reproduce the data of matrix *D* properly.

As it was referred in **Section 6.3.2**, the CPV and scree graph were employed to determine (*l*). **Figure 6.5(a)** shows the distribution of the twenty six (26) factors obtained for the case study using the CPV indicator, **Figure 6.5(b)** shows the scree graph associated.

(a) **(b)**

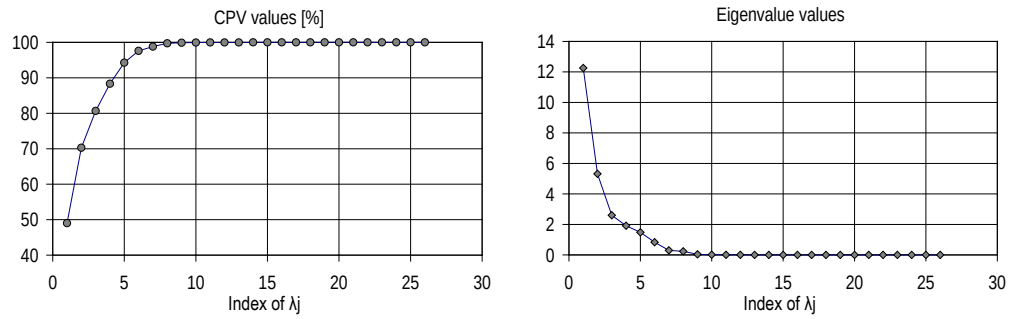

Figure 6.5 Distribution of eigenvalues. **(a)** CPV values. **(b)** Scree graph.

It is observed that both criteria suggest at least the first seven (7) principal components (from a total of 26) of the loading matrix *L* in order to reproduce more than 98% of the total variation of matrix *D*.

One-cycle transient simulation

This step focuses on to obtain all the possible ATAD's temperature profiles in one-cycle evaluation when a large variability is applied in some of the inputs and parameters of operation that affect the sludge temperature profile.

Therefore, according to the steps described in **Section 6.3.3**, it was assumed a total of q=5000 new profiles to be generated, a LHS is applied to the matrix L (26 x 7) to generate the vectors ($\hat{r}$), ($\hat{p}$) and ($\hat{x}$). From the total of terms in the vectors ($\hat{r}$) and ($\hat{p}$), just the terms $\left[f_{Xr}, f_{Xs}, COD\right]$ in ($\hat{r}$) and $\left[Q_{air}\right]$ in ($\hat{p}$) were selected in order to apply a high variability according to the bounds established in **Table 6.1**.

The profiles obtained are classified into two groups: *U*-type profiles (with bending-point, i.e., profiles where the organic substrate was digested) and *V*-type profiles (with no bending-point, i.e., profiles where the organic substrate has not been digested). These profiles are drawn in **Figure 6.6(a)** and **6.6(b)** respectively. *U* and *V* profiles will be employed in the tuning algorithm parameters explained in the next section.

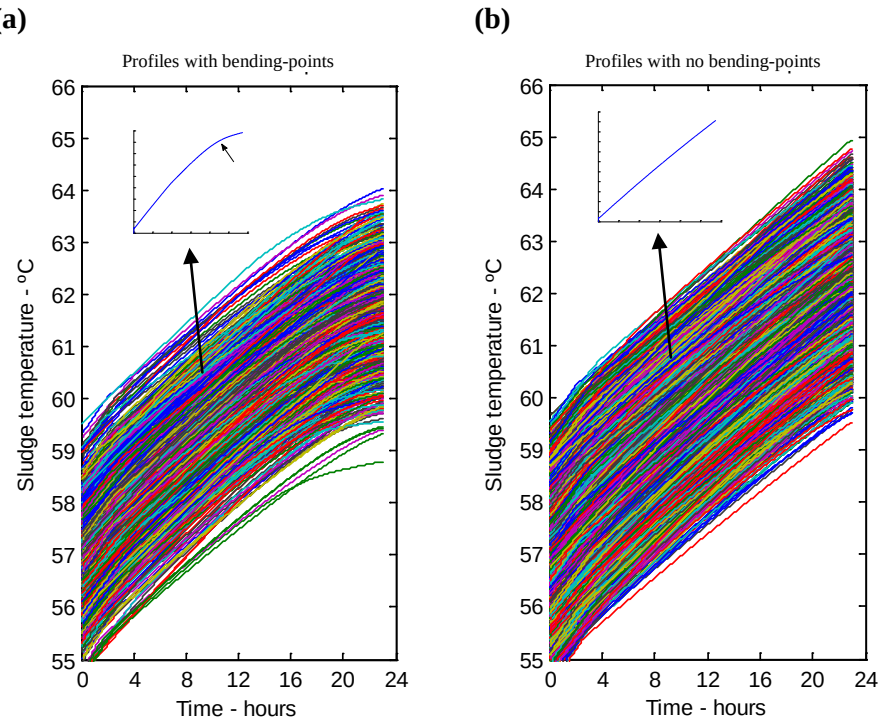

Figure 6.6 Profiles obtained alter one-cycle transient evaluation. **(a)** Profiles with bending-point. **(b)** Profiles with no bending-point. (5000 runs).

It can be observed the band of all possible profiles obtained after applying the once-cycle transient evaluation. The detail of one profile with a bending-point occurrence is shown in **Figure 6.6(a)**, in the same way, the detail of one profile with no bending-point occurrence is shown in **Figure 6.6(b)**.

Tuning algorithm parameters

As referred in the methodology, this step focuses on to obtain proper values for the parameters of the bending-point detection algorithm, in this particular case, the parameters are N and α. From **Equations 6.5** the optimization problem for the case study is expressed as follows:

$$\min_{[N;\alpha]}\left\{\frac{1}{U}\sum_{u=1}^{U}\left(t_b^{(u)}-t_a^{(u)}\right)+\frac{1}{V}\sum_{v=1}^{V}t_b^{(v)}\right\} \tag{6.7}$$

$$\text{subject to: } \begin{cases}\left[t_b^{(u)}-t_a^{(u)}\right]\geq 0 \quad \text{for every} \quad u\in U \\ \\ \qquad N\in[2;60]\,;\ \alpha\in[1;15]\end{cases}$$

The bounds for N and α were considered in order to delimit the solution of the algorithm parameters to a range of reasonable values. Therefore, departing from the *U* and *V* profiles obtained in the one-cycle transient evaluation and the **Equation 6.7** for the optimization problem, the best pair of (N; α) parameters can be obtained.

As it was referred previously in the methodology, t_a denotes the detection time theoretically expected, and t_b denotes the bending-point detection time obtained when the algorithm is applied. For a typical sludge temperature profile with bending-point, these times can be represented as follows in **Figure 6.7**.

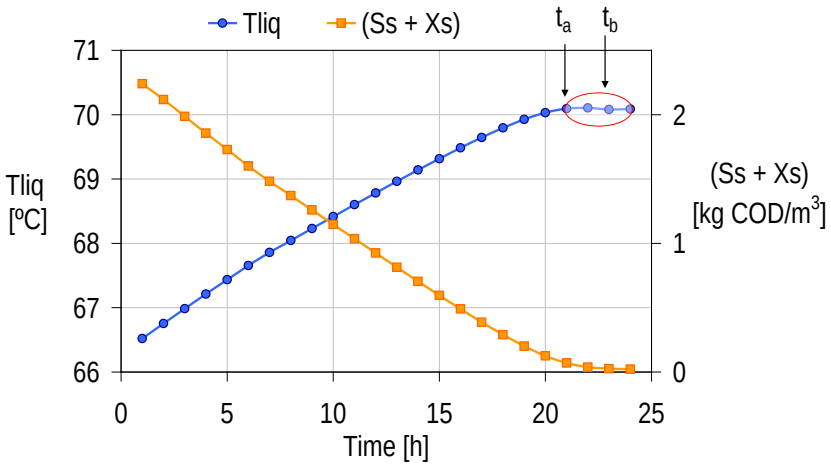

Figure 6.7 Representation of t_a and t_b in the ATAD bending-point temperature profile.

The detection time t_a is related to the moment when the amount of readily and slowly biodegradable substrate was consumed (bending-point effect in the sludge temperature); therefore this detection time is obtained if an ideal biodegradable substrate sensor is connected to the ATAD, allowing to measure the substrate digestion rate. For this purpose, it was defined that t_a is obtained when 95% of the initial biodegradable substrate is consumed (see the detection time t_a in **Figure 6.7**). This ideal detection time is compared with the time obtained from the algorithm (t_b). Hence, the bending-point detection algorithm was subject to give a detection time t_b equal or higher than the time t_a. The zone in the temperature profile where t_b is expected to be detected is represented in **Figure 6.7** with red color.

From the set of requirements defined in **Equation 6.6** for the tuning algorithm parameters, the best pair of parameters (N; α) are obtained, these results are shown in **Table 6.2**.

Table 6.2 Results for the parameters optimization

N [size]	**α [°]**	$mean\left(t_b^{(u)} - t_a^{(u)}\right)\Big\|_U$ **[minutes]**
56	3	24.32

In order to check the results given by the tuning algorithm parameters, the true detections and the mean detection time obtained for the total of bending-point profiles obtained are recorded in matrices (N *x* α); checkerboard plots of these matrices are depicted in **Figure 6.8**.

(a)

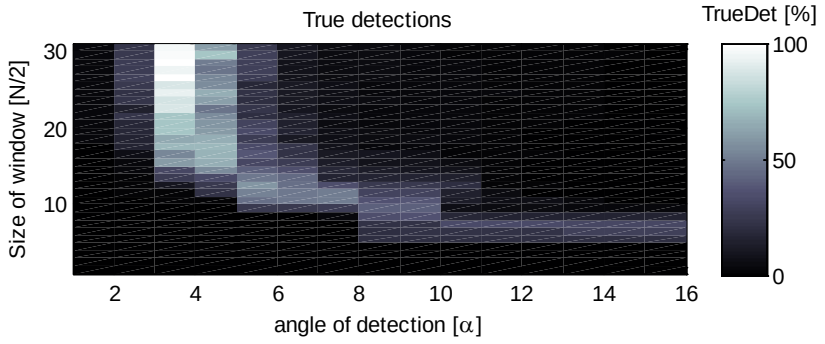

(b)

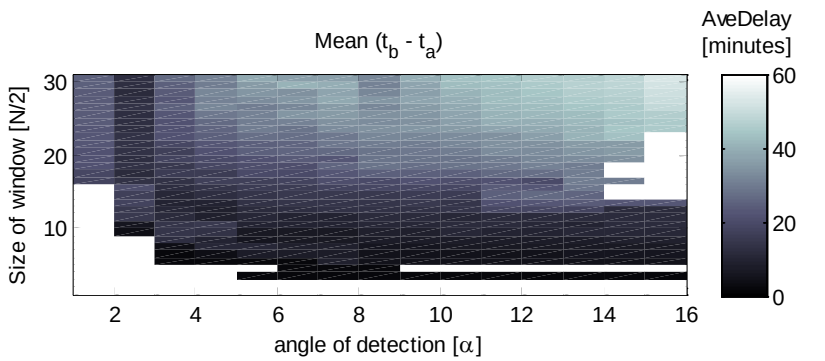

Figure 6.8 Checkerboard plots indicating the detections obtained (matrices N x α). **(a)** True detection matrix. **(b)** Mean detection time matrix.

Where two indices were defined: TrueDet [%] and AveDelay [minutes]. TrueDet refers to the percentage of true detections achieved by the algorithm, and AveDelay refers to the mean delay obtained between the detection time obtained by the algorithm and the detection time expected. The AveDelay is defined by:

$$AveDelay = \frac{1}{U}\sum_{u=1}^{U}\left(t_b^{(u)} - t_a^{(u)}\right) \tag{6.8}$$

TrueDet takes values from 0% (minimum of true detections) to 100% (maximum of true detections). AveDelay takes values from 0min (minimum delay obtained) and 60min (maximum delay obtained). These regions are indicated by gray scales in **Figure 6.8**.

It can be observed in this figure that there is a region for (N; α) where high TrueDet can be obtained (zone in white color). Moreover, as expected, low values of TrueDet are obtained for low values of N considering any α. A similar behavior is found for a low α considering any N. This shows the sensitivity of the algorithm to false detections in these zones.

It can be observed from the TrueDet and AveDelay matrices that, for certain parameters values, low values of AveDelay don't mean high values in the TrueDet matrix. On the other hand, high values in AveDelay don't mean to obtain worse TrueDet values. Therefore, the parameters optimization tries to find the best pair of values to maximize the true detection, to minimize the false detection and to obtain a low delay from the total of different profiles evaluated.

6.5. Considering the noise effect

Until now and without loss of generality, the application of the methodology has considered an ideal signal value in the sludge temperature, i.e. a temperature signal without noise. In this case, before and after the slope changing, the signal follows two perfect lineal dependences. This allows easy bending-point detections because the corner to be detected is well defined.

Real signals include the noise effect, which can lead to a bad response of the bending-point algorithm if the parameters values obtained assuming no-noise conditions are used in noise conditions.

Therefore, a further step in this study is to incorporate the noise effect in the temperature profile. This is done by adding the noise to the target signal previously considered. Under this new consideration, a new pair of values (N; α) is obtained. **Figure 6.9** shows the adaptation of **Figure 6.1** when the noise signal is considered.

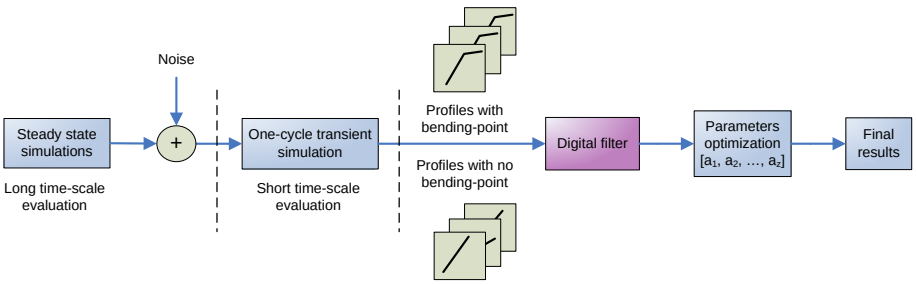

Figure 6.9 Noise and digital filter included in the methodology

Consequently, due to the new features of the signal obtained, it was necessary to apply a signal filter, thus some common digital filters were considered in this study. This will lead to evaluate the effect of the filters performance into the final results.

Indeed, since the filter parameters will adequate the signal, these parameters will affect the results of the optimization problem. In this study the digital filter effects were analyzed separately, but it would be possible to include the filters parameters in the tuning algorithm parameters (**Equation 6.5**) in order to solve the optimization problem in a more general way.

In the next sections, the noise model is described, then a basic description of digital filters is introduced, and finally, results for the methodology applied to the ATAD are shown when the noise effect is considered in the sludge temperature signal.

6.5.1. The noise signal model

A simplified noise description is included in the sensor temperature. The idea is not to model the noise exactly; this leads to require a complex model, but just to take into account its main effects.

The noise effect (and sensor models) was studied by Rieger et al. (2003) and Rosen et al. (2008), where a relative standard deviation is defined to model the noise variation depending on the actual measuring value.

In this methodology, the noise signal was generated using the Gaussian Noise Generator box in Matlab/Simulink®. Accordingly, the noise signal is a sequence of serially uncorrelated random variables with zero mean and finite variance. From typical temperature sensors, a variance of $1.5 \cdot 10^{-3}$ ºC was assumed in the study. Effects of drift, delay and response time were not considered. The temporal evolution and histogram of the noise signal adopted are depicted in **Figure 6.10(a)** and **6.10(b)** respectively. The histogram was obtained considering 662400 samples in **Figure 6.10(a)**.

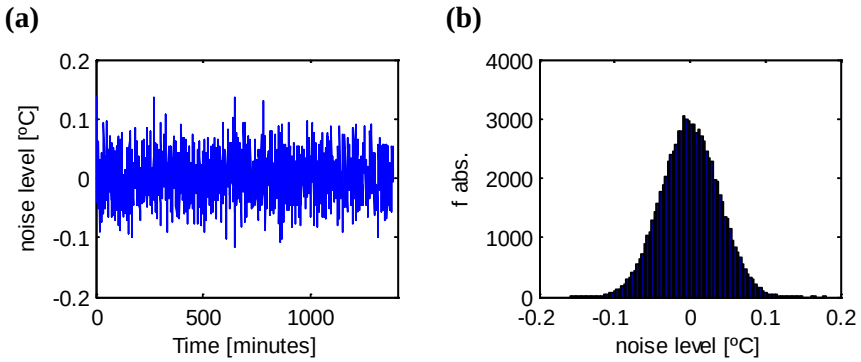

Figure 6.10 The noise signal. **(a)** Temporal evolution. **(b)** Histogram.

6.5.2. The digital filters

Like in any sampled signal, the signal provided by the sludge temperature sensor is a discrete-time signal (non continuous). Due to this signal behavior plus the noise effect added, a kind of filter has to be applied to enhance the signal obtained. Digital filters are systems that perform mathematical operations on a discrete-time signal to reduce or enhance its aspects, although this enhancement is obtained at expenses of some loss of information from the raw signal. The following diagram shows this system.

Figure 6.11 Block diagram representing a digital filter

Due to the discrete-time form of the signal to be filtered, the equation of a digital filter is written by means of differences, the general form of this equation is as follows:

$$y(n) = \sum_{k=0}^{N} a(k) \cdot x(n-k) - \sum_{k=1}^{N} b(k) \cdot y(n-k) \quad (6.9)$$

Where *y(n)* is the current filter output, the *y(n-k)* are previous filter outputs, the *x(n-k)* are the current or previous filter inputs, *a(k)* and *b(k)* are the filter coefficients, *N* is the number of samples considered in the filter.

6.5.3. ATAD: Considering noise in the sludge temperature signal

From the vast amount and types of digital filters found in the signal processing field, just two types of digital filters were considered in this study: CIC filter and Tukey Window. These filters consider only previous filter inputs in their equations.

It was decided to leave the extensive theory and the mathematics that digital filters requires, thus just basic ideas and principles are shown. For more information related to this subject, the specialized literature and the proposed references have been included in this thesis.

For practical purpose, it was assumed that the original signal (from the sludge temperature sensor) is sampled every 1 second, and the considered digital filters have a sample time of 1 minute, therefore, decimation by 60 is applied to the original signal.

CIC filter

The Cascade-Integrator-Comb (CIC) filter was introduced in signal-processing by Hogenauer (1981). The CIC filter is considered as an equivalent form of the *moving averager*. The CIC filter expression applied for the sludge temperature signal of the ATAD is as follows:

$$T_{liq}^{(f)}(n) = \frac{1}{N}\sum_{k=0}^{N} T_{liq}(n-k) \tag{6.10}$$

Where $T_{liq}^{(f)}$ denotes the sludge temperature signal already filtered (filter output), $T_{liq}(n-k)$ denotes the previous samples of the sludge temperature signal to be filtered. Comparing to **Equation 6.9**, the filter coefficients *a(k)* of the CIC filter take the value 1.

Tukey Window

A variant of the CIC filter is the Tukey Window, in this filter is possible to modify the weight of the filter coefficients. Let consider N as the total of samples to be filtered, the Tukey Window can be described as a cosine lobe of width (β/2)·N, convolved with a rectangle of width (1 to β/2)·N. Where β is ranged from 0 to 1, and represents a parameter that defines the window coefficients. For instance, the mathematical model of the weighted coefficients for a Tukey Window with β =0.1 is given as follows:

$$b(n) = \begin{cases} 0.5[1-cos(\cdot\pi n)] & for \quad 0 \le n \le 0.1N \\ 1 & for \quad 0.1N \le n \le 0.9N \\ 0.5[1-cos(\pi n)] & for \quad 0.9N \le n \le N \end{cases} \tag{6.11}$$

The weighted coefficients in time domain for a Tukey Window with β values of 0.25; 0.5 and 0.75 are shown in **Figure 6.12**.

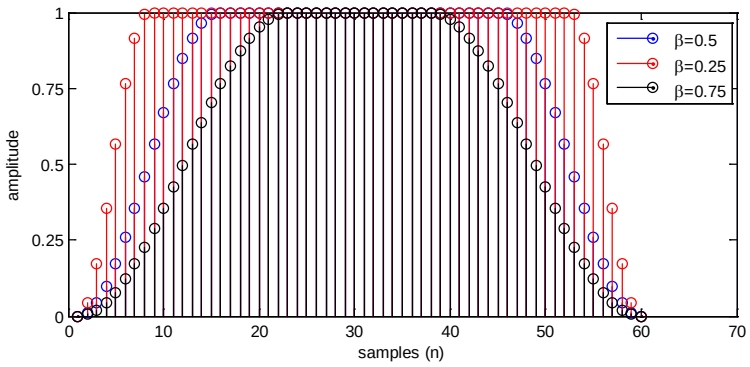

Figure 6.12 Weighted coefficients of a Tukey Window for different values of β.

Hence, after applying the Tukey Window to the sludge temperature signal, the filter output can be expressed as follows:

$$T_{liq}^{(f)}(n) = \sum_{k=0}^{N} b(n) \cdot T_{liq}(n-k) \tag{6.12}$$

Figure 6.13 shows the effect of the noise signal in the sludge temperature signal, and the filter outputs obtained after applying the CIC and Tukey Window filters.

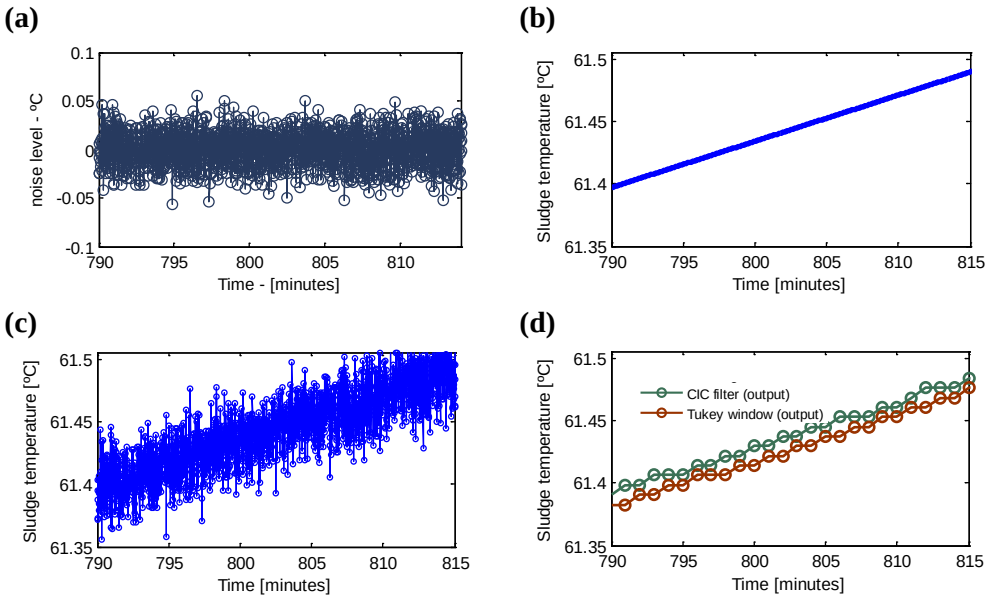

Figure 6.13 (a) Noise signal, **(b)** Ideal sludge temperature signal, **(c)** sludge temperature signal + noise, **(d)** Different filters response for the signal depicted in **(c)**.

It can be observed that the output signal obtained from the digital filters reduces the noise effect added to the ideal signal, but will never give a signal identical to the ideal one.

After applying the methodology, considering the noise signal and the digital filters previously explained, the results of the tuning algorithm parameters are listed in **Table 6.3.**

Table 6.3 Bending-point parameters for different digital filters

Digital Filter	Noise?	N/2 [samples]	α [º]	$mean\left(t_b^{(u)} - t_a^{(u)}\right)_U$ [minutes]
CIC	No	28	3	24.32
CIC	Yes	29	6	27.26
Tukey Window	Yes	27	5	25.61

It can be observed that in ideal conditions (no noise) the mean detection time obtained was the lowest. When the noise is considered, possible false detection may occur, therefore, an increase in both the number of samples of the moving-window and the angle of detection were obtained by the tuning algorithm in order to guaranty the best pair of values (N; α) for correct detections.

6.6. Conclusions

It was demonstrated that, for a robust tuning of control algorithms based on the bending-point detection of a target signal, the decoupling of the dynamics that affect this signal allowed obtaining different profiles to be evaluated by the algorithm. A sub-conjunct of these profiles will give a solution of the algorithm parameters that will not work properly for a real case.

The incorporation of the PCA technique in the methodology allowed finding the uncertainty space of the variables involved in the generation of the profiles to be evaluated.

The noise signal and the digital filters showed an important effect in the bending-point study. As part of a real signal, the noise effect can not be neglected in the trending analysis.

The proposed methodology has a practical application; it can be applied to any other sequential processes (SBR, Biodenitro/Biodenipho, etc.) that require the tuning of bending-point detection algorithms for specific target signals. Therefore, for the application of this methodology in other processes, it is necessary to know the following aspects: the operational point of the process; the target signal to be monitored for bending-point occurrences, and the set of inputs and model parameters (bounds of variability) that can originate the bending-point profiles.

7

Validation of controllers by simulations

Chapter 7 Performance analysis of controllers

In this chapter, the validation of the controllers ST1 and ST2 developed in **Chapter 4** is presented. This validation was assessed following a set of guidelines according to the benchmark detailed in **Chapter 5**.

The chapter is organized as follows: **Section 7.1** details the software implementation of the AT_BSM benchmark, showing the structure adopted for the simulator. Using the methodology described in the AT_BSM benchmark, the results for the control strategy performance are presented in **Section 7.2**. These results are summarized in indices of evaluation that give information about the plant performance in closed-loop operation. Additionally, for a better quantification of controller performance, the simulation study has also analyzed the effect of uncertainty in some coefficients of the mathematical model. This study is presented in **Section 7.3**. Preliminary results from an experimental validation of the ST2 are presented in **Section 7.4**. Finally, some conclusions are given in **Section 7.5**.

7.1. Software implementation of the AT_BSM

A typical implementation for control systems basically consists of five different subsystems: (1) process; (2) online sensors; (3) actuators; (4) controller devices, that implement the control algorithms; and (5) the supervisory control and data acquisition (SCADA), it is the interface to the operator.

A similar architecture applied for automation and control in full-scale WWTP was recently presented by Brockmann et al. (2011), where a multilayer architecture is proposed. This architecture separates mathematical modeling of components related to the treatment process from instrumentation, actuators, and components related to automation and control. In the case of the AT_BSM implementation, the architecture adopted for the subsystems is depicted in **Figure 7.1**.

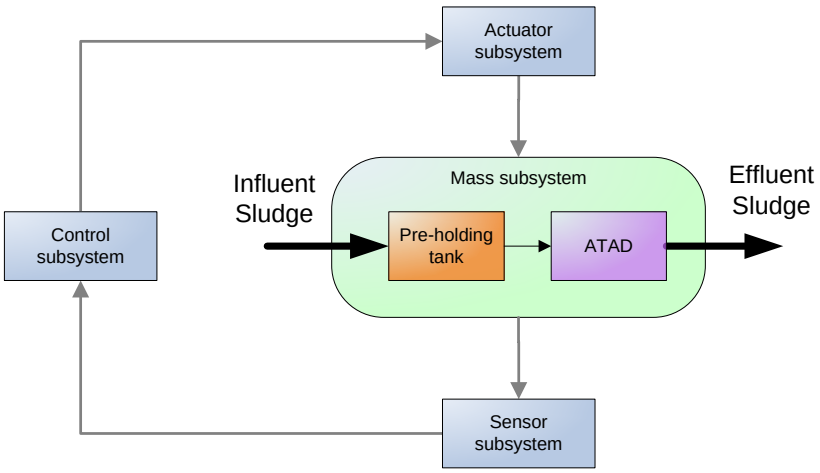

Figure 7.1 Subsystem architecture adopted for the AT_BSM. Black arrows represent mass and energy flows, gray arrows represent data flows.

Based on the subsystems architecture, Matlab/Simulink® was adopted as the simulation platform for this study. **Figure 7.2** shows the structure of subsystems applied for the AT_BSM. The block structure in Matlab/Simulink® allows the interconnection between blocks with different tasks (modeling, control, plotters, registers, switches, etc.). Thus, any variable can be plotted in scopes and can be recorded in vectors for further analysis.

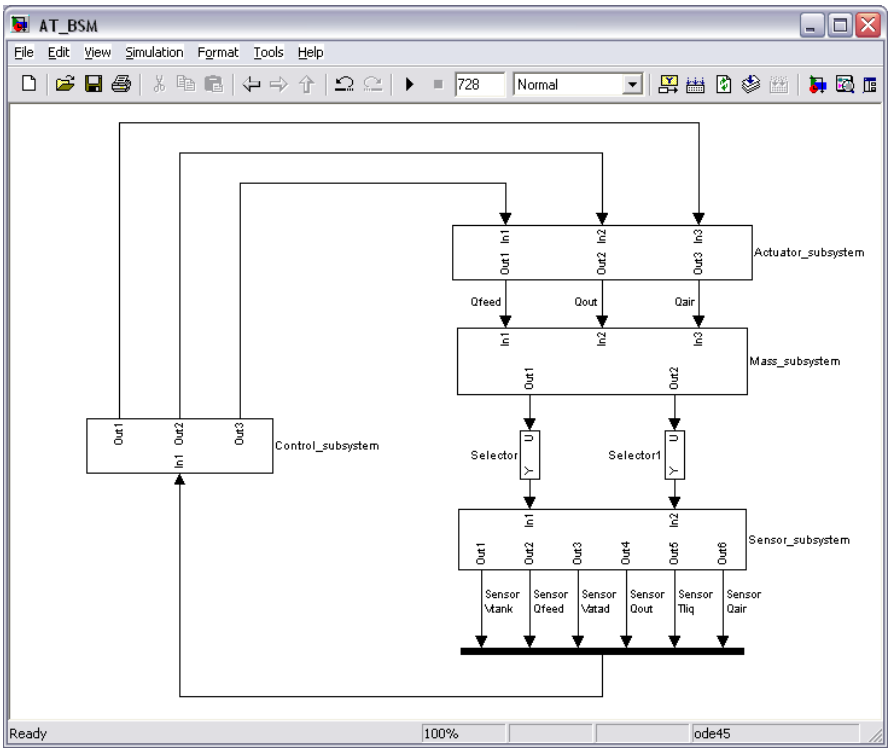

Figure 7.2 Architecture of subsystems applied to the AT_BSM

The idea of the modeling based on subsystems is to establish a clear separation between the mathematical modeling of components related to the process (tanks, reactors, hydraulic flow) and components related to the automation and control devices (sensors, actuators, information flow). In this respect, this architecture includes four basic layers for: mass, sensors, controllers and actuators. Every layer in the general schema is described as follows:

The Mass Subsystem

The mass subsystems contain the physical processes to control. This subsystem includes the hydraulics and the mathematical models of the pre-holding tank and ATAD (see **Figure 7.3**). The model of these two processes is based on the

mathematical model detailed in **Chapter 3**. The software implementation was based on *S-functions* in C-code, while model coefficients, initial states, and general setting of the processes were implemented using *m-files*.

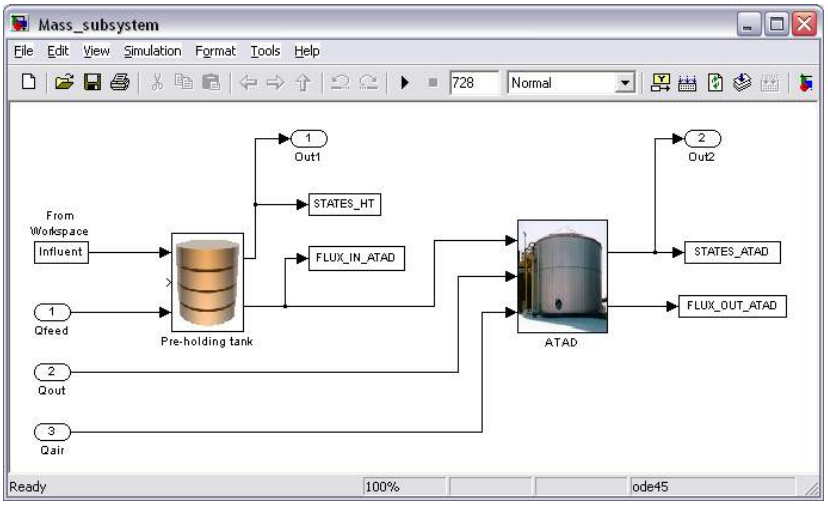

Figure 7.3 The Mass Subsystem

The Sensor Subsystem

This subsystem receives different ideal measurements from the mass subsystem, and appropriate signals for the control layer are generated. Every sensor is modeled like an independent subsystem, as is depicted in **Figure 7.4**. Only ideal sensors (instantaneous dynamic response and no-noise) were considered in this implementation for the principal signals (V_{tank}, V_{atad}, Q_{air} and T_{liq}).

However, in the sensor subsystem generic models of sensors were included like those studied by Rieger et al. (2003), these sensor models can be configured to include delay and noise effect in the measurement, depending on the control problem requirements.

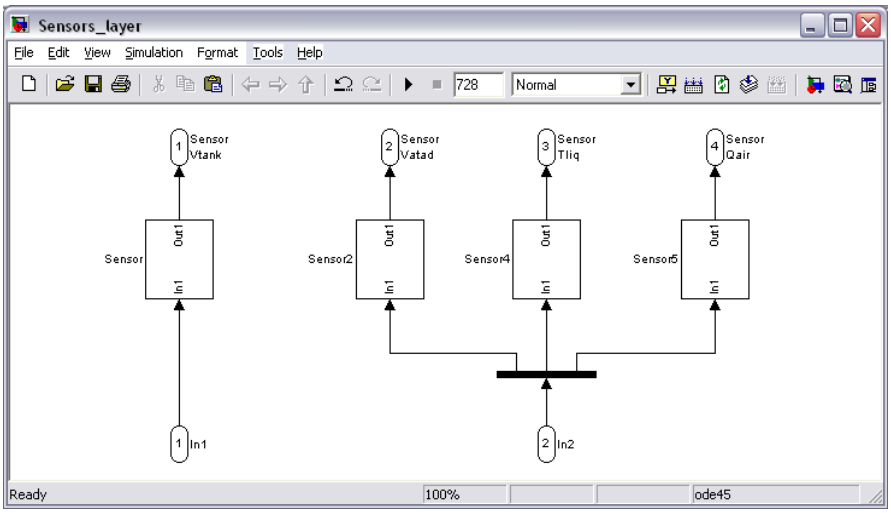

Figure 7.4 The Sensor Subsystem

The Actuator Subsystem

This subsystem contains the manipulate variables of the processes. Once the control action is calculated in the control subsystem, this information is received in the actuator subsystem in order to adjust the associated manipulate variables of the processes. In this implementation, the air flow-rate (Q_{air}) and the feeding flow-rate to the ATAD (Q_{feed}) were considered as manipulate variables. Although it was assumed an ideal action in these actuators, generic models of actuators were included inside the AT_BSM for future applications, similarly to those considered for the sensor subsystem.

The Control Subsystem

This subsystem includes a Low and a High Level Control. The low level control is in charge of feeding and emptying actions. The high level control is in charge of the air flow-rate manipulation; here ST1 and ST2 are programmed. This subsystem receives the following signals: operational mode of the plant

(manual/automatic), indicators, cycle time, set-points and control parameters. The low and high levels were implemented using *S-functions* in C-code.

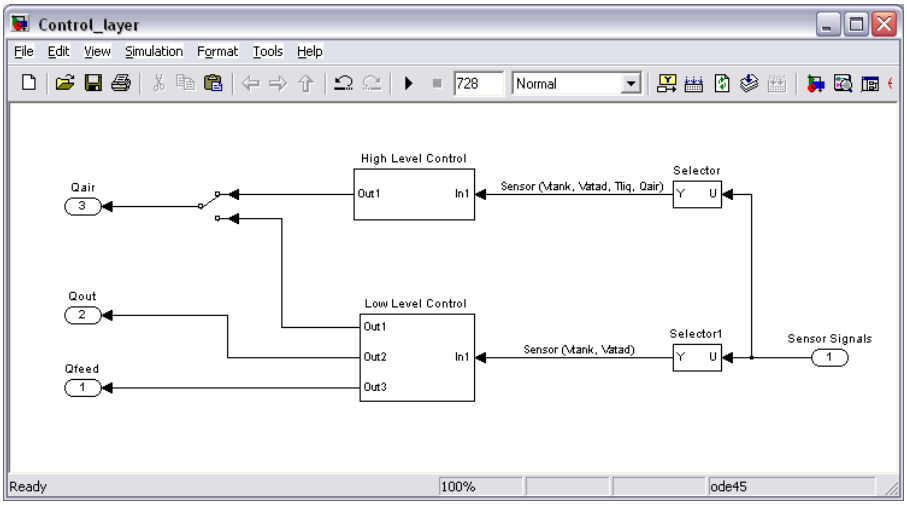

Figure 7.5 The Control Subsystem

7.2. Performance analysis of the ST1 and ST2 controllers

The results obtained for the validation of the control strategies ST1 and ST2 are detailed in this section. The purpose is to quantify the global benefits in the long term when these control strategies are applied, comparing the performance with a conventional open loop (OL) operation.

In order to obtain objective conclusions, both control strategies were evaluated according to the validation protocol established in the AT_BSM benchmark, obtaining the set of indices that give information about the global operation in every case. The results obtained by applying the open loop strategy (OL) are taking as reference values for performance comparison.

Regarding the validation, the general equations of the control strategies and the parameters considered are depicted in **Table 7.1**.

Table 7.1 Equation of the control strategies implemented

Strategy	General equation	Control parameter considered (1)	Bending-point parameters (2)
ST1	$Q_{air}^{(i)}(t) = k_a^{(i)}(t) \cdot Q_{air}^{(o)}$	$Q_{air}^{(o)}$ = 65000 $m^3 \cdot d^{-1}$	N=56 ; α = 3°
ST2	$Q_{air}^{(i)} = k_a^{(i)}(t) \cdot \left[Q_{air}^{(i-1)} + k_b^{(i-1)} \cdot \Delta Q \right]$	ΔQ_{up} = 2.55 $m^3 \cdot m^{-3}_{atad} \cdot d^{-1}$; ΔQ_{down} = -0.42 $m^3 \cdot m^{-3}_{atad} \cdot d^{-1}$; max ($Q_{air}$) = 1.3·$Q_{air}^{(o)}$	

(1) ΔQ_{up} and ΔQ_{down} are normalized to a V_{atad} = 2350 m^3.

(2) Values obtained in **Chapter 6** (see **Table 6.2**)

Recalling that the principal objective of ST2 is to maximize the number of stabilized cycles, it was decided to adopt different values for the increment (ΔQ_{up}) and decrement (ΔQ_{down}) action for the air flow-rate. In this study, it was prioritized the increment than the decrement action in order to find more bending-points during the operation. After different tests, the parameters selected for this purpose are depicted in **Table 7.1**.

The results of the performance indices for OL and the closed-loop cases (ST1 and ST2) are given in **Table 7.2**.

Table 7.2. Results of the performance indices for ST1 and ST2

Strategy	PQI(1) [%]	Knees(2) [#]	StQI(3) [%]	WV_{out}(4) [$m^3 \cdot d^{-1}$]	ThE_{out}(5) [$Mcal \cdot d^{-1}$]	$bCOD_{out}$(6) [$kg\ O_2 \cdot d^{-1}$]	OCI(7) [$kWh \cdot d^{-1}$]	AE(8) [$kWh \cdot d^{-1}$]
OL	100		100	166.94	11772	552	5368	2475
ST1_ideal	100	161	100	166.93	11844	563	5279	2386
ST1	100	151	100	166.94	11842 (0.59%)	557 (0.9%)	5290 (-1.45%)	2396 (-3.19%)
ST2_ideal	100	312	100	166.94	11873	465	5390	2496
ST2	100	312	100	166.94	11859 (0.73%)	452 (-18.11%)	5428 (1.11%)	2535 (2.42%)

In brackets, performance results expressed as percentage with respect to that of the OL strategy.
(1) PQI = Pasteurization Quality Index. (2) Knees = number of bending-points detected. (3) StQI = Stabilization Quality Index. (4) WVout = withdrawal. (5) ThEout = Thermal Energy in the treated sludge. (6) bCODout = Biodegradability in the treated sludge. (7) OCI = Overall Cost Index. (8) AE = Aeration Energy.

Part of the performance of the control strategies ST1 and ST2 obtained by simulations is depicted in **Figure 7.6**.

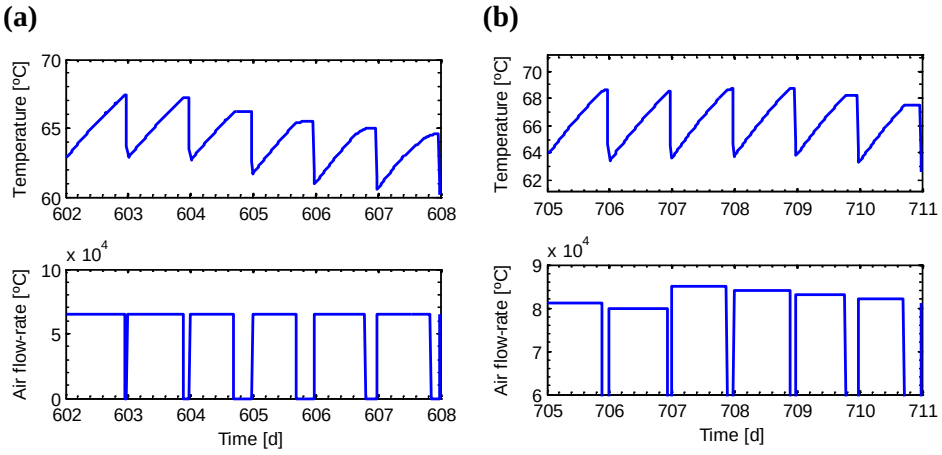

Figure 7.6 Performance of control strategies obtained by simulations. **(a)** Under ST1 mode, **(b)** Under ST2 mode

As an initial comparison, the control strategies based on the bending-point detection in the temperature profile (ST1 and ST2) were also implemented assuming an "ideal" sensor of Xs+Ss (slowly and readily biodegradable substrate respectively), the results are expressed in **Table 7.2** as ST1_ideal and ST2_ideal. In this respect, it was established that more that 95% of reduction in Xs+Ss is traduced in a lacking of organic matter.

It can be observed that the result indices obtained for ST1 and ST1_ideal, as well as for ST2 and ST2_ideal are similar; this reflects that effectively, control strategies based on processing the temperature profiles give a similar behavior than strategies that would implement an organic matter sensor.

As expected, ST1 produces the same sludge quality as the OL strategy (PQI, ThE_{out}, StQI and $bCOD_{out}$ values). In contrast, save on aeration costs is achieved with ST1 (≈ -1.5%), but less than anticipated. An analysis of the 141 "bCOD knees" observed in ST1 revealed that most of them occurred close to the end of the operation phase, explaining the reason of such a small reduction in the aeration costs. Nevertheless, higher energy saving would have been obtained with ST1, if air flow-rates greater than 65000 $m^3 \cdot d^{-1}$ had been employed in the OL strategy.

For instance, setting the air flow-rate to 80000 $m^3 \cdot d^{-1}$, aeration savings increase up to 4%. Similarly, the smaller the pre-holding tank the larger the difference in aeration costs between ST1 and OL. With a smaller pre-holding tank, under-loads become more noticeable, "bCOD knees" more frequent and, consequently, ST1 more effective.

In comparison to OL and ST1, ST2 leads to a significantly smaller value of $bCOD_{out}$ (≈ -17%), which means a more stabilized treated sludge. The increase in the number of "bCOD knees" (141 in ST1 versus 312 in ST2) reaffirms the above conclusion. Nevertheless, these results are achieved at the expense of higher aeration (21%). Thus, the ST2 strategy should be adopted instead of ST1 only in those operating scenarios where a maximum level of stabilization is mandatory (due, for example, to more stringent local regulations).

The analysis of the ThE_{out} index for the three strategies reveals that ST2 leads to lower temperatures in the ATAD than those reached with ST1 or OL. This result contradicts the initial assumption that the application of the ST2 strategy would cause higher temperatures in the ATAD. However, the reason for this behavior lies in the heat losses associated with the water evaporation. Since water evaporation is proportional to the air flow-rate, as the ST2 strategy increases the air flow-rate from batch to batch in order to find a maximum stabilization of the sludge, the evaporative heat losses also increase.

Within the normal operating range (i.e., air flow-rates of around 65000 $m^3 \cdot d^{-1}$), changes in the air flow-rate do not affect significantly the evaporative losses. Conversely, at very high air flow-rates, the cooling effect due to evaporation prevails over the heat generated biologically, and causes a decrease in the sludge temperature. In this respect, simulation results agree with experimental observations of this cooling effect in ATADs operated under over-aerated conditions (Cheng and Zhu, 2008).

7.3. Model uncertainty considerations

The validation of the proposed controllers in terms of the AT_BSM benchmark has allowed quantifying objectively the control strategy ST1 and ST2. In spite of it, control studies of biological processes based on mathematical modeling involve several sources of uncertainty. For instance, it is more and more frequent to see studies (in designing, modeling, etc.) considering uncertainty in model kinetic and stoichiometric coefficients (Sin et al., 2009).

Recall **Chapter 5**, the evaluation assessed in the AT_BSM benchmark considered fixed values in some coefficients of the mathematical model. Departing from the fact that the control study is performed by simulations, a rigorous validation has to consider the uncertainty associated to those most significant model coefficients. This allows evaluating the controller sensitivity

with respect to the range of considered uncertainties, as well as it evaluates the controller performance for different operational conditions.

In order to evaluate the sensitivity of control strategies, every strategy was validated considering uncertainty in some of the kinetic and stoichiometric coefficients.

On the basis of default general parameters adopted in the model study of ATADs given by Gomez et al. (2007a) and Gomez (2007b); some coefficients were considered for the model uncertainty study. **Table 7.3** depicts the selected coefficients for this study, assuming uniform distribution for the range of variability showed.

Table 7.3 Uncertainty in the model parameters

Coefficient	Default value	Min value	Max value	Unit
k_H	1.7	1.65	2	day^{-1}
b_H	0.5	0.45	0.55	day^{-1}
μ_H	17	14	18	day^{-1}
Ks	0.02	0.015	0.025	$kg\ COD \cdot m^{-3}$
Y_H	0.4	0.38	0.45	$kg\ COD \cdot (kg\ COD)^{-1}$

The model uncertainty study involved three steps: (i) random generation of the uncertainty coefficients defined in **Table 7.3**; (ii) propagation of the sampled uncertainty coefficients through the AT_BSM benchmark and (iii) statistical representation of performance indices is performed. These steps are depicted in **Figure 7.7**. For step (i) Latin Hypercube Sampling was used, for (ii) a total of 500 simulations were adopted.

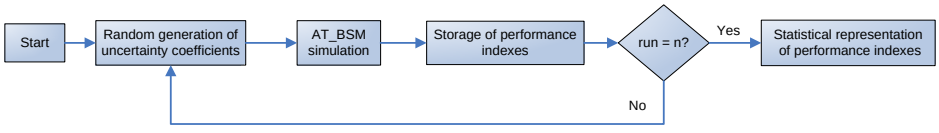

Figure 7.7 Procedure for the uncertainty study

7.3.1. Results obtained

The statistical results of some of the most important evaluation indices for OL, ST1 and ST2 are summarized in **Table 7.4**, indicating the mean and standard deviation (StD) values. Recalling the AT_BSM benchmark, the indices ThE_{out}, $bCOD_{out}$ and AE were selected for the uncertainty study. The true and false detections (obtained from the algorithm of bending-point detections) were also included as part of the statistical results. These true and false detections were calculated with respect to real (ideal) detections, i.e., defined as the moment when 95% of the initial biodegradable substrate is consumed during the cycle.

In the same way as it was implemented in **Section 7.2**, the parameters values assigned to the bending-point detection algorithm for ST1 and ST2 were obtained after applying the tuning methodology explained in **Chapter 6**.

Table 7.4 Index results considering uncertainty

	Mean / StD				
Strategy	ThEout	bCODout	AE	(True/Real) detections(*)	(False/Real) detections(*)
	[Mcal·d^{-1}]	[kg O_2·d^{-1}]	[kWh·d^{-1}]	[%]	[%]
OL	11726 / 60.83	550 / 14.86	2475 / 0.02	-	-
ST1	11822 / 30.59 (0.81%)	555 / 14.35 (0.9%)	2370 / 32.54 (-4.2%)	87.05 / 4.44	13.36 / 7.56
ST2	11839 / 52.68 (0.96%)	474 / 33.4 (-13.8%)	2516 / 142 (1.69%)	86.02 / 1.24	13.39 / 1.45

In brackets, the mean values expressed as percentage with respect to that of the OL strategy

(*) True/Real and False/Real detections represent the percentage of true and false detections with respect to real detections respectively.

In addition to the statistical results showed above, probability density functions (PDF) for the indices ThE_{out}, $bCOD_{out}$ and AE were obtained. The PDF are depicted in **Figure 7.8**.

(a)

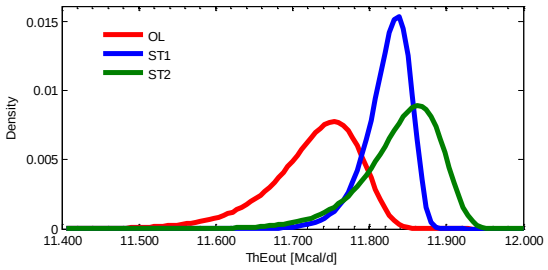

(b)

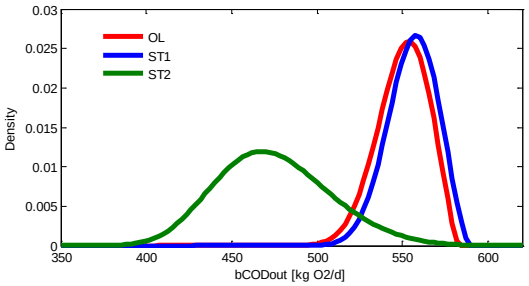

(c)

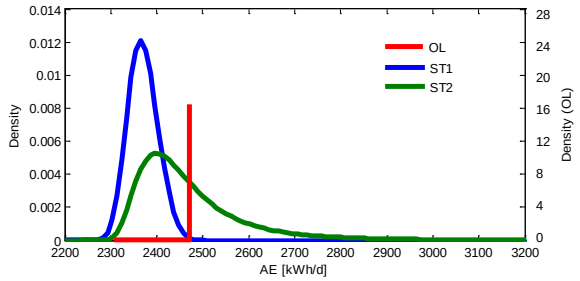

(d)

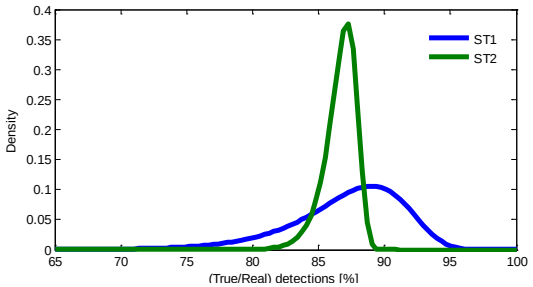

Figure 7.8 Probability density functions of: **(a)** ThE_{out}, **(b)** $bCOD_{out}$, **(c)** AE and **(d)** (True/Real) detections.

Analysis of ST1

The results listed in **Table 7.4** show that, comparing with OL, the important reduction obtained was related to the aeration energy (AE) (-4.2%), the thermal energy (ThE_{out}) and the effluent biodegradable COD ($bCOD_{out}$) are similar to that given by the OL.

Compared to OL, the PDF of ThE_{out} showed a slightly increase in the mean value and a reduction in the standard deviation. This was a direct consequence of stopping the air injection when the bending-point (lack of biodegradable substrate during digestion cycles) occurred.

The index results and the previous figure led to conclude that ST1 operation, which it was proposed for AE reduction, besides of giving a band of AE reduction, also reduces the sensibility to the uncertainty in terms of ThE_{out}.

Analysis of ST2

The **Table 7.4** shows that, compared to OL, the important reduction obtained was in terms of $bCOD_{out}$ (-13.8%), but this required an increase in AE (1.69%). The $bCOD_{out}$ obtained was similar to that given by the ST1.

Although the mean value of $bCOD_{out}$ is reduced, the standard deviation obtained was higher, revealing that the system is reacting based on the objective of reducing the $bCOD_{out}$. Therefore, the dispersion to the right side for AE is a consequence of the corrective action taken by this controls strategy.

Regarding the ThE_{out}, although the mean value obtained was slightly higher when compared to OL and ST1, the PDF showed a tendency to increase the final thermal energy. Naturally, higher values for AE (high value of air injected) can give a reduction in this index.

The index results and the previous figure led to conclude that ST2 operation, which it was proposed for a best effluent quality (more sludge stabilized), mainly gave a lower $bCOD_{out}$ and a higher ThE_{out} with a data dispersion that can not be neglected.

Concerning the True/Real detections, similar mean values were obtained for ST1 and ST2, although the dispersion is higher for ST1. This suggests a better respond of the bending-point detection in ST2, since the parameters adopted for the detection algorithm were obtained considering variation in the air flow-rate, therefore, a wide diversity of profiles were taken into account for the tuning procedure.

7.3.2. Correlation analysis

In order to indentify the parameters with major effect in the performance of control strategies, a correlation study between the model parameters considered in the sensitivity study and the evaluation indices selected was assessed. This analysis was developed for every control strategy; the results are summarized in **Table 7.5**.

Table 7.5 Correlation between indices and model coefficients

Strategy	Index	k_H	b_H	μ_H	Ks	Y_H
OL	ThEout	0.06	0.21	0.02	-0.04	-0.97
	bCODout	-0.03	-0.88	0.02	0.07	-0.36
	AE	-0.06	-0.01	-0.03	0.05	-0.01
ST1	ThEout	0.11	0.06	-0.02	-0.04	-0.93
	bCODout	-0.09	-0.88	-0.02	-0.01	-0.31
	AE	-0.13	0.29	-0.03	-0.01	-0.93
ST2	ThEout	0.36	-0.24	-0.03	-0.05	-0.16
	bCODout	-0.11	-0.54	-0.01	-0.01	0.79
	AE	-0.22	0.33	0.02	0.02	-0.69

From the correlation coefficients listed in **Table 7.5**, the lysis rate coefficient (b_H) and the yield of heterotrophic biomass (Y_H) gave an important effect in the control strategies. The effect of maximum specific hydrolysis rate (K_H), the maximum specific growth rate (μ_H) and the half-saturation coefficient for growth (Ks) were not considered in the following analysis. **Figure 7.9** shows

the correlations between the parameters Y_H and b_H for the indices ThE_{out}, $bCOD_{out}$ and AE.

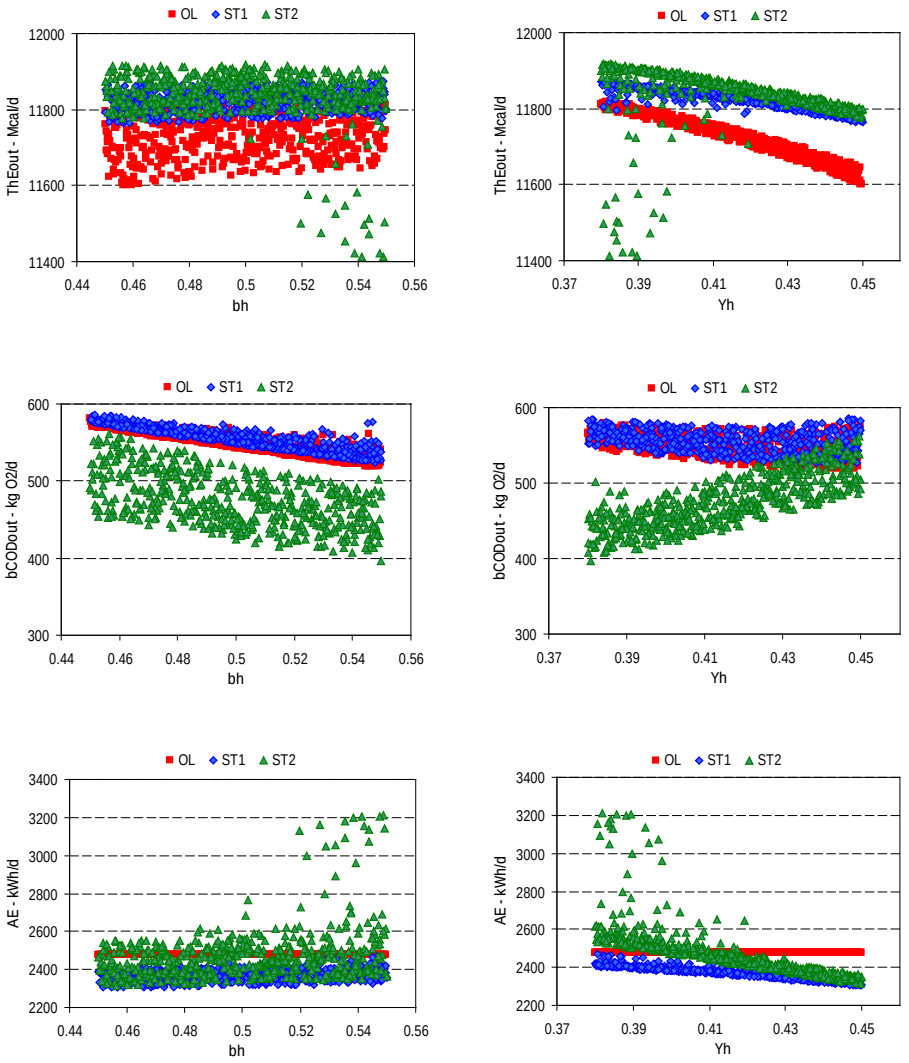

Figure 7.9 Correlation between ThE_{out}, $bCOD_{out}$ and AE and the parameters b_H and Y_H.

As an overview, it was observed that high values of Y_H led to obtain a similar effluent quality ($bCOD_{out}$) for the different strategies. This is because high value in Y_H means low oxygen required per COD of biomass generated, promoting a reduction in the air injection required (low values in AE) and a reduction in the heat generated by the biological activity (low values in ThE_{out}). Moreover, it was observed that the decreasing rate in ThE_{out} was higher in OL than in ST1 and ST2. Some low values for ThE_{out} were obtained in ST2, due to the cooling effect obtained by over-aeration.

The dispersion of the sample data in $bCOD_{out}$ is similar for any value of Y_H when OL and ST1 are applied. For ST2, low values of Y_H led to an air adaptation in order to reduce the COD that is still available in the sludge.

In the same way, higher values in Y_H tend to give similar air consumption by ST1 and ST2 (in OL the air injection is fixed, so there is not variation expected for this index), but for lower values in Y_H the air flow-rate required is becoming higher.

Regarding the parameter b_H, compared to the OL operation, the dispersion of the sample data in ThE_{out} is reduced for any value of this parameter when ST1 and ST2 are applied. The dispersion observed in $bCOD_{out}$ due to b_H is similar for OL and ST1, and it is higher for ST2 while the mean value is lower.

7.4. Preliminary experimental results

In this section, preliminary results obtained from an ATAD pilot plant are presented. The main propose of this experimentation was to test the viability to implement control strategies and consequently, to analyze the performance assessed.

7.4.1. Experimental setup

The raw sludge

The experiments were performed with a sludge obtained from a wastewater treatment plant located in Loiola (Gipuzkoa, Spain). This plant was aimed at carbon removal process and has not a primary settling tank, so after a bar screen and a grit chambers the wastewater is passed trough a series of activated sludge reactors, which are followed by secondary settling tank. The hydraulic retention time in the biological reactors is lower compared to a conventional plant because the effluent is discharged to the sea. After the secondary clarifier the sludge is thickened and then piped to a holding tank from which it is fed to the digester via a pump. This kind of sludge is similar to a mixed and low stabilized sludge.

The pilot plant

The architecture of the ATAD pilot plant is depicted in **Figure 7.10**. This reactor consisted in a 12.7m^3 cylindrical stirred reactor tank with 9m^3 active volume; 3mm of stainless steel AISI type 316 is used for the interior wall, 1.2mm of stainless steel AISI type 304 is used for the exterior wall; the manifold is insulated using 50mm of compressed rock wool. The reactor was aerated by 1.5kW air-blower, and the sludge was sufficiently mixed using a Seepex spiral screw recirculation 4kW motor pump. The aeration of the substrate resulted in a dense foam layer which needed to be controlled; therefore, foam level was monitored by a radar instrument VEGAPULS61 top-mounted, and its level was controlled by pumping the foam to the reactor trough aspiration. Besides keeping the foam in a certain level, this system performs the oxygen transfer due to the gases recirculation. This effect was assessed in other plants (Scisson, 2003) and therefore it was decided to implement this aeration way in the pilot plant.

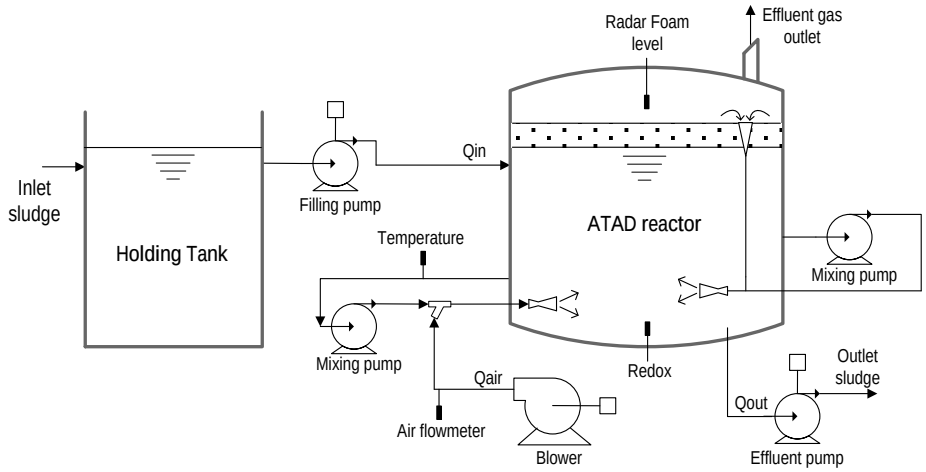

Figure 7.10 Scheme of the ATAD pilot plant

The followed signal were measured and registered: sludge and foams level, liquid and gas temperature inside the reactor, ORP. Moreover, flow-rate and temperature of air injected, ambient temperature, and blower energy consumption were online registered.

The experimental phase was carried out during less than 1 month. Therefore, due to the limited time for validation, the ATAD was operated in batch mode of 12 hours per cycle: 0.5 hours for sludge feeding, 11 hours for reaction and 0.5 hours for sludge withdrawal.

7.4.2. Results

Checking the bending-point detection algorithm

At the beginning of the experimentation the ATAD was operated in open-loop mode but emulating the bending-point detection algorithm. This action was useful since it allowed verifying both the signal treatment and the correct bending-point detection of the sludge temperature signal. The block diagram of the signal treatment is depicted in the **Figure 7.11**.

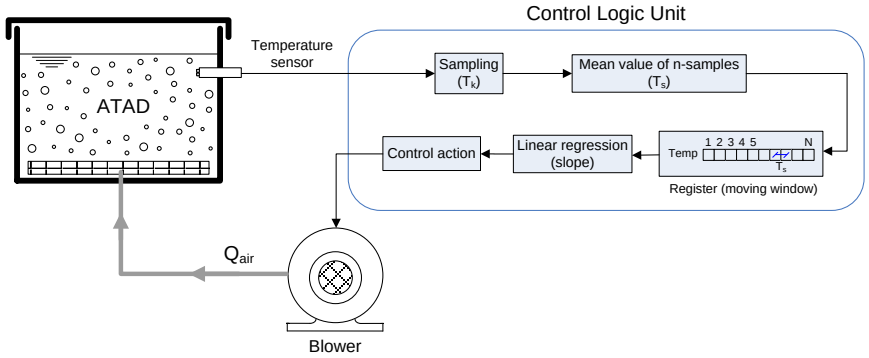

Figure 7.11 Signal treatment implemented for the bending-point detection.

Basically, the signal from the temperature sensor was sampled every T_k seconds. After n-samples a mean value is calculated and stored in a register of size N, thus every T_s minutes (T_s=n·T_k), a new sample is stored, the oldest sample is removed and the rest of samples are shifted. The linear regression gives the value α of the register; this value is used in the control action of the air injected to the ATAD (see **Section 4.3.3** for details of this procedure).

Typical profiles with bending-point occurrence were selected in order to test the performance of the detection algorithm. For a fast checking, an adequate value of α was adopted and different tests were done varying both the moving-window size (N) and the sample time (T_s), to establish suitable values of these parameters for the controller.

From these first preliminary values for the algorithm, several digestion cycles were monitored, checking that the algorithm for the bending-point detection was working properly. **Figure 7.12(a)** shows a typical sludge temperature profile obtained form the ATAD pilot plant, observing a bending-point occurrence. **Figure 7.12(b)** shows different bending-point detection times obtained from the profile shown in **Figure 7.12(a)** varying the value of the window-size (N) and the sample-time (Ts).

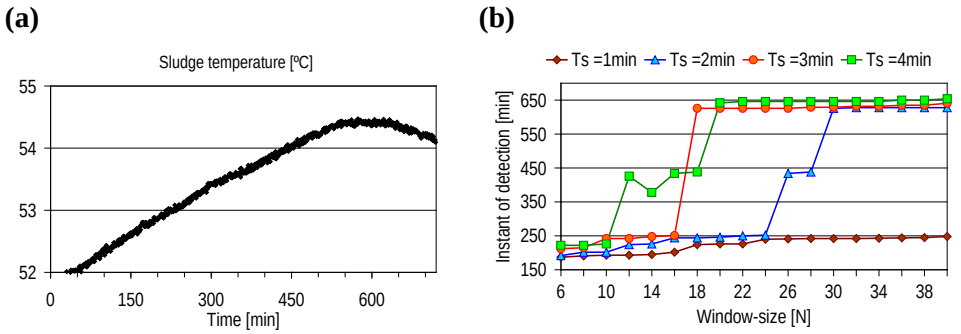

Figure 7.12 (a) Typical sludge temperature profile with bending-point. **(b)** Bending-point detection moments for different N and Ts values.

From the profile showed in **Figure 7.12(a)** the zone of knee detection occurs around the minute 600. The detections obtained with Ts=1min never give the expected value, this was not the case for Ts of 2, 3 and 4 minutes. According to this, after some checks in different bending-point profiles, a window-size of N=30 and Ts=2 minutes were selected as the algorithm parameters.

Figure 7.13(a) shows one cycle in open-loop operation, indicating in circle the moment when the sludge temperature pending value starts to change. **Figure 7.13(b)** shows a zoom of the circle indicated in **Figure 7.13(a)**, where the calculation of the α-profile is also included.

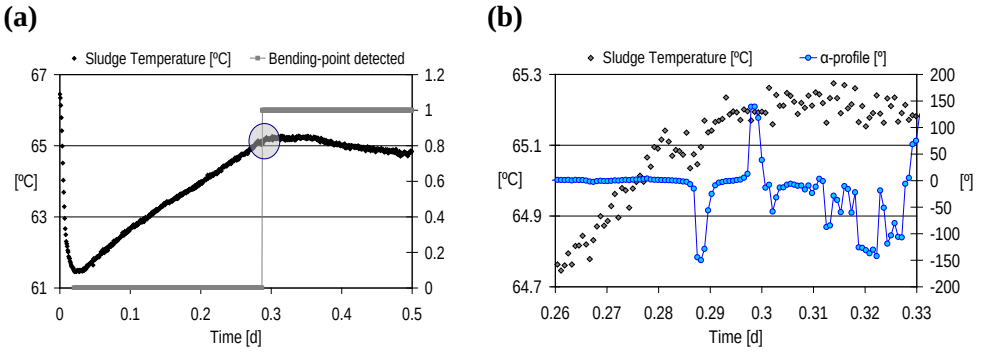

Figure 7.13 ATAD in OL mode. **(a)** Sludge temperature profile and indication of bending-point detection; **(b)** Zoom of circle indicated in **(a)**, the α-profile is included.

It can be observed that the α-profile is close to zero before the bending-point zone, and just when the bend-point appears the α -profile changes to a negative value, this is because the pending from newest data (W_{new}) is lower than the pending from oldest data (W_{old}). The behaviour of the α-profile from the sludge temperature measurement during the knee-zones allows applying the detection algorithm as part of control strategies in the ATAD pilot plant.

Activation of controller

In this section, some results are shown when a close-loop strategy is applied to the ATAD pilot plant. Due to limitation in time for the experimental period, it was decided to test just the ST2 strategy; therefore, the experimental time includes the operation in open-loop (OL) mode and then the operation in ST2 mode. **Figure 7.14** shows the ATAD sludge temperature profile, first in OL and then when ST2 is activated.

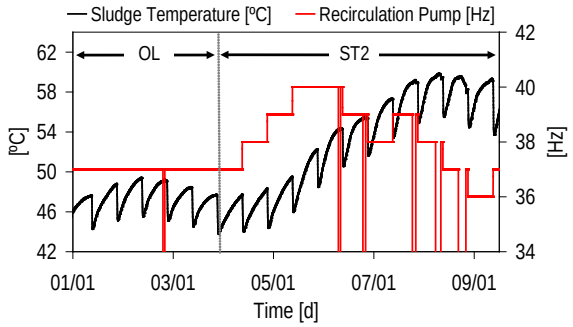

Figure 7.14. Sludge temperature and air flow-rate action when ATAD is working in OL and in ST2.

It can be observed that, during the OL mode, the fixed amount of air applied to the ATAD produces two main effects: a maximum value in the sludge temperature if the substrate is not digested, or a cooling effect if the substrate is digested.

Next, when the ATAD is operated in ST2, it can be observed that the sludge temperature profile increases after some digestion cycles, i.e. the sludge temperature at the end of every cycle is becoming higher. This increasing in the sludge thermal energy allows having a higher sludge pasteurization time, letting the sludge to be above 55 ºC during a longer time during the digestion. The effect of OL and ST2 operation can be observed in detail in **Figure 7.15(a)** and **Figure 7.15(b)** respectively.

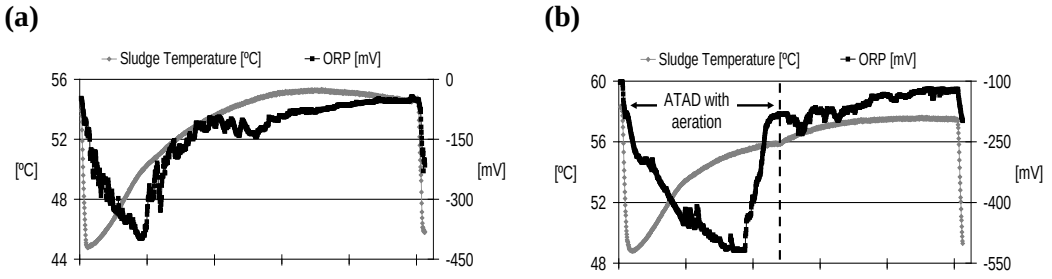

Figure 7.15. Air flow-rate effect in the ORP and sludge temperature during one cycle. **(a)** Under OL mode; **(b)** Under ST2 mode.

In **Figure 7.15(a)**, if bending-point is not detected under OL mode, and although the air flow-rate produces a cooling effect in the sludge temperature, the ORP acts as an indirect indicator of the substrate digestion status. In **Figure 7.15(b)**, if the aeration is stopped when the bending-point is detected in ST2 mode, the cooling effect can be avoided. This detection time corresponds to a zone where the ORP signal is already in aerobic conditions. Therefore, under ST2 mode, the bending-point detections are close to the zone where the substrate is already digested.

In **Figure 7.16** the effect in terms of pasteurization, aeration time and energy consuming are shown, both under OL and ST2 mode.

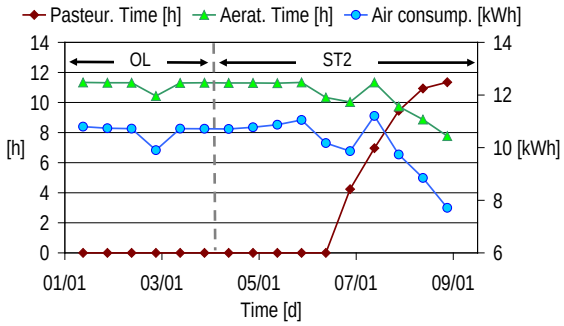

Figure 7.16. Pasteurization time, aeration time and energy consumption obtained under OL and ST2 mode.

After some cycles with bending-points, the air requirements tend to decrease; consequently the energy consumption also decreases. Therefore, after some digestion cycles, the adaptive action of the air injected overcomes the cooling effect obtained under OL mode and increases the final sludge temperature, seeking for a maximum of the biodegradable substrate reduction. In this way, it can be observed that under ST2 mode the air requirement is automatically adjusted depending on the occurrence of bending-points in the sludge temperature. The aeration energy (AE) and thermal energy (ThE_{out}) indices under OL and ST2 mode are depicted in **Table 7.6**.

Table 7.6 Results in OL and ST2 mode

Index	OL mode	ST2 mode
AE [kWh·d^{-1}]	10.7	10.1
ThE_{out} [Mcal·d^{-1}]	48.7	54.3

7.5. Conclusions

Performance of control strategies by simulation

It was showed in this chapter the validation of control strategies ST1 and ST2 by simulation. Comparing to a conventional open-loop operation, the main advantage of ST1 was to save aeration costs in cycles when there is a lack of substrate to be digested. On the other hand, the main advantage of ST2 was to obtain a maximum level of stabilization in the final sludge, but this result requires a higher aeration cost.

Certain limits in the air injected have to be defined, since high values in the aeration can promote a cooling effect in the sludge temperature, promoting the inhibition of the biological activity in the reactor. In fact, the pasteurization and stabilization can be affected if an over aeration is continuously applied.

When requirement for maximum sludge stabilization is a priority, ST2 must be implemented. When the air saving is prioritized, the ST1 strategy must be adopted.

The control strategies performance obtained are associated to the influent characteristics of the raw sludge and the plant-layout sizing adopted. A bigger volume for the pre-holding tank could avoid having overflow or emptied effects; however it must be considered that an over-sized tank will lead to a useless controller in terms of perturbations rejection due to the lamination effect obtained. Consequently, both the plant-layout and the controllers design are the key factors considered, where the compromised between the operational costs and a good operational performance has to be established.

Concerning the control strategies design, the previous study led to consider the range of uncertainty in the kinetic parameters as an important factor to obtain a proper performance study of the proposed controllers, and also, in order to guaranty good results of these strategies under the entire band of the considered uncertainty space.

Preliminary experimental results

The bending-point detection algorithm was applied successfully. In this way, the signal treatment adopted for the experimental sludge temperature was crucial for the control strategy implementation.

When ST2 was activated after the OL operation, an increment in the final temperature of the sludge and a reduction in the aeration energy were obtained. Nevertheless, it must be necessary to validate this operation in a longer time.

The ORP signal was useful to confirm the good performance of the algorithm for bending-point detections. As further research, both the sludge temperature and the ORP signal can be used together to support each other in new control strategies applied to the aeration.

Requiring few sensors and simple control algorithms, it was possible to implement a control law allowing a reduction in the aeration energy at pilot plant scale, its implementation in full scale ATADs will be an interesting step.

8

Conclusions and perspectives

Chapter 8 Conclusions and Perspectives

8.1. Summary of results

This thesis proposed two control solutions for the treatment of raw sludge when using an Autothermal Thermophilic Aerobic Digester (ATAD). These control strategies were designed taking into account a conventional industrial scenario: a pre-holding tank followed by the digester.

As a single treatment, the ATAD must operate as a batch process in order to obtain pasteurized and stabilized final sludge. The different control solutions proposed took these requirements into account. The strategies proposed in this study were based on a trend analysis of the sludge temperature signal; one solution prioritizes air cost savings, and the other prioritizes a more stabilized final sludge.

As in any control solution, a tuning step was required. Due to the lack of tuning procedures in batch process controllers, where the trend analysis is crucial, a new methodology for this kind of controllers was developed. This methodology took uncertainty into consideration in order to obtain a robust tuning of the control algorithm. Concerning the ATAD as case study, where the control algorithms are based on the sludge temperature analysis, the tuning procedure proposed was applied.

In order to have an objective validation of the control strategies proposed, a new protocol test or benchmark adapted for the case study was presented in this thesis. This benchmark allowed the performances of the proposed control strategies to be quantified and compared to other strategies; it also allowed the advantages of the control operations in the case study to be evaluated by means of a systematic procedure.

Some conclusions related to different parts of this study are as follows:

8.1.1. The mathematical model and simulation study

The mathematical model employed in this study was an important tool for a systematic control study by simulation. In this way, the mathematical model implemented was able to represent the plant-layout that needed to be controlled. Furthermore, the model proved to be appropriate for design and validation of controllers.

The benchmark implementation in Matlab/Simulink made it handy to develop and validate the controllers; this facilitates testing different control strategies applied to real scenarios.

8.1.2. The control problem studied

The objectives and restrictions of the proposed control solutions were subjected to the case study features such as plant-layout, tanks sizing, influent flow-rate and concentration characteristics, and the availability of measurements and control actions.

The validation of control solutions following a benchmark methodology showed important results in terms of performance evaluation of the overall plant, such as the operational cost index, the biodegradability of the treated sludge, the reduction of volatile solids, and the thermal energy in the treated sludge.

8.1.3. The performance of the control solutions

In this thesis, it was possible to employ the sludge temperature signal from the ATAD as a signal for control algorithms. As a result, a bending-point algorithm based on this signal was developed.

The control strategy ST1 was oriented toward reducing air consumption, while ST2 was oriented toward maximizing the volatile solids reduction. The stability of the process was maintained in all of the control solutions proposed

The performance of control solution ST1 versus the open loop strategy (OL) gave a reduction in aeration energy of almost 2%. On the other hand, the performance of control solution ST2 versus the OL strategy resulted in a biodegradable COD reduction of almost 17%, but with the disadvantage of an increase in air consumption. These values have to be taken as reference, since they depend of the plant-layout design and the process uncertainty.

Regarding the case study features, including fast changes in flow-rates and concentrations, as well as the limited volume of the pre-holding tank, these factors determine the control strategy behavior from the hydraulic point of view.

It was possible to carry out a practical implementation of ST2, obtaining good results in terms of thermal energy recovering and a fast response of the process, although effluent quality measurements must be incorporate in future validations.

8.1.4. The methodology for robust tuning of bending-point algorithm

The new methodology for a robust tuning of bending-point strategies gave a solution for the tuning of the kind of control strategies proposed here, taking into account uncertainty in inputs and considering both fast and slow dynamics. The aim was to produce a large amount of possible profiles in order to be analyzed by the bending-point detection algorithm.

In the case of the ATAD process, due to the fact that some control strategies applied to the ATAD were based on the bending-point detection in the temperature profile, it was useful to apply this methodology in order to obtain suitable parameter values for the algorithm.

Moreover, in order to analyze more realistic temperature profiles, this methodology was applied considering the noise effect. Under this consideration, the algorithm found suitable parameters for the algorithm.

Regarding the noise effect, it showed to be an important factor to consider in the methodology proposed. In this way, parameters values for the bending-point algorithm obtained if the noise effect is not considered, will not give a good performance in real conditions.

8.2. Topics for Further Research

Departing from the study presented in this thesis, some interesting topics for further studies arise:

8.2.1. Control strategies

ST2 strategy proposed can be modified in order to automatically regulate the increment and decrement control action for the air flow-rate in the next cycle according to the time when the bending-point is detected in the actual cycle.

On the other hand, one avenue of further study in ATAD controllers is the development of control strategies that take into account additional manipulated variables like the pure-oxygen supply and the feeding volume per cycle.

An advantage of using pure-oxygen systems is that the heat losses from evaporation are considerably reduced. Therefore, since air is not effective at very high flow-rates, ST2 combined with an automatic on/off system for the oxygen supply might be an effective solution to ensure maximum sludge stabilization with no risk of cooling effects due to water evaporation. The air system would work alone (i.e., with the oxygen supply switched off), unless the air flow-rate set-point reached a preset upper limit value. In that case, ST2

would set the air flow-rate to its upper limit and, simultaneously, the pure oxygen supply would be switched on. Under these circumstances, any perturbation in the oxygen demand would be handled by regulating the pure oxygen flow-rate. ST2 combined with automatic regulation of the feeding volume from batch to batch would also allow greater control on the evaporative losses. ST2 would work as the original approach (see the previous section), unless the air flow-rate set-point reached a preset upper limit value. In that case, ST2 would set the air flow-rate to its upper limit and, simultaneously, the feeding volume would be reduced. Under these circumstances, any perturbation in the oxygen demand would be handled by regulating the feeding volume.

8.2.2. The AT_BSM

With slight modifications, the AT_BSM might be easily adapted to face with control solutions for diverse ATAD configurations, some of which are as follows:

- ATAD operating as a pre-treatment unit of a conventional anaerobic digester, where the ATAD, working in continuous-fashion, will help to solubilise the raw sludge in order to improve the anaerobic digester's performance.
- The pre-heating of raw sludge using the heat recovered from the final digested product through a heat exchanger.
- A pre-holding tank followed by multiple serially configured ATAD reactors.

In this way, the software implementation based on subsystems can facilitate the development of the above scenarios.

8.2.3. The methodology for bending-point detection tuning

Regarding the general aspects of the methodology for tuning bending-point detection algorithms, many other different detection algorithms can be studied

with this approach. Hence, depending on the parameters that these detection algorithms require, the set of optimization restriction will be modified.

Although the methodology was applied to the ATAD technology, it can be also applied to any other biological technology that treats waste (either liquids or solids) in a batch or semi-batch operation, such as Sequencing Batch Reactors and Biodenitro/Biodenipho processes.

a

Annexes

Annex A Mathematical modeling aspects

In this Annex the different aspects considered in the mathematical model are presented. In **Section A.1** the stoichiometry matrix is depicted, the matrix summarizes all the components and the biochemical, chemical and physico-chemical transformations considered in the study. In **Section A.2** the set of default values for the model transformations parameters is listed, classified by stoichiometric, physico-chemical and kinetics parameters.

The equations employed for the kinetics of transformations are detailed in **Section A.3**. Finally, some equations employed in the algebraic variables calculations that are considered in the mass and energy balances for the liquid and gaseous phase (including volumes, enthalpy flows, temperatures, pressures) are detailed in **Section A.4**.

A.1 Stoichiometric calculus

A.1.1 Stoichiometry matrix

The mathematical model of ATAD is defined by a total of 22 variables: 14 variables are dissolved, 4 are particulate and 4 are gaseous. There are 12 biological processes considered. It is based on a COD balance of the system and is usually presented in a matrix format suggested by (Petersen, 1965). The matrix representation allows rapid and easy recognition of the fate of each component.

Table A.1 Process kinetics and stoichiometry

Components	i	1	2	3	4	5	6	7	8	9	10	11	12	13	14	15	16	17	18	19	20	21	22	
	Process	Sh2o	Ss	Si	So2	Shco3	Sco2	Sn2	Snh4	Snh3	Sh	Soh	Sh2po4	Shpo4	Xs	Xr	Xbh	Xi	Xinor	Gh2o	Gco2	Go2	Gn2	
j																								
1	Hydrolysis	$v_{1,1}$	1		$v_{4,1}$		$v_{6,1}$		$v_{8,1}$		$v_{10,1}$		$v_{12,1}$		-1									Nitrogen gas [kg N·m-3]
2	Solubilization	$v_{1,2}$	1		$v_{4,2}$		$v_{6,2}$		$v_{8,2}$		$v_{10,2}$		$v_{12,2}$			-1								Oxygen gas [kg O·m-3]
3	Aerobic growth of biomass	$v_{1,3}$	$-1/Y_H$		$-(1-Y_H)/Y_H$		$v_{6,3}$		$v_{8,3}$		$v_{10,3}$		$v_{12,3}$				1							Carbon dioxide gas [kg C·m-3]
4	Lysis	$v_{1,4}$			$v_{4,4}$		$v_{6,4}$		$v_{8,4}$		$v_{10,4}$		$v_{12,4}$		1- f_{xi}		-1	f_{xi}						Vapour of water [kg H2O·m-3]
5	CO2 dissolution	$v_{1,5}$			$v_{4,5}$		-1				$v_{10,5}$		$v_{12,5}$								1			Inorganic matter
6	O2 dissolution	$v_{1,6}$			-1		$v_{6,6}$		$v_{8,6}$		$v_{10,6}$		$v_{12,6}$									1		Particulate inert organic matter [kg COD·m-3]
7	N2 dissolution	$v_{1,7}$			$v_{4,7}$		$v_{6,7}$	-1			$v_{10,7}$		$v_{12,7}$										1	Active heterotrophic biomass [kg COD·m-3]
8	C inorganic	$v_{1,8}$			$v_{4,8}$	-1	1		$v_{8,8}$		$v_{10,8}$		$v_{12,8}$											Readily solubilizable substrate [kg COD·m-3]
9	N inorganic	$v_{1,9}$			$v_{4,9}$		$v_{6,9}$		$v_{8,9}$	-1	$v_{10,9}$		$v_{12,9}$											Slowly biodegradable substrate [kg COD·m-3]
10	P inorganic	$v_{1,10}$			$v_{4,10}$		$v_{6,10}$		$v_{8,10}$		$v_{10,10}$		$v_{12,10}$											Hydrogen phosphate [kg P·m-3]
11	Equilibrium of water	$v_{1,11}$			$v_{4,11}$		$v_{6,11}$		$v_{8,11}$		$v_{10,11}$	-1	$v_{12,11}$											De-hydrogen phosphate [kg P·m-3]
12	Evaporation of water	-1			$v_{4,12}$		$v_{6,12}$		$v_{8,12}$		$v_{10,12}$		$v_{12,12}$							1				Ion of hydroxyl [kg H·m-3]
																								Ion of hydrogen [kg H·m-3]
																								Ammonia [kg N·m-3]
																								Ammonium [kg N·m-3]
																								Nitrogen [kg N·m-3]
																								Carbon dioxide [kg C·m-3]
																								Bicarbonate [kg C·m-3]
																								Dissolved oxygen [kg O_2·m-3]
																								Soluble inert organic matter [kg COD·m-3]
																								Readily biodegradable substrate [kg COD·m-3]
																								Water [kg H_2O·m-3]

A.2 Model transformations parameters

The total of parameters is divided in three groups: (1) stoichiometric coefficients; (2) the physico-chemical parameters that are involved in the acid-base equilibrium and in transferences between phases, and (3) the kinetic coefficients that are involved in the biological transformations. The following Tables show this set of parameters.

Table A.2 Stoichiometric parameters

Symbol	Description	Unit
Yh	Heterotrophic yield	kg COD·(kg COD)$^{-1}$
fxi	Fraction of inert COD generated by lysis	kg COD·(kg COD)$^{-1}$
v_{ij}	Stoichiometric coefficient of component i in the transformation j	UE·m^{-3}

Table A.3. Physico-chemical parameters

Symbol	Description	Dependency respect to the temperature (T)	Unit
$C_{p,i}$	Specific heat of component i	-	kJ·kg^{-1}·^{o}C^{-1}
D_{gas}	Diffusivity of gaseous component	-	m^2·d^{-1}
R	Gas constant	-	bar·m^3·kmol^{-1}·^{o}K^{-1}
ΔH^o	Heat of reaction in standard conditions	-	J·mol^{-1}
$K_{eq,i}$	Acid-base equilibrium of component i	$K_{eq}(T) = K_{eq(25^oC)} \cdot e^{\left[\frac{K^0}{R \cdot 100}\left(\left(\frac{1}{298.15}\right)-\left(\frac{1}{T}\right)\right)\right]}$	UEi·m^{-3}
$K_{H,i}$	Henry's law constant of gas i	$K_H(T) = K_{H(25^oC)} \cdot e^{\left[\frac{K_H^0}{R \cdot 100}\left(\left(\frac{1}{298.15}\right)-\left(\frac{1}{T}\right)\right)\right]}$	UEi·m^{-3}·bar^{-1}

Table A.4. Kinetic parameters

Symbol	Description	Equation	Unit
kla_{o2}	Transfer coefficient for O_2	$kla_{o2}(Q_{air,ref}) + \left(f_{mix} + (1 - f_{mix}) \frac{Q_{air}}{Q_{air,ref}} \right)$	d^{-1}
kla_{gas}	Transfer coefficient for a gas	$kla_{gas} = kla_{o2} \cdot \sqrt{D_{gas} / D_{o2}}$	d^{-1}
G_{h2o}^{sat}	Saturated water vapour	$0.0313 \cdot e^{\left[5290 \cdot \left(\frac{1}{298.15} - \frac{1}{Tgas}\right)\right]} \cdot \left(\frac{18}{T_{gas} \cdot R}\right)$	kg H_2O·m^{-3}

Next, the default values for the model parameters are detailed:

A.1.2 Stoichiometric parameters

Table A.5 Stoichiometric parameters

Parameter	Value	Unit
Yh	0.5	kg COD·(kg COD)$^{-1}$
fxi	0.1	kg COD·(kg COD)$^{-1}$

A.1.3 Physico-chemical parameters

Table A.6 Specific heat and gas constant

Parameter	Value	Unit
$c_{p,h2o}$	4.184	kJ·kg^{-1}·ºC^{-1}
$c_{p,co2}$	0.892	kJ·kg^{-1}·ºC^{-1}
$c_{p,o2}$	0.929	kJ·kg^{-1}·ºC^{-1}
$c_{p,n2}$	1.042	kJ·kg^{-1}·ºC^{-1}
R	0.08314	bar·m^3·kmol^{-1}·ºK^{-1}

Table A.7 Acid-base equilibrium coefficients

Parameter	Value	Unit
$K_{eq,co2}$	$10^{-6.35}$	kg H m^{-3}
$K_{eq,nh4}$	$10^{-9.25}$	kg H m^{-3}
$K_{eq,h2o}$	10^{-14}	kg H m^{-3}
K^0_{co2}	7646	J·mol^{-1}
K^0_{nh4}	51965	J·mol^{-1}
K^0_{h2o}	55900	J·mol^{-1}
K^{co2}_{dis}	10^7	m^3·kgH·d^{-1}
K^{nh4}_{dis}	10^7	m^3·kgH·d^{-1}
K^{h2po4}_{dis}	10^7	m^3·kgH·d^{-1}
K^{h2o}_{dis}	10^9	m^3·kgH·d^{-1}

Table A.8 Henry's constants

Parameter	Value	Unit
$K_{H,co2}$	$3.45 \cdot 10^{-2}$	UE·m^{-3}·bar^{-1}
$K_{H,o2}$	$12.8 \cdot 10^{-4}$	UE·m^{-3}·bar^{-1}
$K_{H,n2}$	$6.02 \cdot 10^{-4}$	UE·m^{-3}·bar^{-1}
$K^0_{H,co2}$	-2400	J·mol^{-1}
$K^0_{H,o2}$	-1500	J·mol^{-1}
$K^0_{H,n2}$	-1300	J·mol^{-1}

A.1.4 Kinetics parameters

Table A.9 Kinetic parameters of transformations

Parameter	Description	Value	Unit
K_{sol}	Maximum specific thermal solubilization rate	100	d^{-1}
K_H	Maximum specific hydrolysis rate	1.7	d^{-1}
μ_H	Maximum specific growth rate	10	d^{-1}
b_H	Lysis rate coefficient	0.5	d^{-1}
K_s	Half-saturation coefficient for growth	0.02	kg COD·m^{-3}
K_X	Half-saturation coefficient for hydrolysis	0.03	kg COD·(kg COD)$^{-1}$
K_{OXI}	Saturation/Inhibition coefficient for oxygen	0.0002	kg O_2·m^{-3}

Table A.10 Specific parameters of the model

Parameter	Description	Value	Unit
$KlaO_2(Q_{ref})$	O_2 gas transfer coefficient	250	d^{-1}
Do2	O_2 diffusivity	$2.16 \cdot 10^{-4}$	m^2·d^{-1}
Dco2	CO_2 diffusivity	$1.69 \cdot 10^{-4}$	m^2·d^{-1}
Dn2	N_2 diffusivity	$1.64 \cdot 10^{-4}$	m^2·d^{-1}

A.3 Kinetics of transformations

In the following table the kinetic equations associated to every transformation considered in the model are described.

Table A.11. Kinetic equations of transformations

j	Transformation	Kinetic equation [kg m^{-3} t^{-1}]
1	Hydrolysis	$\rho_1 = K_H \cdot \frac{Xs / Xbh}{Kx + (Xs / Xbh)} \cdot Xbh$
2	Solubilization	$\rho_2 = K_{sol} \cdot X_R$
3	Aerobic growth of biomass	$\rho_3 = \mu_H \cdot \frac{Ss}{Ks + Ss} \cdot \frac{S_{o2}}{S_{o2} + K_{OXI}} \cdot Xbh$
4	Lysis	$\rho_4 = b_H \cdot Xbh$
5	CO2 dissolution	$\rho_5 = kla_{CO2} \cdot (S_{CO2} - PM_{CO2} \cdot H_{CO2} \cdot Pp_{CO2})$
6	O2 dissolution	$\rho_6 = kla_{O2} \cdot (S_{O2} - PM_{O2} \cdot H_{O2} \cdot Pp_{O2})$
7	N2 dissolution	$\rho_7 = kla_{N2} \cdot (S_{N2} - PM_{N2} \cdot H_{N2} \cdot Pp_{N2})$
8	Equilibrium of carbon	$\rho_8 = K_{dis}^{CO_2} \cdot (S_{HCO3} \cdot S_H - K_{eq(CO2)} \cdot S_{CO2})$
9	Equilibrium of nitrogen	$\rho_9 = K_{dis}^{NH_4} \cdot (S_{NH_3} \cdot S_H - K_{eq(NH_4)} \cdot S_{NH_4})$
10	Equilibrium of phosphorus	$\rho_{10} = K_{dis}^{H_2PO_4} \cdot (S_{HPO_4} \cdot S_H - K_{eq(H_2PO_4)} \cdot S_{H_2PO_4})$
11	Equilibrium of water	$\rho_{11} = K_{dis}^{H_2O} \cdot (S_{OH} \cdot S_H - K_{eq(H_2O)})$
12	Evaporation of water	$\rho_{12} = k_{ma(Qair)} \cdot (G_{h2o}^{sat} - G_{h2o})$

A.4 Algebraic calculus

A.1.5 Mass and energy balance in the liquid phase

In this section the different mathematical expressions to calculate the algebraic variables involved in the mass and energy balances are shown. Some parameters are taken from the values listed in **Section A.2**.

Table A.12. Parameters

Parameter	Description	Value	Unit
δ_{h2o}	Volumetric density of water	1000	kg $H_2O \cdot m^{-3}$
R_{HT}	Pre-holding tank radius	7.51	m
R_{ATAD}	ATAD radius	7.93	m
$h_{liq,ATAD}$	ATAD liquid phase height	11.9	m
$h_{gas,ATAD}$	ATAD gaseous phase height	2	m
k_{walls}	Coefficient of heat conduction through walls	25	$kJ \cdot d^{-1} \cdot m^{-2} \cdot {}^{o}C^{-1}$
k^{0}_{qa}	Heat conduction coefficient	480	$kJ \cdot d^{-1} \cdot m^{-2} \cdot {}^{o}C^{-1}$
k^{0}_{ma}	Water evaporation rate coefficient	240	d^{-1}
λ_{qa}	Heat conduction kinetic factor	0.15	$kJ \cdot m^{-5} \cdot {}^{o}C^{-1}$
λ_{ma}	Water evaporation rate factor	0.08	m^{-3}
k_{gas}	Gas flow rate coefficient	1058200	$m^{3} \cdot d^{-1} \cdot atm^{-1}$
P_m	Power consumption from equipments	10368	$MJ \cdot d^{-1}$
Ø	Humidity	70	%

Areas:

Considering a cylindrical shape in both the pre-holding tank and the ATAD reactor, the area in the liquid phase that is in contact with the reactor's walls is as follows:

$$A_{liq,HT} = \pi \cdot R_{HT}^2 + 2 \cdot \frac{V_{liq,HT}}{R_{HT}} \quad \text{(A.1)}$$

$$A_{liq,ATAD} = \pi \cdot R_{ATAD}^2 + 2 \cdot \frac{V_{liq,ATAD}}{R_{ATAD}} \quad \text{(A.2)}$$

The area that separates the liquid from the gaseous phased is calculated considering the same area as the tank base.

$$A_{phs,HT} = \pi \cdot R_{HT}^2 \quad \text{(A.3)}$$

$$A_{phs,ATAD} = \pi \cdot R_{ATAD}^2 \quad \text{(A.4)}$$

Heat flows

- Influent and effluent heat flows:

$$HF_{\inf} = Q_{\inf} \cdot \delta_{h2o} \cdot c_{p,h2o} \cdot T_{\inf} \quad \text{(A.5)}$$

$$HF_{weir} = Q_{weir} \cdot \delta_{h2o} \cdot c_{p,h2o} \cdot T_{weir,HT} \quad \text{(A.6)}$$

$$HF_{feed} = Q_{feed} \cdot \delta_{h2o} \cdot c_{p,h2o} \cdot T_{feed,ATAD} \quad \text{(A.7)}$$

$$HF_{out} = Q_{out} \cdot \delta_{h2o} \cdot c_{p,h2o} \cdot T_{liq,ATAD} \quad \text{(A.8)}$$

- Gain heat by motors (HF_{mot}): This is the power gave by the motors from the aeration and mixing equipments. It is calculated as the electric power consumed by the equipments (P_m) multiplied by a factor (η_m).

$$HF_{motor,HT} = P_{m,HT} \cdot \eta_m \quad \text{(A.9)}$$

$$HF_{motor,ATAD} = P_{m,ATAD} \cdot \eta_m \quad \text{(A.10)}$$

- The heat lost from walls corresponds to the difference between the inside and outside temperature:

$$HF_{walls,HT} = k_{walls(l)} \cdot \left(T_{liq,HT} - T_{amb}\right) A_{liq,HT} \quad \text{(A.11)}$$

$$HF_{walls(l),ATAD} = k_{walls(l)} \cdot \left(T_{liq,ATAD} - T_{amb}\right) A_{liq,ATAD} \quad \text{(A.12)}$$

- Heat lost by phase conduction $\left(H^{cond}_{phases}\right)$: is the interchange heat between the liquid and gaseous phases trough the surface that separate them. It is calculated as follows:

$$HF_{phs,HT} = k_{qa} \cdot \left(T_{liq,HT} - T_{amb}\right) A_{phs,HT} \quad \text{(A.13)}$$

$$HF_{phs,ATAD} = k_{qa_{(Q_{air})}} \cdot \left(T_{liq,ATAD} - T_{gas}\right) A_{phs,ATAD} \quad \text{(A.14)}$$

- Production of biological heat (HF_{bio}): This is produced by the aerobic reactions. This heat generation is proportional to the oxygen consumption

rate and to the specific biological heat production during the heterotrophic biomass growth (Y_{heat})

$$HF_{bio} = \Delta H_{bio} \cdot \rho_3 \cdot V_{liq,ATAD} = Y_{heat} \cdot \left[\frac{1 - Yh}{Yh} \right] \cdot \rho_3 \cdot V_{liq,ATAD} \quad \text{(A.15)}$$

Where Y_{heat} is the specific biological heat production. ($(1-Y_h)/ Y_h$) denotes the kg of consumed oxygen per kg of biomass heterotrophy generated [COD/COD]. ρ_3 (see **Table A.5**) is the kinetic associated to the heterotrophic biomass growth [kg COD·m^{-3}·d^{-1}].

- Heat loss by water evaporation: It is calculated considering the latent heat of evaporation $\left(\Delta H_{evap(Tliq,ATAD)}\right)$ at 100 ºC ($\Delta H_{evap(100ºC)}$) obtained from the following expression:

$$\Delta H_{evap(Tliq,ATAD)} = \Delta H_{evap(100ºC)} + c_{p,h2o(l)} \cdot \left(100\,ºC - T_{liq,ATAD}\right) + c_{p,h2o(g)} \cdot \left(T_{liq,ATAD} - 100\,ºC\right) \quad \text{(A.16)}$$

Therefore, this heat loss can be expressed as:

$$HF_{evap} = \Delta H_{evap(Tliq,ATAD)} \cdot \rho_{evap} \cdot V_{gas} \quad \text{(A.17)}$$

Where the ρ_{evap} equation is referred in **Table A.11** as ρ_{12}.

Temperature:

The temperature in the liquid phase is calculated from the enthalpy. It is assumed that the temperature only depends on the mass of water in the liquid phase, it is calculated as follows.

$$T_{liq,HT} = \frac{H_{liq,HT}}{M_{h2o,HT} \cdot c_{p,h2o}} \quad \text{(A.18)}$$

$$T_{liq,ATAD} = \frac{H_{liq,ATAD}}{M_{h2o,ATAD} \cdot c_{p,h2o}} \quad \text{(A.19)}$$

A.1.6 Mass and energy balance in the gas phase

The gas volume in the ATAD is obtained dynamically as the difference between the total volume and the liquid volume, as follows:

$$V_{gas} = V_{ATAD} - V_{liq} \tag{A.20}$$

Area

Considering a cylindrical shape in the ATAD reactor, the area in the gas phase in contact with the reactor's walls is as follows:

$$A_{gas} = \pi \cdot R_{ATAD}^2 + 2 \cdot \frac{V_{gas}}{R_{ATAD}} \tag{A.21}$$

Pressure

The partial pressure of every gas component in the gaseous phase is obtained from the law of ideal gases:

$$p_{gas,h2o} = \frac{G_{h2o} \cdot R \cdot T_{gas}}{18} \tag{A.22}$$

$$p_{gas,co2} = \frac{G_{co2} \cdot R \cdot T_{gas}}{12} \tag{A.23}$$

$$p_{gas,o2} = \frac{G_{o2} \cdot R \cdot T_{gas}}{32} \tag{A.24}$$

$$p_{gas,n2} = \frac{G_{n2} \cdot R \cdot T_{gas}}{28} \tag{A.25}$$

The total pressure in the gaseous phase is the sum of the gases partial pressures obtained before:

$$P_{gas} = P_{gas,h2o} + P_{gas,co2} + P_{gas,o2} + P_{gas,n2} \quad \text{(A.26)}$$

The water vapor partial pressure is obtained from the water vapor partial pressure in saturated state at certain temperature:

$$Pp_{h2o} = Pp_{sat,h2o} \cdot \frac{\phi}{100} \quad \text{(A.27)}$$

Where

$$Pp_{sat,h2o} = 6.2509 + 0.3365 \cdot (T_{gas,in}) + 0.0259 \cdot (T_{gas,in})^2 \quad \text{(A.28)}$$

Gas influent flow-rate

The influent flow-rate is conformed by the four gaseous components of the model, which are generated from the influent air flow-rate, considering the following air composition: N_2 (78%); O_2 (21%); CO_2 (1%). Therefore, the flow-rate for every gaseous component is obtained as follows:

$$G_{h2o(in),ATAD} = \frac{Pp_{h2o} \cdot Q_{gas,in} \cdot 18}{R(T_{gas,in} + 273.15)} \quad \text{(A.29)}$$

$$G_{n2(in),ATAD} = \frac{0.78 \cdot Q_{gas,in} \cdot 28}{R \cdot (T_{gas,in} + 273.15)} \quad \text{(A.30)}$$

$$G_{o2(in),ATAD} = \frac{0.21 \cdot Q_{gas,in} \cdot 32}{R \cdot (T_{gas,in} + 273.15)} \quad \text{(A.31)}$$

$$G_{o2(in),ATAD} = \frac{0.01 \cdot Q_{gas,in} \cdot 12}{R \cdot \left(T_{gas,in} + 273.15\right)} \tag{A.32}$$

Gas effluent flow-rate

The gas effluent flow-rate is obtained based on the difference of pressures between the total gas in the gaseous phase and the outside, this difference is regulated by a coefficient that represents the flow resistance in the off-gas hole:

$$Q_{gas,out} = k_{gas} \cdot \left(P_{gas} - P_{atm}\right) \tag{A.33}$$

Heat flows

- Influent and effluent heat flows:

The influent ($HF_{in,(g)}$) and effluent ($HF_{out(g)}$) gaseous heat flows considers the heat flow of every gaseous component:

$$HF_{in(g)} = T_{inf(g)} \cdot Q_{gas,in} \cdot \begin{pmatrix} G_{h2o(in),ATAD} \cdot c_{p,h2o} + G_{co2(in),ATAD} \cdot c_{p,co2} + \\ + G_{o2(in),ATAD} \cdot c_{p,o2} + G_{n2(in),ATAD} \cdot c_{p,n2} \end{pmatrix} \tag{A.34}$$

$$HF_{out(g)} = T_{gas} \cdot Q_{gas,out} \cdot \begin{pmatrix} G_{h2o,ATAD} \cdot c_{p,h2o} + G_{co2,ATAD} \cdot c_{p,co2} + \\ + G_{o2,ATAD} \cdot c_{p,o2} + G_{n2,ATAD} \cdot c_{p,n2} \end{pmatrix} \tag{A.35}$$

The heat lost from walls corresponds to the difference between the inside and outside temperature:

$$HF_{walls(g),ATAD} = k_{walls(g)} \cdot \left(T_{gas,ATAD} - T_{amb}\right) A_{gas,ATAD} \tag{A.36}$$

Temperature

The temperature in the gaseous phase is obtained from its enthalpy:

$$T_{gas,ATAD} = \frac{H_{gas,ATAD}}{V_{gas} \cdot \left(G_{h2o} \cdot c_{p,h2o} + G_{co2} \cdot c_{p,co2} + G_{o2} \cdot c_{p,o2} + G_{n2} \cdot c_{p,n2} \right)} \qquad \text{(A.37)}$$

Annex B The Latin Hypercube Sampling Method

Latin hypercube sampling (LHS) is a statistical method for generating distribution of plausible collections of parameter values from a multidimensional distribution. The sampling method is often applied in uncertainty analysis. The technique was first described by (McKay et al., 1979). It was further elaborated by (Iman et al., 1981).

In the context of statistical sampling, a square grid containing sample positions is a Latin square if (and only if) there is only one sample in each row and each column. A Latin hypercube is the generalization of this concept to an arbitrary number of dimensions, whereby each sample is the only one in each axis-aligned hyperplane containing it.

When sampling a function of N variables, the range of each variable is divided into M equally probable intervals. M sample points are then placed to satisfy the Latin hypercube requirements; note that this force the number of divisions, M, to be equal for each variable. Also note that this sampling scheme does not require more samples for more dimensions (variables); this independence is one of the main advantages of this technique. Another advantage is that random samples can be taken one at a time, remembering which samples were taken so far.

Consider the case when is required to sample M points in the N dimensional vector space. Therefore, the Latin hypercube sampling strategy can be explained as follows:

- Divide the interval of each dimension into M non-overlapping intervals having equal probability (considering a uniform distribution, so the intervals should have equal size).
- Sample randomly from a uniform distribution a point in each interval in each dimension.
- Pair randomly (equal likely combination) the point from each dimension.

The maximum number of combinations for a Latin Hypercube of M divisions and N variables (i.e. dimensions) can be computed with the following expression:

$$\left[\prod_{n=0}^{M-1}(M-n)\right]^{N-1} = (M!)^{N-1} \qquad \text{(B.1)}$$

For example, a Latin hypercube of M=4 divisions with N=2 variables (i.e., a square) will have 24 possible combinations. A Latin hypercube of M=4 divisions with N=3 variables (i.e., a cube) will have 576 possible combinations. In two dimensions the main difference between random sampling and LHS are:

- In random sampling new sample points are generated without taking into account the previously generated sample points. One does thus not necessarily need to know beforehand how many sample points are needed.
- In LHS one must first decide how many sample points to use and for each sample point remember in which row and column the sample point was taken.

Consider two input variables (x_1 and x_2) in the range [0; 1]. If a random and a LHS are applied to this parameters space, the following distributions are obtained:

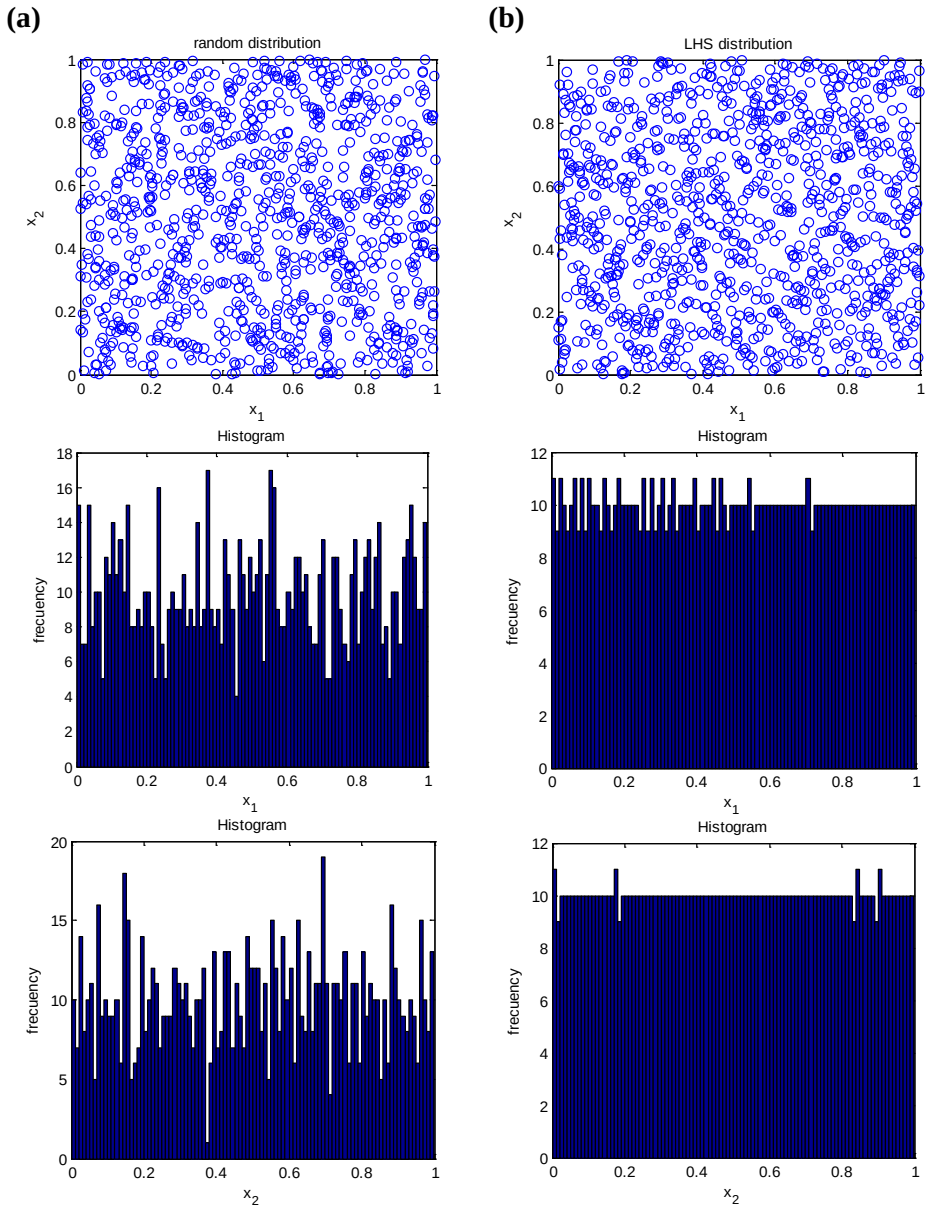

Figure B.1 Parameters distribution. **(a)** Applying a random sampling. **(b)** Applying a LHS sampling.

It can be observed in **Figure B.1(a)** the variables distribution when a random sampling is applied, detailing a non-uniform distribution for x_1 and x_2. When a LHS sampling is applied, **Figure B.1(b)** shows an improvement in these distributions to a quasi-uniform behavior.

Thus, LHS ensures that the ensemble of random numbers is representative of the real variability whereas traditional random sampling (sometimes called brute force) is just an ensemble of random numbers without any guarantees.

Annex C Principal Components Analysis

C.1 Definition

Principal Components Analysis (PCA) is a mathematical procedure that uses an orthogonal transformation to convert a set of observations of possibly correlated variables into a set of values of uncorrelated variables called *principal components (PCs)*. The goal of PCA is to reduce the dimensionality of the data while retaining as much as possible of the variation present in the original dataset.

The transformation is defined in such a way that the first component has as high a variance as possible (that is, accounts for as much of the variability in the data as possible), and each succeeding component in turn has the highest variance possible under the constraint that it be orthogonal to (uncorrelated with) the preceding component.

C.2 Example showing the PCA technique

Suppose we had measured two variables, length and width, and plotted them as shown in **Figure C.1(a)**. Both variables have approximately the same variance and they are highly correlated with one another. We could pass a vector through the long axis of the cloud of points and a second vector at right angles to the first, with both vectors passing through the centroid of the data.

(a) **(b)**

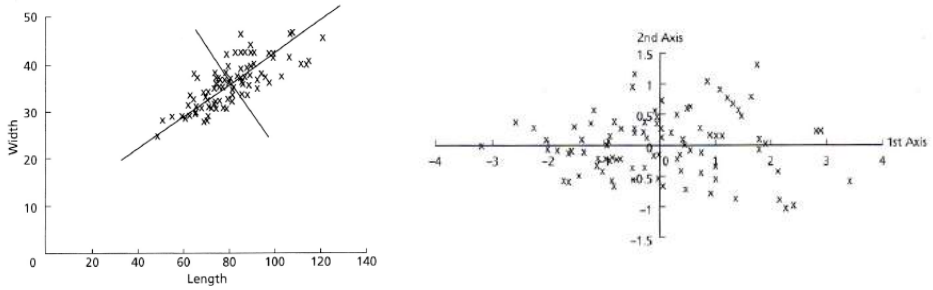

Figure C.1. **(a)** Original data plot. **(b)** Two perpendicular vectors of the original data.

Once we have made these vectors, new coordinates of all the data points relative to these two perpendicular vectors is obtained (see **Figure C.1(b)**). In this new reference frame, note that the variance is greater along the axis 1 than it is on axis 2. Also note that the spatial relationship of the points are unchanged; this process has merely rotated the data. Finally, note that the new vectors, or axes, are uncorrelated. By performing such a rotation, the new axes might have particular explanation. In this case, axis 1 could be regarded as a size measure, with samples on the left having both small length and width and samples on the right having large length and width. Axis 2 could be regarded as a measure of shape, with samples at any axis 1 position (that is, on a given size) having different length to width ratios. PC axes will generally not coincide exactly with any of the original variables.

Although these relationships may seem obvious, when one is dealing with many variables, this process allows one to assess much more quickly any relationships among variables. For data sets with many variables, the variance of some axes may be great, whereas others may be small, such that they can be ignored. This is known as reducing the dimensionality of a data set, such that one might start with thirty original variables, but might end with only two or three meaningful axes. PCA produces linear combinations of the original variables to generate the axes, i.e. the principal components.

C.3 Computation

Given a data matrix with p variables and n samples, the data are first centered on the means of each variable. This will ensure that the cloud of data is centered on the origin of the principal components, but does not affect the spatial relationship of the data nor the variances along our variables. The first principal component (Y_1) is given by the linear combination of the variables X_1, X_2, …, X_p.

$$Y_1 = a_{11}X_1 + a_{12}X_2 + ... + a_{1p}X_p \qquad \text{(C.1)}$$

Or in matrix notation:

$$Y1 = a_1^T X \qquad \text{(C.2)}$$

The first principal component is calculated such that it accounts fir the greatest possible variance in the data set. Of course, one could make the variance of Y_1 as large as possible by choosing large values for the weight a_{11}, a_{12}, …, a_{1p}. To prevent this, weights are calculated with the constraint that their sum of squares is 1.

$$a_{11}^2 + a_{12}^2 + ... + a_{1p}^2 = 1 \qquad \text{(C.3)}$$

The second principal component is calculated in the same way, with the condition that it is uncorrelated with the principal component and that it accounts for the next highest variance.

$$Y_2 = a_{21}X_1 + a_{22}X_2 + ... + a_{2p}X_p \quad \text{(C.4)}$$

This continues until a total of p principal components have been calculated, equal to the original number of variables. At this point, the sum of the variances of all of the principal components will equal the sum of the variances of all of the variables, that is, all of the original information has been explained or accounted for. Collectively, all of these transformations of the original variables to the principal components are:

$$Y = AX \quad \text{(C.5)}$$

The rows of matrix *A* are called the eigenvectors. The elements of an eigenvector are the weights a_{ij}, and are also known as loading. The elements in the diagonal of matrix Y are known as the eigenvalues. Eigenvalues are the variances explained by each principal component, and are constrained to decrease monotonically from the first principal component to the last. These eigenvalues are commonly plotted to show the decreasing rate at which variance is explained by additional principal components (see **Figure C.2**).

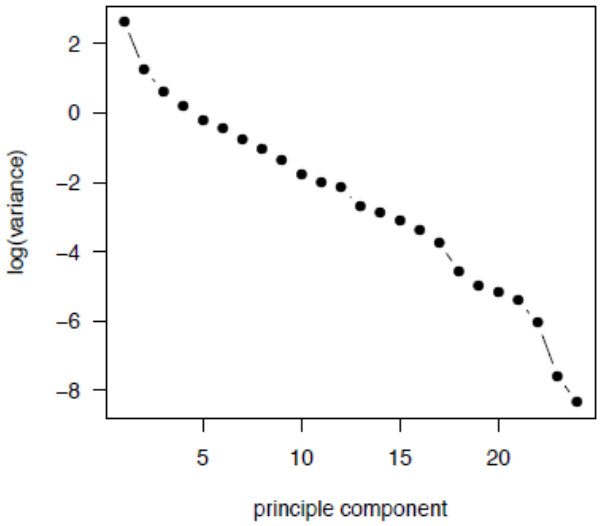

Figure C.2. Plot of eigenvalues

The positions of each observation in this new coordinate system of principal components are called scores and are calculated as linear combinations of the original variables and the weights a_{ij}.

C.4 Number of PCs

Applying PCA a reduction of dimensionality is obtained, that is, few principal components (PCs) versus many variables, therefore several criteria have been proposed for determining how many PCs should be taken into account and how many should be ignored. One common criterion is to ignore PCs at the point at which the next PC offers little increase in the total variance explained. A second criterion is to include all those PCs up to a predetermined total percent variance explained, such as 90%. A third criteria is to ignore components whose variance explained is less than 1 when a correlation matrix is used or less than the

average variance explained when a covariance matrix is used, with the idea being that such a PC offers less than one variable's worth of information. A fourth standard is to ignore the last PCs whose variance explained is all roughly equal.

Annex D Checkerboard plots considering noise signal

In this section the rest of results from the methodology application for the robust tuning of bending-point detection algorithm parameters (see **Chapter 6**) are presented. These results were obtained considering a Gaussian noise in the temperature sensor and different responses of digital filters.

D.1 Applying the Cascaded integrator-comb (CIC) filter

(a)

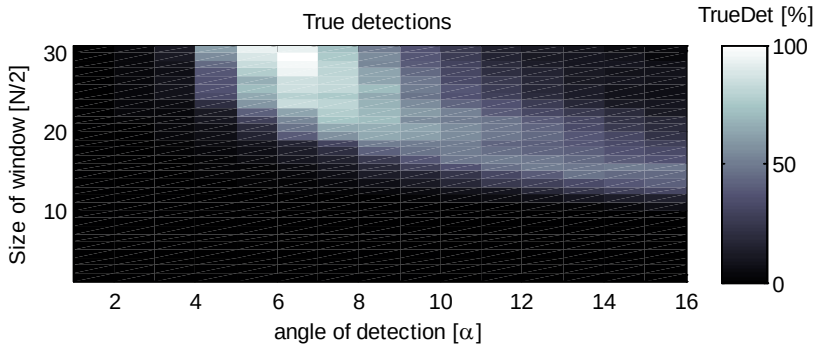

(b)

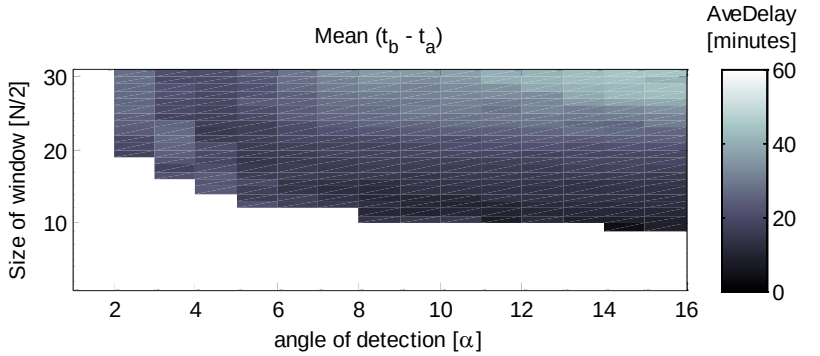

Figure D.1 Checkerboard plot considering noise signal (CIC filter applied). **(a)** True detection matrix. **(b)** Mean detection time matrix.

D.2 Applying the Tukey Window filter

(a)

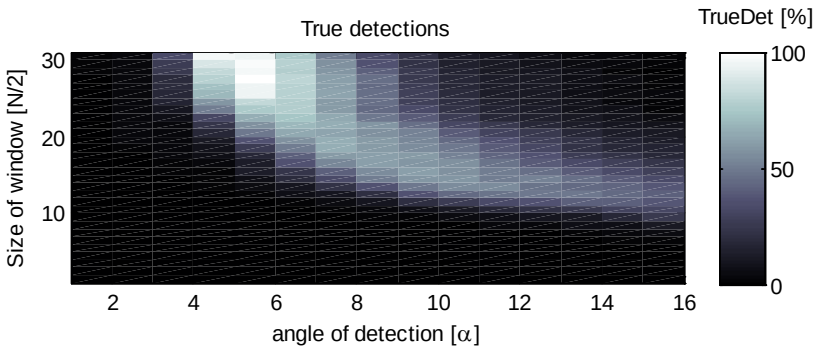

(b)

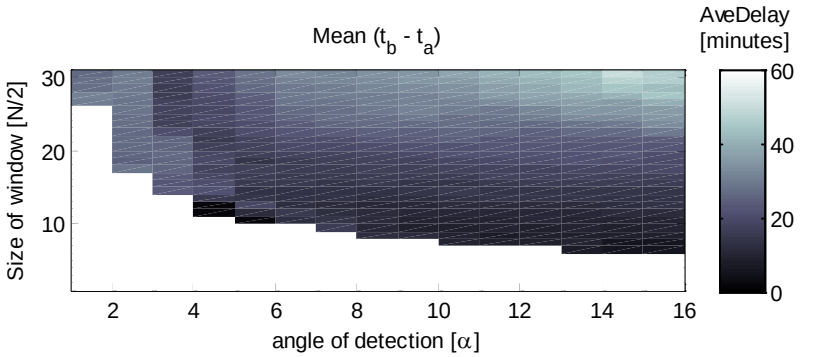

Figure D.2 Checkerboard plot considering noise signal (Tukey window applied). **(a)** True detection matrix. **(b)** Mean detection time matrix.

Annex E **Notation & Acronyms**

Table E.1 Glossary (Notations, abbreviations)

AE	Aeration Energy	PTime	Pasteurization Time
ASM	Activated Sludge Model	Q_{air}	Volumetric air flow-rate
ATAD	Autothermal Thermophilic Aerobic Digestion	Q_{feed}	Influent volumetric flow-rate to the
AT_BSM	ATAD Benchmark Simulation Model	Q_{in}	Influent volumetric flow-rate to the plant
AveDelay	Mean delay	Q_{out}	Effluent volumetric flow-rate from the
bCOD	Biodegradable Chemical Oxygen Demand	$\bar{p}$	Vector of parameters
BSM	Benchmark Simulation Model	$\bar{r}$	Vector of inputs
COD	Chemical Oxygen Demand	RI	Robustness Index
c_p	Specific heat	SOUR	Specific Oxygen Uptake Rate
CPV	Cumulative Percent Variance	SP	Sludge Production
EQ	Effluent Quality	SRT	Solid Retention Time
G_i	Concentration in gaseous phase	ST1	Strategy 1
H	Enthalpy	ST2	Strategy 2
HF	Heat flux	StD	Standard deviation
HT	Pre-holding tank	StQI	Stabilization Quality Index
k_a	Flag of bending-point detection acting during the cycle	t	Time
k_b	Flag of bending-point detection acting the next cycle	T	Temperature
K_La	Oxygen transfer coefficient	T_{cycle}	Time of cycle duration
K_{paste}	Indicator of pasteurized cycle	TCI	Total Cost Index
K_{st}	Indicator of stabilized cycle	ThE	Thermal Energy
L_i	Concentration in liquid phase	TrueDet	True Detections
LHS	Latin Hypercube Sampling	t_{sim}	Time of simulation
M	Mass	TSS	Total Suspended Solids
ME	Mixing Energy	TWV	Total Withdrawal Volume
N	Total number of batch cycles	V	Volume
OCI	Overall Cost Index	VS	Volatile Solids
OL	Open-Loop Strategy	W_{new}	Window with newest data
ORP	Oxidation Reduction Potential	W_{old}	Window with oldest data
PCA	Principal Component Analysis	WV_{out}	Withdrawal
PE	Pumping Energy	WWTP	Waste Water Treatment Plant
PQI	Pasteurization Quality Index	$\bar{x}$	Vector of state variables

Table E.2 Greek letters

α	Angle of detection
β	Parameter of the Tukey Window
Δ	Difference
v_{ij}	Stoichiometric coefficient for a specific component X*i* in the transformation *j*
ρ_j	Kinetic of transformation *j*

Table E.3 Subscript

i	Specific model component
j	Specific transformation
k	Volume in which de component is defined

Table E.4 Superscript

i	Specific batch number respect to the total batches
u	u-type profile (profile with bending-point)
v	v-type profile (profile with no bending-point)

Annex F Main papers generated

F.1 Patent

Irizar I., Zambrano J. A. Método de detección del agotamiento de la materia orgánica biodegradable en reactores aerobios autotérmicos. Oficina Española de Patentes y Marcas. **P200901328**. (Submitted).

F.2 International Journal

Zambrano J. A., Gil-Martinez M., Garcia-Sanz M. and Irizar I. (2009b). Benchmarking of control strategies for ATAD technology: A first approach to the automatic control of sludge treatment systems. *Water Science and Technology*. **60**(2), 409-417.

Zambrano J. A. and Irizar I. (2011). New methodology for robust tuning of bending-points detection algorithm considering uncertainty. *Water Science and Technology*. (Submitted).

F.3 Proceedings

Zambrano J. A., Gil-Martinez M., García-Sanz M. and Irizar I. (2009a). Benchmarking of control strategies for ATAD technology: a first approach to the automatic control of sludge treatment systems. In: *Proceedings 10th IWA Conference on Instrumentation, Control and Automation (ICA2009)*. Cairns, Australia, June 14-17 2009. (on CD-ROM).

Bibliography

Alferes, J., Irizar, I., 2010. Combination of extremum-seeking algorithms with effective hydraulic handling of equalization tanks to control anaerobic digesters. *Water Science and Technology* 61, 2825-2834.

Al-Ghusain, I., Hao, O., 1995. Use of pH as Control Parameter for Aerobic/Anoxic Sludge Digestion. Journal of Environmental Engineering 121, 225-235.

Al-Ghusain, I., Huang, J., Hao, O., Lim., B., 1994. Using pH as Real-Time Control Parameter for Wastewater Treatment and Sludge Digestion Processes. Water Science & Technology 30, 159-168.

APHA, 1995. Standard Methods, 19 ed. American Public Health Association, Washington, DC / U.S.A.

ASCE & WEF, 1998. Design of Municipal Wastewater Treatment Plants. Nº 76.

BOC Gases, 1998. Equipment Spec.

Booth, M.G., Tramontini, E., 1983. Thermophilic Sludge Digestion Using Oxygen and Air, in Anonymous Sewage Sludge Stabilization and Disinfection. Ellis, Chichester, England, pp. 293-311.

Bouhouche, S., Lahreche, M., Moussaoui, A., Bast, J., 2007. Quality monitoring using principal component analysis and fuzzy logic application in continuous casting process. American Journal of Applied Sciences 4, 637-644.

Breider, E.J., Drnevich, R.F., 1981. Control of Sludge Temperature in Autothermal Sludge Digestion. United States patent 4276174.

Breitenbucher, K., 1984. Engineering and Practical Experiences of Autoheated Aerobic-Thermophilic Digestion, in Strach, D., Havellar, A., LHermite, P. (Eds.), Inactivation of Microorganisms in Sewage Sludge by Stabilization Processes. Elsevier Applied Science, London, pp. 192-205.

Brockmann, D., Steyer, J.P., De Keyser, W., Nopens, I., Claeys, F., Urchegui, G., Ayesa, E., 2011. ADD CONTROL: advanced control solutions for waste water treatment. Rev Environ Sci Biotechnol 10, 3-7.

Bruce, A.M., Newman, P.J., 1992. Processing of organic sludges and liquid agricultural wastes, in Hall, J.E., Newman, P.J., LHermite, P. (Eds.), Treatment and use of Sewage Sludge and Liquid Agricultural Wastes. Commission of the European Communities, Brussels.

Burnett, C., 1994. Technology and Process Options for Autothermal Thermophilic Aerobic Digestion. *Proceedings Water Environment Federation 67th Annual Conference & Exposition*, Chicago, Illinois, 658.

Cattell, R.B., 1966. The scree test for the number of factors. Multivariate Behavioral Research 1, 245-276.

Chen, K., Chen, C., Peng, J., Houng, J., 2002. Real-time control of an immobilized-cell reactor for wastewater treatment using ORP. Water Research 36, 230-238.

Cheng, J.H., Zhu, N.W., 2008. Effect of Autothermal Thermophilic Aerobic Digestion Operation on Reactor Temperatures. In. 2nd Conference on Bioinformatics and Biomedical Engineering (ICBBE 2008), Shangai, June (2008).

Cheremisinoff, N.P., 2002. Handbook of Water and Wastewater Treatment Technologies. Butterworth-Heinemann, Boston, USA.

Cohen, D.B., Puntenney, J.L., 1973. Metro Denver's experience with large-scale aerobic digestion of waste activated sludge. Presented at the 47th Annual Conference Water Pollution Control Federation, Cleveland, Ohio, October (1973).

Copp, J., 2002. The COST Simulation Benchmark - Description and Simulation Manual. Office for Official Publications of the European Communities, Luxembourg.

Deeny, K., Hahn, H., Leonhard, D., Heidman, J., 1991. Autoheated thermophilic aerobic digestion. Water Environment and Technology 3, 65-72.

Deeny, K., Heidman, J., Smith, J., 1985. Autothermal Thermophilic Aerobic Digestion in the Federal Republic of Germany. 40th Annual Purdue Industrial Waste Conference, West Lafayette, Indiana, 14–16 May 1985. pp. 1–17.

Eleyan, A., Demirel, H., 2005. Face recognition system based on PCA and feedforward neural networks. Computational Intelligence and Bioinspired Systems, LNCS, vol. 3512, pp. 935-942.

European Commission, 2000. Working document on sludge - 3rd draft. ENV.E.3/LM.

Eyma, R., Tansel, B., Helfrich, C., 1999. Thermophilic Aerobic Digestion to Achieve Class A Biosolids. Florida Water Resource Journal December, 24-28.

Farmer, S.A., 1971. An investigation into the results of principal component analysis of data derived from random numbers. Statistician 20, 63-71.

Fuchs, L., Fuchs, M., 1991. Process for the Disinfection and Aerobic Stabilization of Sewage Sludge. United States patent 4983298.

Ga, C.H., Ra, S.C., 2009. Real-time control of oxic phase using pH(mV)-time profile in swine wastewater treatment. Journal of Hazardous Materials 172, 61-67.

García, J., Gomez, J., Lasheras, A., Huete, E., Echeverría, N., García-Heras, J.L., 2007. Advancing with ATAD. Water Environmental and Technology 19, 48-55.

Giffin, T., 2009. ATAD Process for the Treatment of Biosolids for Beneficial Re-Use. 72nd Annual Water Industry Engineers and Operators' Conference Bendigo Exhibition Centre, 1 to 3 September, 2009.

Gomez, J., de Gracia, M., Ayesa, E., Garcia-Heras, J.L., 2007a. Mathematical modelling of autothermal thermophilic aerobic digesters. Water Research 41, 959-968.

Gomez, J., 2007b. Digestión Aerobia Termófila Autosostenida (ATAD) de fangos. Estudio experimental a escala real y modelización matemática del reactor. PhD's Thesis. Escuela Superior de Ingenieros, Universidad de Navarra, San Sebastian, España.

Gujer, W., Henze, M., Mino, T., van Loosdrecht, M.C.M., 1999. Activated Sludge Model No. 3. Water Science & Technology 39, 183-193.

Gurjar, B.R., 2001. Sludge Stabilization at Small Works, in Anonymous Sludge Treatment and Disposal. A.A. Balkema Publishers, India, pp. 102-106.

Haner, A., Mason, C.A., Hamer, G., 1994. Death and lysis during aerobic thermophilic sludge treatment: characterization of recalcitrant products. Water Research 28, 863-869.

Haug, T.R., 1993. , in Anonymous The Practical Handbook of Compost Engineering, 2nd edition ed. Lewis Publishers, Boca Raton, FL, pp. 268.

Hogenauer, E.B., 1981. An economical class of digital filters for decimation and interpolation. IEEE Transactions on Acoustic, Speech and Signal Processing 29, 155-162.

Iman, R.L., Helton, J.C., Campbell, J.E., 1981. An Approach to sensitivity analysis of computer models. Part 1. Introduction, input variable selection and preliminary variable assessment. Journal of Quality Technology 13, 174-183.

Jakob, J., Roos, H., Siekmann, K., 1989. Aerobic Thermophilic Methods for Disinfecting and Stabilizing Sewage Sludge, in Dirkwager, A., L'Hermite, P. (Eds.), Sewage Sludge Treatment and use, New Developments, Technological Aspects and Environmental Effects. Elsevier Applied Science, London, UK., pp. 378-389.

Jeppsson, U., Pons, M.N., 2004. The COST benchmark simulation model - current state and future perspective. Control Engineering Practice 12, 299-304.

Jeppsson, U., Pons, M.N., Nopens, I., Alex, J., Copp, J.B., Gernaey, K.V., Rosen, C., Steyer, J.P., Vanrolleghem, P., 2007. Benchmark simulation model no 2: General protocol and exploratory case studies. Water Science and Technology 56, 67-78.

Jeppsson, U., Rosen, C., Alex, J., Copp, J., Gernaey, K.V., Pons, M.N., Vanrolleghem, P.A., 2006. Towards a benchmark simulation model for plant-wide control strategy performance evaluation of WWTPs. Water Science and Technology 53, 287-295.

Jewell, W.J., Kabrick, R.M., 1980. Autoheated aerobic thermophilic digestion with aeration. Journal of Water Pollution and Control Federation 52, 512-523.

Jolliffe, I.T., 2002. Principal Component Analysis, 2nd ed. Springer, New York, USA.

Kambhu, K., Andrews, J.F., 1969. Aerobic Thermophilic Process for the Biological Treatment of Wastes - Simulation Studies. Journal of the Water 41, 127-141.

Kelly, H., Warren, R., 1995. What's in a name? - Flexibility. Water Environment & Technology 7, 46-50.

Kelly, H.G., 1999. Comparing North American biosolids treatment of thermophilic digestion, thermal-chemical and heat drying technologies. 4th European Conference on Sludge Management, Wakefield, West Yorkshire, UK, November 1999.

Kelly, H.G., 1990. Demonstration of an Improved Digestion Process for Municipal Sludges. Supply and Services Contract KE405-8-6575/01-SE, (1990), Ottawa, Canada.

Kelly, H.G., 2006. ATADigesters in Review: Operations and other issues. In 23rd annual operators training conference (IWEA 2006).

Kelly, H.G., Warren, R., 1997. Autothermal Thermophilic Aerobic Digestion Design, Proceedings ASCE/CSCE Joint Environmental Engineering Conference, Edmonton, Alberta, Canada, July 1997.

Keohan, P.W., Connelly, P.J., Prince, A.B., 1981. Engineering and Economic Assessment of Autoheated Thermophilic Aerobic Digestion with Air Aeration. EPA-600/S2-81-171.

Kim, J., Chen, M., Kishida, N., Sudo, R., 2004. Integrated real-time control strategy for nitrogen removal in swine wastewater treatment using sequencing batch reactors. Water Research 38, 3340-3348.

Kim, Y.K., Oh, B.K., 2009. Aeration Control of Thermophilic Aerobic Digestion Using Fluorescence Monitoring. Journal of Microbiology and Biotechnology 19, 93-98.

Koch, F., Oldham, W., Wang, H., 1988. ORP as a Tool for Monitoring and Control in Bio-Nutrient Removal Systems. Proc. of Joint ASCE/CSCE Envir. Engng Conf.12–19 July, Vancouver, BC (1988), pp. 162–170.

Koers, D.A., Mavinic, D.S., 1977. Aerobic Digestion of Waste Activated Sludge at Low Temperatures. Journal of Water Pollution and Control Federation 49, 460.

Kovacs, R., Mihaltz, P., Csikor, Z., 2007. Kinetics of autothermal thermophilic aerobic digestion - Application and extension of Activated Sludge Model No 1 at thermophilic temperatures. Water Science and Technology 56, 137-145.

Langeland, G., Paulsrud, B., 1984. Aerobic Thermophilic Stabilization, in Strach, D., Havellar, A., LHermite, P. (Eds.), Inactivation of Microorganisms in Sewage Sludge by Stabilization Processes. Elsevier Applied Science, London, pp. 38-47.

Lapara, T.M., Alleman, J.E., 1999. Thermophilic aerobic biological wasterwater treatment. Water Research 33, 895-908.

Layden, N.M., 2007. An evaluation of autothermal thermophilic aerobic digestion (ATAD) of municipal sludge in Ireland. Journal of Environmental Engineering and Science 6, 19-29.

Le, M.S., 2006. Thermophilic Biological Pre-treatments for MADs. Advances in Technology for Anaerobic Digestion of Municipal Sludge. Aqua Enviro, Manchester.

Loll, U., 1984. Combined Aerobic, Thermophilic and Anaerobic Digestion of Sewage Sludge. Abwasser-Abfall-Aquatechnik , 20-27.

Loll, U., Pawletta, G., Reinert, D., 1986. The Influence of Heavy Metals on Aerobic-Thermophilic Sewage Sludge Stabilization. EF-Verlag, Berlin.

Marsili-Libelli, S., Spagni, A., Susini, R., 2008. Intelligent monitoring system for long-term control of Sequencing Batch Reactors. Water Science & Technology 57, 431-438.

Mason, C., Hamer, G., Fleischmann, T., Lang, C., 1987. Aerobic Thermophilic Biodegradation of Microbial Cells. Applied Microbiology and Biotechnology 25, 568-576.

Matsch, L.C., Drnevich, R.F., 1977. Autothermal Aerobic Digestion. Journal of Water Pollution and Control Federation 49, 296-310.

Mavinic, D.S., Koers, D.A., 1979. Performance and Kinetics of Low Temperature, Aerobic Sludge Digestion. Journal of Water Pollution and Control Federation 51, 2088.

McKay, M.D., Beckman, R.J., Conover, W.J., 1979. A Comparison of three methods for selecting values of input variables in the analysis of output from a computer code. Technometrics 21, 239-245.

Messenger, J.R., de Villiers, H.A., Ekama, G.A., 1990. Oxygen utilization rate as a control parameter for the aerobic stage in dual digestion. Water Science and Technology 22, 217-227.

Morgan, S., Gunson, H.G., 1987. Aerobic Thermophilic Digestion of Sludge Using Air, in Bruce, A., Colin, F., Newman, P.J. (Eds.), Treatment of

Sewage: Thermophilic Aerobic Digestion and Processing Requirements for Land Filling. Elsevier Applied Science, London, pp. 29-37.

Morgan, S., Winstanley, R., Littlewood, M.H., Gunson, H.G., 1986. The Design of an Aerobic Thermophilic Sludge Digestion System. Institute Chemical Engineering Symposium Series 96, 393-402.

Morgan, S.F., Gunson, H.G., Littlewood, M.H., Winstanley, R., 1983. Aerobic Thermophilic Digestion of Sludge Using Air, in Anonymous Sewage Sludge Stabilization and Disinfection. Ellis Horwood Ltd., Chichester, England., pp. 278-292.

Pavselj, N., Hvala, N., Kocijan, J., Ros, M., Subelj, M., Music, G., Strmcnik, S., 2001. Experimental design of an optimal phase duration control strategy used in batch biological wastewater treatment. ISA Transactions 40, 41-56.

Peddie, C.C., Koch, F.A., Jenkins, C.J., Mavinic, D.S., 1988. ORP as a Tool for Monitoring and Control of SBR Systems for Aerobic Sludge Digestion. Proceedings of the Joint CSCE-ASCE National Conf. Env. Eng., Vancouver, B.C. (refereed), July 12-15, 1988, pp. 171-178.

Petersen, E.E., 1965. Chemical Reaction Analysis. Prentice Hall Inc., Englewood Cliffs, New Yersey, USA.

Piovoso, M., Kosanovich, K., Yuk, J., 1992. Process data chemometrics. IEEE Transactions on Instrumentation and Measurement 41, 262-268.

Plisson-Saune, S., Capdeville, B., Mauret, M., Deguin, A., Baptiste, P., 1996. Real-Time control of nitrogen removal using three ORP bending-points: signification, control strategy and results. Water Science and Technology 33, 275-280.

Ponti, C., Sonnleitner, B., Fiechter, A., 1995. Aerobic thermophilic treatment of sewage sludge at pilot plant scale. 2. Tecnical solutions and process design. Journal of Biotechnology 38, 183-192.

Pöpel, F., Ohnmacht, C., 1972. Thermophilic bacteria oxidation of highly concentrated substrates. Water Research 6, 807-815.

Prats-Montalbán, J.M., de Juan, A., Ferrer, A., 2011. Multivariate image analysis: A review with applications. Chemiometrics and Intelligent Laboratory Systems (*in press*).

Prescott, L.M., Harkey, J.P., Klein, D.A., 2002. Microbiology, 5th edition ed. McGraw-Hill.

Raich, A.C., Çinar, A., 1995. Multivariate statistical methods for monitoring continuous processes: assessment of discrimination power of disturbance models and diagnosis of multiple disturbances. Chemometrics and intelligent laboratory systems 30, 37-48.

Reid Crowther and Partners Ltd., 1987. Autoheated Thermophilic Aerobic Digestion of Wastewater Sludges.

Rieger, L., Alex, J., Winkler, S., Boehler, M., Thomann, M., Siegrist, H., 2003. Progress in sensor technology - progress in process control? Part I: Sensor

property investigation and classification. Water Science and Technology 47, 103-112.
Riley, D.W., Forster, C.F., 2002. An evaluation of an autothermal aerobic digestion system. Process Saf. Environ. Prot. 80, 100-104.
Rosen, C., Jeppsson, U., Vanrolleghem, P., 2004. Towards a common benchmark for long-term process control and monitoring performance evaluation. Water Science and Technology 50, 41-49.
Rosen, C., Olsson, G., 1998. Disturbance detection in wastewater treatment plants. Water Science & Technology 37, 197-205.
Rosen, C., Rieger, L., Jeppsson, U., Vanrolleghem, P.A., 2008. Adding realism to simulated sensors and actuators. Water Science and Technology 57, 337-344.
Samuelsson, P., Halvarsson, B., Carlsson, B., 2007. Cost-efficient operation of a denitrifying activated sludge process. Water Research 41, 2325-2332.
Scherfig, J., Schleisner, L., Brond, S., Kilde, N., 1996. Dynamic temperature changes in wastewater treatment plants. Water Environment Research 68, 143-151.
Schwinning, H.G., 1996. Autoheated thermophilic digestion of industrial sewage sludge. WEFTEC '96, Water Environment Federation 69th Annual Conference & Exposition, October 5–9, 1996. pp. 101–109.
Schwinning, H.G., Deeny, K.J., Hong, S.N., 1997. Experience with autothermal thermophilic aerobic digestion (ATAD) in the United States. WEFTEC '97, Water Environment Federation, 70th Annual Conference & Exposition. October 18–22, 1997. pp. 275–285.
Scisson, J.P., 2003. ATAD, The Next Generation: Design, construction, start-up and operation of the first municipal 2nd generation ATAD. WEF/ AWWA/ CWEA Joint Residuals and Biosolids Management Conference and Exhibition 2003.
Sedory, P.E., Stenstrom, M.K., 1995. Dynamic prediction of wastewater aeration basin temperature. Journal of Environmental Engineering 121, 609-618.
Shammas, N.K., Wang, L.K., 2007. Aerobic Digestion, in Wang, L.K., Shammas, N.K., Hung, Y. (Eds.), Biosolids Treatment Processes. Human Press, Totowa, New Jersey, USA, pp. 177-205.
Sin, G., Gernaey, K.V., Neumann, M.B., van Loosdrecht, M.C.M., Gujer, W., 2009. Uncertainty analysis in WWTP model applications: A critical discussion using an example from design. Water Research 43, 2894-2906.
Smith, J., Young, K., Dean, R., 1975. Biological oxidation and disinfection of sludge. Water Research 9, 17-24.
Song, Y., Nie, F., Zhang, C., Xiang, S., 2008. A unified framework for semi-supervised dimensionality reduction. Pattern Recognition 41, 2789-2799.

Sonnleitner, B., 1983. Biotechnology of Thermophilic Bacteria - Growth, Products and Application, in Fiechter, A. (Ed.), Advances in Biochemical Engineering/Biotechnology. Springer-Verlag, New York, USA, pp. 68-138.

Sonnleitner, B., Fiechter, A., 1983a. Bacterial Diversity in Thermophilic Aerobic Sewage Sludge II. Types of Organisms and their Capacities. European Journal of Applied Microbiology and Biotechnology 18, 174-180.

Sonnleitner, B., Fiechter, A., 1983b. Bacterial Diversity in Thermophilic Aerobic Sewage Sludge. I. Active biomass and its Fluctuations. European Journal of Applied Microbiology and Biotechnology 18, 47-51.

Stare, A., Vrecko, D., Hvala, N., Strmcnik, S., 2007. Comparison of control strategies for nitrogen removal in an activated sludge process in terms of operating costs: A simulation study. Water Research 41, 2004-2014.

Staton, K.L., Alleman, J.E., Pressley, R.L., Eloff, J., 2001. 2nd Generation Autothermal Thermophilic Aerobic Digestion: Conceptual Issues and Process Advancements. , 1484.

Stentiford, E.I., 2001. Aerobic digestion, in Spinosa, L., Vesilind, P.A. (Eds.), Sludge into Biosolids: Processing, Disposal, Utilization. IWA Publishing, pp. 209-222.

Stover, E.L., Joshua Samuel, G., 1998. High rate thermophilic pretreatment of high strength industrial wastewaters. 52nd Purdue Industrial Waste Conference, Purdue University, West Lafayette, IN (May 5-7, 1997).

Tomita, R., Park, S., Sotomayor, O., 2002. Analysis of activated sludge process using multivariate statistical tools - a PCA approach. Chemical Engineering Journal 90, 283-290.

Trim, B.C., 1984. Sludge Stabilization and Disinfection by means of Autothermal Aerobic Digestion using Oxygen. IWPC Biennal Conf. Durban 27-30 May.

Tsang, K.R., Smith, J.E., 2005. Challenges in Sludge Stabilization: Regulatory Compliance in the Design and Operation of Facilities. Journal of Environmental Engineering , 834-837.

USEPA, 1993. Environmental regulations and technology: control of pathogens and vector attraction in sewage sludge. EPA/625/R-92/013.

USEPA, 1990. Environmental regulations and technology: Autothermal thermophilic aerobic digestion of municipal wastewater sludge. Technical report. EPA/625/10-90/007.

Vanrolleghem, P.A., Gillot, S., 2002. Robustness and economic measure as control benchmark performance criteria. Water Science & Technology 45, 117-126.

Vanrolleghem, P.A., Jeppsson, U., Carstensen, J., Carlsson, B., Olsson, G., 1996. Integration of wastewater treatment plant design and operation – a systematic approach using cost function. Water Science and Technology 34, 159-171.

Vesilind, P.A., 2001. Introduction to Stabilization, in Spinosa, L., Vesilind, P.A. (Eds.), Sludge into Biosolids - Processing, Disposal and Utilization, First ed. IWA Publishing, London, UK, pp. 206-208.

Vismara, R., 1985. A model for autothermic aerobic digestion: Effects of scale depending on aeration efficiency and sludge concentration. Water Res. 19, 441-447.

Volcke, E.I.P., Gernaey, K.V., Vrecko, D., Jeppsson, U., van Loosdrecht, M.C.M., 2006. Plant-wide (BSM2) evaluation of reject water treatment with a SHARON-Anammox process. Water Science and Technology 54, 93-100.

Vrecko, D., Gernaey, K.V., Rosen, C., Jeppsson, U., 2006. Benchmark Simulation Model No 2 in Matlab-Simulink: Towards plant-wide WWTP control strategy evaluation. Water Science and Technology 54, 65-72.

Wareham, D.G., Mavinic, D.S., Hall, K.J., 1994. Sludge Digestion Using ORP-Regulated Aerobic-Anoxic Cycles. Water Research 28, 373-384.

Wolf, P., 1982. Aerobic thermophilic stabilization of sludge versus anaerobic digestion and other kinds of sludge treatment at middle-sized plants with respect to power conservation and economy. Water Science & Technology 14, 727-738.

Wolinski, W.K., 1985. Aerobic Thermophilic Sludge Stabilization Using Air. Water Pollution Control , 433-455.

Won, S.G., Ra, C.S., 2011. Biological nitrogen removal with a real-time control strategy using moving slope changes of pH(mV)- and ORP-time profiles. Water Research 45(1), 171-178.

Yoon, S., MacGregor, J., 2001. Fault diagnosis with multivariate statistical models part I: using steady state fault signatures. Journal of Process Control 11, 387-400.

Yu, R.-., Liaw, S.-., Chang, C.-., Lu, H.-., Cheng, W.-., 1997. Monitoring and control using on-line ORP on the continuous-flow activated sludge batch reactor system. Water Science and Technology 35, 57-66.

Zambrano, J.A., Gil-Martinez, M., García-Sanz, M., Irizar, I., 2009a. Benchmarking of control strategies for ATAD technology: a first approach to the automatic control of sludge treatment systems. Water Science and Technology 60, 409-417.

Zambrano, J.A., Gil-Martinez, M., Garcia-Sanz, M., Irizar, I., 2009b. Benchmarking of control strategies for ATAD technology: A first approach to the automatic control of sludge treatment systems. In: Proceedings 10th IWA Conference on Instrumentation, Control and Automation (ICA2009). Cairns, Australia, June 14-17 2009. (on CD-ROM).

Acknowledgment

My greatest gratitude goes to Ion Irizar, for giving me the opportunity to work with him, his help, encouragement and guidance during these years. To Eduardo Ayesa, for receiving me and also for being there in the most complicated moments, I'll never forget our talks in Isaba and the mountains trekking. To the directive at CEIT and Tecnun, I always felt in a good atmosphere.

Money matters. Therefore, I am grateful to Asociación de Amigos de la Universidad de Navarra for financing part of my PhD period, and CEIT where I worked as a researcher in some projects.

My sincere gratitude to Mentxu Blanco for let me work as an assistant in some courses of Mathematics. Also thanks to Manuel Pargada, Juan Flaquer and Bea Pereda, as well as to Maria Trueba, Aitor Luque and Goretti Etxegaray. It was completely a pleasure to work with all of you.

Thanks to Elena, Albizuri et al., Maite, Carmen, Alain, Enrique, Naiara, Tamara, Maider, Elena G., Mikel Maiza, Susana and all the others. All my gratefulness goes to Luis Larrea, Luis Sancho, Antonio, Paloma, Jaime Luis, Bixent and Jaime. Thanks to the "latin-group": Janelcy, Claudia, Adriana Ortiz & Tim, Lorena, Nirko, Carlos, Lucho, Fer, Lalo & Adriana, Charly, Yunesky and Alaine, we had great moments together. Also thanks to Rossi, Patricia, Nacho, Sabine and JuanJo. Also thanks to Inma (aupa Mendaza!), may your energy never change!, to Larraitz, Natalie, Ramona and Annie. Thanks to Jose Manuel (no va más!) & Imanol, all the best for you guys!

Susan Alustiza, Joseba Campos, you always gave me a good energy and enthusiasm, I wish you the best! Also thanks to Tomás Gomez-Acebo and Raúl Antón. Thanks to Patxi, Paqui, Carmele, Patrick and Manolo, I always got a big help from all of you. Verónica, thank you for having a lot of patient with me in these last months preparing documents. Thanks to Rober for the great disposition in printing my thesis. Don JuanJo, Don Patxi, Don Rafa (the holy

friends), I really appreciated those coffee breaks and advises. My gratitude to Josune Otxotorena, Estitxu, Ana and all the others, for those good moments we have had enjoying the music.

I'll never forget those friends I met in Barcelona: Ruth, Thomas, Sabine O., GertJan and Emmy, Mathias and Marisabel, Marta, Micky, Patricia U. and Rosa. All of you are fantastic! I can't forget the friendship I received from Poland (Grazyna, Thomaz, Edyta, Magda, Pawel, Asia), I always felt like part of the family. Lila, Angela, Maria, Dbee, Edgar and Brian, I know you since the college, may the life give you the best.

Thanks to Marco, Hayley, Marie, Luke, Ornella, Pj Kahuna (and the Biurrun family). I'll never forget your great friendship and the musical moments. Also to "Mapu", Leo, Juan Pablo, Diana, Amilcare, Pier-Luigi, thank you guys!

Lucy, Patricia, Ivedt, Sandra, thanks for every word and your best wishes from Venezuela. Thanks to my family: Omar, Marlene, Jhon, Kelly, Tío Rodolfo, Tía Flor and sons, and all the others.